Sample-Efficient Reinforcement Learning for Flight Control

Advancing Fault-Tolerant Control

Wing Chan

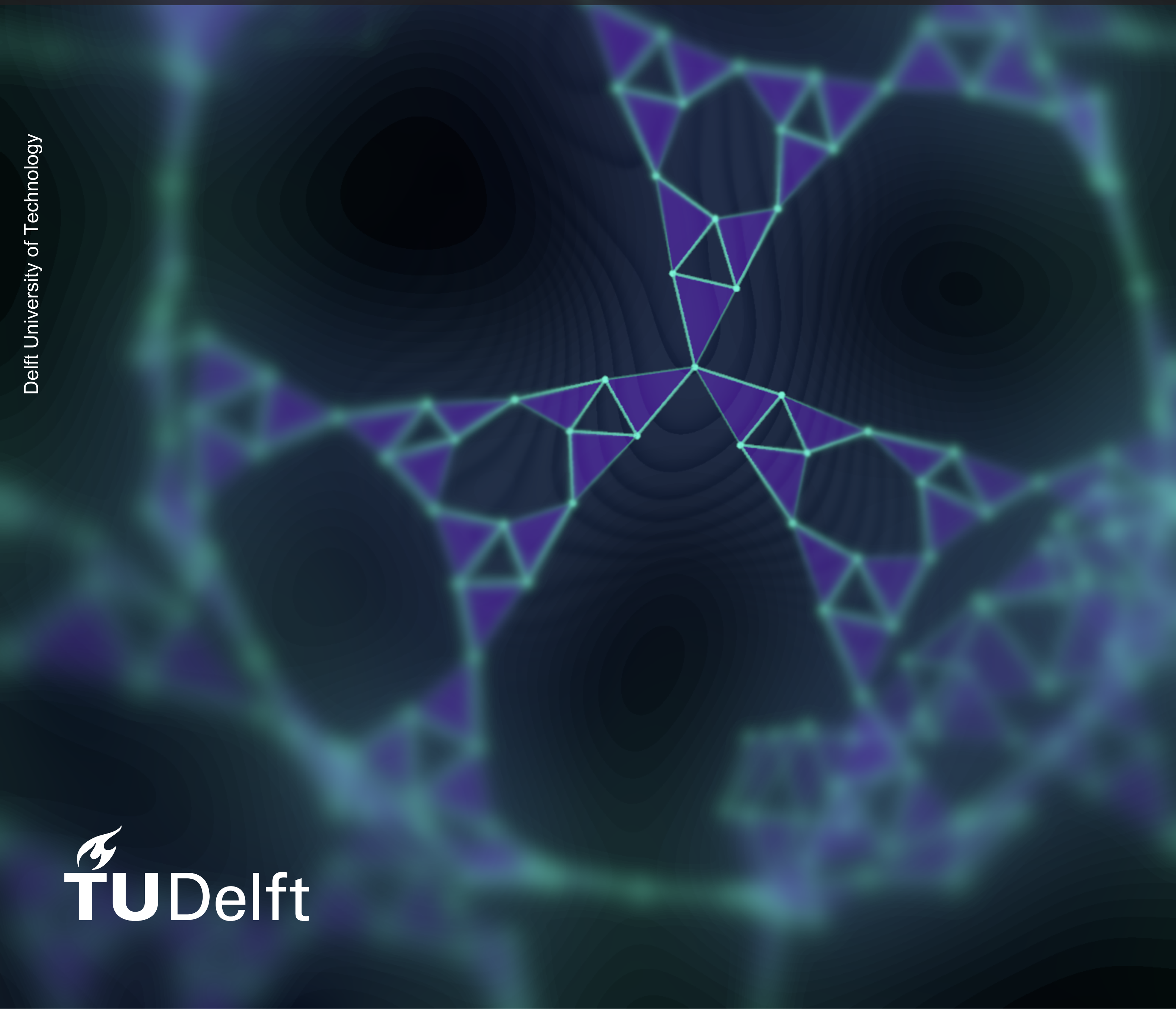

TU Delft

Sample-Efficient Reinforcement Learning for Flight Control

Advancing Fault-Tolerant Control

Thesis report

by

Wing Chan

to obtain the degree of Master of Science
at the Delft University of Technology
to be defended publicly on August 30, 2024 at 14:00

Thesis committee:	
Chair:	Dr.Ir. Rene van Paassen
Supervisor:	Dr.Ir. Erik-Jan van Kampen
External examiner:	Dr.Ir. Erwin Mooij
Additional member:	Ir. Isabelle El-Hajj
Place:	Faculty of Aerospace Engineering, Delft
Project Duration:	January, 2024 - August, 2024
Student number:	5002265

Faculty of Aerospace Engineering · Delft University of Technology

Preface

This is my Master's thesis, which I wrote to fulfil my graduation criteria for the Aerospace Engineering Master's programme at TUDelft, and I am very happy to be able to say that it was a great joy to do so. While I started this thesis knowing very little about the technical aspects of Reinforcement Learning (RL), I'm happy to say that I've come out of it knowing a great deal more -but I still have much more to learn-. I find it extremely fascinating that a collection of mathematical models can build something resembling how animals learn from experience, and it is my hope that continued research in this field will one day way down the line build us a complete model of something that can learn just like humans.

A copy of the ACD (a kind of RL) algorithm developed, and all the notes which I took during this thesis, can be found on Github[1][2].

Thanks to my friends in Delft for their support, and my thesis supervisor Erik-Jan for the fun and interesting conversations we'd have in our progress meetings, I consider myself fortunate to have been given the opportunity to do this thesis under his tutelage. And thank you to my girlfriend Kate for always being there even when we live behind different borders.

Enjoy the read.

Wing Yin Chan
Delft, 2024

[1] RL Algorithm: `https://github.com/wingos80/RL4AFCS`
[2] Notes: `https://github.com/wingos80/thesis_notes`

Contents

List of Figures

List of Tables

List of Algorithms

List of Symbols

Operators & Functions

$p()$	Probability distribution	$[-]$
$f()$	State transition function	$[-]$
$g()$	Input/action transition function	$[-]$
$\pi()$	Policy function	$[-]$
$v_\pi()$	State-value function under policy π	$[-]$
$q_\pi()$	Action-value function under policy π	$[-]$
$\mathbb{E}()$	Expectation operator	$[-]$

Variables

a	Action variable	$[-]$
s	MDP state variable	$[-]$
x	Dynamics model state variable	$[-]$
r	Reward variable	$[-]$
A_t	Action at t	$[-]$
S_t	MDP state at t	$[-]$
R_t	Reward at t	$[-]$
G_t	Return at t	$[-]$
$\mathcal{T}$	Trajectory	$[-]$
γ	Reward discount rate	$[-]$
$\mathbf{E}_t$	Eligibility trace at time t	$[-]$
λ	Eligibity trace decay rate	$[-]$
$W_{a,t}$	Actor network weights at time t	$[-]$
$W_{c,t}$	Critic network weights at time t	$[-]$
θ	Function approximator parameters	$[-]$
η	Learning Rate	$[-]$
τ	Target critic mixing factor	$[-]$
T	Episode final timestep/episode termination time	$[-, \mathrm{s}]$
Q	LQR state cost matrix	$[-]$
R	LQR action cost matrix	$[-]$
q	Pitch rate	[deg/s or rad/s]
V_{TAS}	True airspeed	[m/s]
ϕ	Roll angle	[deg or rad]
θ	Pitch angle	[deg or rad]
ψ	Yaw angle	[deg or rad]
α	Angle of attack	[deg or rad]
β	Angle of attack	[deg or rad]
δ_e	elevator deflection at time t	[deg or rad]
Θ	RLS estimator parameter matrix	$[-]$
Σ	RLS estimator covariance matrix	$[-]$
X	RLS estimator states	$[-]$
ρ	RLS estimator forgetting factor	$[-]$
k	RLS estimator gain	$[-]$
ϵ	RLS estimator innovation	$[-]$
L_{CAPS}	CAPS score	$[-]$
λ_s	CAPS spatial smoothness weight	$[-]$
λ_t	CAPS temporal smoothness weight	$[-]$

Nomenclature

Abbreviations

RL	Reinforcement Learning
MDP	Markov Decision Process
HDP	Heuristic Dynamic Programming
DHP	Dual Heuristic Programming
GDHP	Globalized Dual Heuristic Programming
AD	Action-Dependent
ACD	Actor-Critic Design
ADP	Approximate Dynamic Programming
VI	Value Iteration
PI	Policy Iteration
LQR	Linear Quadratic Regulator
MC	Monte Carlo
TD	Temporal Difference
HJB	Hamilton-Jacobi-Bellman
RLS	Recursive Least Squares
TD	Temporal Difference
IHDP	Incremental Heuristic Dual Programming
IDHP	Incremental Dual Heuristic Programming
MIDHP	Multi-step Incremental Dual Heuristic Programming
DRL	Deep Reinforcement Learning
DNN	Deep Neural Network
CNN	Convolutional Neural Network
RNN	Recurrent Neural Network
DQN	Deep Q Network
SGD	Stochastic Gradient Descent
TRPO	Trust Region Policy Optimization
PPO	Proximal Policy Optimization
KL	Kullback-Leibler
DPG	Deterministic Policy Gradient
DDPG	Deep Deterministic Policy Gradient
TD3	Twin Delayed Deep Deterministic policy gradient
SAC	Soft Actor Critic
LTI	Linear Time-invariant
DSAC	Distributional SAC
AoA	Angle of Attack
LTV	Linear Time-Varying
IQR	Inter Quartile Range
PID	Proportional Integral Derivative
RSE	Root Squared Error
CAPS	Conditioning for Action Policy Smoothness
VD	Vargha and Delaney

1 Introduction

1.1. Background and Motivation

Civil aviation is a sector that has a good track record in terms of transport safety [1], this excellent record is nonetheless tarnished by individual accidents that involve high fatality rates. The most fatal category of such accident is known as Loss of Control – Inflight (LOC-I), which groups together accidents that occur due to an aircraft deviating from flight path or aircraft operation outside normal flight envelope; 94% of accidents in this category resulted in fatalities [2]. Fault-tolerant or robust controllers are flight control methods that remain stable despite changes in the dynamic properties of an aircraft or operation in extreme conditions. One of the most exciting areas of research in fault-tolerant controllers is the application of Reinforcement Learning (RL) agents to control an aircraft. This approach can allow for directly optimizing a controller for scenarios that lead to LOC-I accidents [3], or even online adaptation of controller parameters in the face of dynamic behaviour changes [4], all of which have the potential of providing the flight controller with greater safety margins.

The limits to operational improvements do not stop at greater safety, as a higher degree of fault-tolerance will improve the feasibility of fully autonomous systems. The benefits from this range from the possibility to deploy pilot-less cockpits, to enhancing swarm-based drone systems for purposes such as offshore inspection or unmanned search and rescue operations in hard-to-access environments, advancing the state-of-the art of aviation.

The potential impact of RL on the control engineering community should be noted as well. Current industry practices for controller synthesis for aerospace engineering are predominantly done by combining Proportional Integral Derivative (PID) control laws with gain scheduling [5], where a different set of PID gains are designed for each discrete point in the flight envelope. While this approach has been proven to work and serves the aviation industry well, it is nonetheless tedious, time-consuming, and thus expensive to perform, requiring the expertise of dedicated control engineers. Furthermore, while such controllers provide guarantees for the automatic flight control system's performance within all considered flight conditions, such guarantees do not extend to portions of the flight envelope not covered by or between the selected flight conditions. This can happen in the case of faults or extreme weather conditions. This is especially true if the aircraft ventures into regions of the envelope where dynamics become nonlinear or experience hysteresis, such as near stall or if a fault occurs on the aircraft.

In addition to flight safety and control design efforts, there is also the matter of sustainability. Based on 2018 data, the aviation industry is responsible for approximately 2.4% of global anthropogenic greenhouse gas emissions [6]. Despite aviation traffic volumes falling drastically as a result of the COVID-19 pandemic, the recovery of air travel has been rapid and the number of flights is expected to recover soon, ultimately resulting in the aviation sector contributing 0.1 degrees Celcius of warming by 2050 [7]. To alleviate the severity of climate change, the aviation industry must therefore become carbon neutral, which will require innovation in all aspects related to aviation. On this front, novel aircraft design concepts such as the Flying-V promise fuel efficiency improvements over current tube-and-wing designs [8], and thus increasing the technological readiness level of such novel designs is of special interest for sustainability. This maturity will require dedicated efforts toward the design of flight control systems, which traditionally involves dedicated expert knowledge of control theory and time-intensive design campaigns [5]. Furthermore, the guarantees that traditional linear control laws promise would be hampered by the relative lack of exact system dynamic models for innovative aircraft designs. By their adaptiveness, RL based flight controllers can be model agnostic and therefore easily be trained to control new aircraft with less expert involvement in controller design, freeing up expertise for tackling other pressing design issues.

With the potential benefits in fault tolerance control, and reduced burden in controlling novel systems due to their system-agnostic nature, RL algorithms stand as an exciting means of improving the automatic flight control system design procedure, especially in the case of innovative aircraft designs such as the Flying-V. Maturing such RL for flight control applications by exploring the challenges associated with such a technology, and methods for overcoming them, will be some of the most crucial steps in advancing this technology's readiness level and yielding the benefits of autonomous flight.

1.2. Research Goal

Driven by the desire to contribute to the state of the art of RL, and motivated by the potential benefits which RL based controllers have for the aviation industry, the present research thesis is commenced.

To define the scope of this research, a research objective stating the high-level aim of the thesis is defined:

Research Objective

To improve the fault-tolerance of RL based flight controllers by advancing the state of the art, through researching novel augmentations to reinforcement learning algorithms.

Breaking down this objective, a set of research questions is formulated to define the direction of research more precisely. These questions help roughly segment the research process into two halves: the literature study phase, and the experimentation phase.

Research Questions

Q1 What promising reinforcement learning algorithm for fault-tolerance and tracking performance should be further studied in the present research?

- *Q1.1* What reinforcement learning algorithms are considered to be state-of-the-art?
- *Q1.2* How is fault-tolerance defined and tested in past research?
- *Q1.3* Which algorithms have been shown to provide the best fault-tolerance?
- *Q1.4* What reference tracking performance have these algorithms shown in past research?
- *Q1.5* What promising augmentations to reinforcement learning algorithms can be made and experimented with?

Q2 How can the identified algorithm be applied to control the PH-LAB research aircraft?

- *Q2.1* How can the identified augmentations be made to the reinforcement learning algorithm studied?
- *Q2.2* How should the flight control system be structured?
- *Q2.3* What are the variables defining the MDP in the case of controlling the PH-LAB?

Q3 How does the developed flight controller perform during nominal flight and in the presence of faults?

- *Q3.1* What flight scenarios should be designed to test the proposed controller's nominal performance and fault tolerance?
- *Q3.2* How should a controller's nominal performance and fault tolerance be measured?
- *Q3.3* What is the implemented controller's nominal performance and fault tolerance?
- *Q3.4* How do the proposed augmentations affect the nominal performance and fault tolerance of the baseline reinforcement learning algorithm?

The literature study phase is used to understand the field of reinforcement learning and that of flight control, and to discover ideas that will be used in the thesis. This phase will be an important first step to take in order to acquire knowledge about the fields, and this is outlined by **Q1**.

The experiment phase is where a reinforcement learning algorithm would be potentially developed, implemented, and experimented with for successful flight control. This phase will involve determining how an experiment on reinforcement learning for flight control needs to be set up, how it can be conducted, and how the experiments can be evaluated to draw conclusions. This phase is outlined by **Q2** and **Q3**.

1.3. Thesis Outline

With the motivation and the goals of the research presented, the remainder of the thesis report is outlined.

Following the thesis report structure of the master's thesis from the department of Control & Simulations in the faculty of Aerospace Engineering in TUDelft, the remainder of the thesis is split into three parts. The first part presents the scientific paper produced in the latter half of the thesis, as part of the fulfilment of the thesis requirements, it constitutes some of the primary results of this thesis and can be read as a standalone document. The second part has two chapters: the first is Chapter 2 which is a study of the published literature on the topics relevant to this thesis, such as adaptive dynamic programming, deep reinforcement learning, and flight control, thus providing the basis knowledge for the conducted research; the second is Chapter 3 which presents the results gathered up until the mid-term of the thesis. The third part contains four chapters of additional results gathered in the latter half of the thesis, but which are better presented distinctly from the scientific paper. The fourth and final part closes the thesis and contains Chapter 8, the overall conclusions of the thesis including the answers to the research questions posed, and Chapter 9, documenting recommendations and aspects that were not touched upon in the present thesis, this may be used for guidance on conducting future research in this direction.

Part I

Scientific Paper

A Multi-step and Eligibility Trace Approach to Incremental Dual Heuristic Programming for Flight Control

W. Chan *
Delft University of Technology, P.O. Box 5058, 2600GB Delft, The Netherlands

Incremental Dual Heuristic Programming (IDHP) is a successor to the Dual Heuristic Programming (DHP) algorithm that uses an online identified incremental system model, this algorithm showed promising flight control performance and tolerance of faults in simulation experiments. This paper studies the potential for extending IDHP through augmenting the computation of agent updates and returns, more specifically, by using eligibility trace updates and multi-step temporal difference error. This results in the IDHP(λ), MIDHP, and MIDHP(λ) algorithms, which are compared against IDHP in several simulated flight control scenarios with faults introduced mid-flight. The results demonstrate that the proposed algorithms have improved flight control performance and fault tolerance in terms of tracking errors when controlling a nominal aircraft and an aircraft with faults introduced, with the most improvement observed in MIDHP(λ).

Nomenclature

λ	=	Eligibility trace decay rate	[-]	ϵ, κ	=	RLS prediction residual, update gain	[-]
$\mathcal{S}, \mathcal{A}$	=	MDP state & action space	[-]	$\mathbf{E}$	=	Eligibility trace	[-]
$\mathcal{P}()$	=	MDP transition function	[-]	L_{CAPS}	=	CAPS score	[-]
n, m	=	No. of MDP states, actions	[-]	λ_T, λ_S	=	CAPS temporal, spatial smoothness weight	[-]
s, s', a, r	=	MDP state, augmented state, action, reward	[-]	$\mathcal{N}$	=	Multivariate normal distribution	[-]
γ	=	MDP reward discount rate	[-]	p, q, r	=	Roll, pitch, yaw rate	[rad/s]
R_t	=	MDP Return	[-]	V_{TAS}	=	True airspeed	[m/s]
$J(), \pi()$	=	Value, policy function	[-]	$\alpha, beta$	=	Angle of attack, sideslip	[rad]
Λ	=	Value gradient function	[-]	ϕ, θ, ψ	=	Roll, pitch, yaw angle	[rad]
Λ'	=	Target value gradient function	[-]	H	=	Height	[m]
W_a, W_c	=	Function parameter of actor, critic	[-]	X_e, Y_e	=	East, north-ward location	[m]
δ	=	Temporal difference error	[-]	θ_r	=	Reference pitch	[rad]
E_t	=	Quadratic δ	[-]	θ_e	=	Pitch error	[rad]
η_a, η_c	=	Actor, critic learning rate	[-]	$\delta_a, \delta_e, \delta_r$	=	Aileron, elevator, rudder deflection angle	[rad]
τ	=	Target critic update fraction	[-]	δ_e'	=	Elevator deflection from trim	[rad]
F, G	=	Incremental state transition, input matrix	[-]	tr_a, tr_e, tr_r	=	Aileron, elevator, rudder trim tab angle	[rad]

*MSc. Student, Faculty of Aerospace Engineering, Control and Simulation Division, Delft University of Technology.

Θ	=	RLS parameter estimates	[-]	δ_f	=	Flaps deflection angle	[rad]
Σ	=	RLS parameter estimate covariance	[-]	T_1, T_2	=	Left, right engine thrust setting	[-]
X	=	RLS states	[-]	k	=	Learning rate factor	[-]
ρ	=	RLS forgetting factor	[-]	Sm	=	Action smoothness	[-]

I. Introduction

The civil aviation sector is undergoing many developments which will redefine what flight means, be it the advent of personal air vehicles, novel airliner designs, hydrogen fuelled concepts, or the increasing usage of drones [1–4]. Flight control on novel systems using model-based control system design methods will require extensive modelling and system identification campaigns, costing a vast amount of resources. An example is in the gain-scheduling approach to flight control system design [5]. As model-based controller synthesis techniques typically focus on flight control in nominal regions of the flight envelope, the occurrence of faults can result in control system failure by introducing new dynamics to the aircraft or venturing into unmodelled regions of the flight envelope, resulting in loss of control [6]. Fault tolerant and adaptive flight control is a trend in flight control design which directly addresses the issue of faults, with promising techniques being actively developed [7–9].

Simultaneously, Reinforcement Learning (RL) has been developing at a rapid pace, from agents trained that can surpass human performance on games [10, 11], to ones with the ability to control real life systems [12, 13]. RL is a method of Machine Learning that predicates on the machine actively learning through sovereign actions, as opposed to other ML methods such as supervised learning where the machine is told what to do or what is correct. Actor-Critic Design (ACD) is a sub-field of RL which approaches the problem of RL from an optimal control perspective [14], where an agent comprises of an actor, a critic, and a system model, the former two modelled using function approximators such as a neural network, and latter modelled as state derivatives. The actor and critic are updated through steps known as policy improvement and policy evaluation respectively. ACD algorithms are generally classified into three categories, all of which have identical architecture for the actor but not the critic: Heuristic Dynamic Programming (HDP), where the critic estimates the actor's value function; Dual Heuristic Programming (DHP), where the critic estimates the actor's value function gradient; and Global Dual Heuristic Programming (GDHP), whose critic estimates both simultaneously [15]. Incremental DHP (IDHP) is a successor to the DHP algorithm, which is extended with an online identified incremental model of the system dynamics to facilitate agent updates, resulting in a sample efficient RL algorithm [16]. Parallel to ACD, there also exist Deep RL (DRL) algorithms where deep neural networks are used to model the agent.

The intersection of these two developments has several promising potentials. The learning emulation that RL methods offer has the potential of making flight controllers truly intelligent, and offers an alternative reward-driven adaptive control method to methods such as Incremental Nonlinear Dynamic Inversion (INDI) or Incremental Back Stepping (IBS). Such a reward-driven adaptive control method can be directed to perform more than only performance tracking, which methods such as INDI and IBS are designed to do. In fact, RL controllers are an approach akin to the Linear Quadratic Regulator (LQR), to which ACD algorithms are closely related. Moreover, challenges in novel aircraft systems and fault tolerant control could be overcome with the successful application of RL based flight controllers, which can learn to fly an aircraft without any prior model. This model agnostic nature further implies the ability to use such controllers to fly systems which vary over time. Or more importantly, experience faults during operation, e.g. a bird strike event on an aircraft mid flight. ACD algorithms are especially suited for this role due to their high adaptiveness and high sample efficiency, allowing them to learn a stabilizing controller online during flight [16]. Success in the application of RL to flight control with faults introduced has been demonstrated in attitude control of the Innovative Control Effectors (ICE) model with a pure ADP controller [17] and an NDI hybrid ACD controller [18], as well as in attitude and velocity control of a business jet using a pure ACD controller [19].

ACD algorithms traditionally use information from one timestep per agent update. However, by using information from more time steps it is possible to speed up agent learning. This can be done in two ways, by using eligibility traces where past function parameter updates are recorded and subsequently reused [20], or by using observed rewards from multiple time steps resulting in multi-step policy evaluations or updates [21]. These ideas have been applied to the HDP and GDHP algorithms with success, improving their learning rate [20–22]. With improved learning rates, the speed at which controllers based on such algorithms recover from sudden system changes could be improved. Additionally, such techniques have yet to be applied to IDHP. Thus, multi-step and eligibility traces for ACD are interesting avenues to explore for fault tolerance controllers based on IDHP.

Therefore, this paper's main contribution is in the extension of IDHP using eligibility trace updates, resulting in IDHP(λ), using the multi-step policy evaluations or Temporal Difference (TD) error, resulting in MIDHP, and a combination of the two, resulting in MIDHP(λ). These algorithms are evaluated both during nominal flight and with faults introduced to give an insight into these augmentation's effects.

This paper is outlined as follows: in Sec. II the background on IDHP, the application of IDHP to flight control, and the idea of multi-step updates and eligibility traces are presented; in Sec. III the proposed methodology for incorporating multi-step updates and eligibility traces to IDHP and the flight control task devised for testing are presented. The main results are presented and discussed in Sec. IV, and finally the main conclusions are drawn in Sec. V.

II. Background

This section presents the background underlying the methodology of this paper. Beginning with introducing the sequential decision making framework used in all RL methods, then introducing IDHP and the sub-field of ACD in which it exists, and finally onto the eligibility trace and multi-step augmentations which exist in the TD learning framework.

A. MDP

Markov Decision Process (MDP) is the mathematical framework used in RL to model the sequential decision making process of some agent interacting with an environment. An MDP is described by the state space $\mathcal{S} \subset \mathbb{R}^n$, the action space $\mathcal{A} \subset \mathbb{R}^m$, a reward signal $r : \mathcal{S} \times \mathcal{A} \to \mathbb{R}$, and a state transition function $\mathcal{P}(s_{t+1}, r_{t+1}|s_t, a_t)$ which may deterministically or stochastically transition the state from s_t to s_{t+1} with reward r_{t+1} given an agent action a_t.

An MDP operates in discrete time. At each time step, an action is performed by the agent on the environment, which the agent responds to by producing the next time step's state and reward, which are both observed by the agent and influence subsequent agent decisions. This notion of sequential decision making has important ramifications. It implies that decisions made at an earlier time may influence what decisions should be made at a later time. In practice, this notion implies that taking suboptimal actions at an earlier time may lead to fewer rewards in the future. Building upon the MDP framework, it is possible to define a *Value function* $J(s)$, which describes the total future reward to be expected by the agent for starting in state s. The main goal of RL is to estimate such a function and use it to maximize reward in the corresponding MDP.

B. ACD and IDHP

RL agents seek to maximize the total expected reward in a given MDP, that is to not only obtain the maximum reward currently but also the maximum cumulative reward -the *return*- in the future. There are several methods of creating such an agent, including ACD algorithms, which this paper will focus on. Such algorithms are composed of three components; the actor, which observes the state of the MDP and chooses an action it thinks is most optimal; the critic, which observes the state of the MDP and outputs either the value function, value function's gradient, or a combination of the two, all capturing information regarding the expected rewards from the current state; and the model, which models the dynamics of the MDP states. Function approximators are used to approximate the true functions which underly each of these components, for example, the true value function. Common options for such approximators are linear functions such as polynomials, radial basis functions, and neural networks.

In traditional ACD, either an offline phase for learning the MDP dynamics or knowing the dynamics a-priori were the two main techniques for applying ACD algorithms [19, 23, 24], as opposed to purely online learning. For pure online learning, there is a need to remove the burden of knowing system dynamics a-priori, and to efficiently identify a usable dynamics model online. In answer to this need, an incremental model identified online using Recursive Least Squares (RLS) was proposed, resulting in IDHP [16]. Such a model came at the cost of only being able to model local dynamics as linear, as opposed to identifying nonlinear dynamics across the entire state space, which furthermore required high enough model update rates to overcome nonlinearities in system dynamics. However, this also has the added benefit of significantly reducing the complexity of model identification, allowing for computationally efficient model identification using a least squares approach.

The IDHP actor, also referred to as the policy, is a function denoted as $\pi : \mathcal{S} \rightarrow \mathcal{A}$. To act, the agent evaluates the policy $\pi()$ and obtains the appropriate a, which is then performed by the agent on the environment. Any function approximator with parameters W_a may be used to represent $\pi()$. To train the agent to maximize future expected reward, the parameters W_a are updated to maximize the return $R_t = r_t + \gamma J(s_t)$ which is an estimate of the total reward or return to be expected in the future, with $J()$ discounted by $\gamma \in [0, 1]$. In ACD, updating W_a to maximize R can then be done using gradient ascent with the following Equations:

$$W_{a,t} = W_{a,t-1} + \eta_a \frac{\partial R_{t-1}}{\partial W_a} \tag{1}$$

$$\frac{\partial R_t}{\partial W_a} = \left(\frac{\partial r_t}{\partial s_t} + \Lambda_t \right) \frac{\partial s_t}{\partial a_{t-1}} \frac{\partial a_{t-1}}{\partial W_a} \tag{2}$$

$$\Lambda_t = \frac{\partial J(s_t)}{\partial s_t} \tag{3}$$

Where η_a is the gradient descent step size, also referred to as the actor's learning rate.

The IDHP critic is a value gradient function denoted as $\Lambda : \mathcal{S} \rightarrow \mathbb{R}^n$, it outputs the gradient of the value function with respect to the MDP states s as expressed in Eq. 3. This value gradient function is internal to the agent and serves only to aid in improving the actor's actions. Similar to the actor, any function approximator with parameters W_c may be used to represent Λ. To stabilize learning, a target critic denoted as Λ' is maintained, though IDHP can function without it. This target critic is identical to the critic except for the function parameters used, which are updated with a slow moving average filter towards the latest critic weights [25], see Eq. 7. The objective of the critic is to accurately estimate the value function's gradient. This is done by updating the critic's parameters to minimize a quadratic E_t of the TD error δ_t, where $E_t = \frac{1}{2}\delta_t \cdot \delta_t$ with $\cdot$ being the dot product, and δ_t defined as follows:

$$\delta_t = \Lambda_{t-1} - \frac{\partial r_{t-1}}{\partial s_{t-1}} - \gamma \Lambda'_t \frac{\partial s_t}{\partial s_{t-1}} \tag{4}$$

Note that the target critic output is used in constructing δ_t, which serves the purpose of smoothing the variation of δ_t over time, as the target critic is updated slowly. In ACD, W_c is updated to minimize E through gradient descent using Eq. 5.

$$W_{c,t} = W_{c,t-1} - \eta_c \frac{\partial E_{t-1}}{\partial W_c} \tag{5}$$

$$\begin{aligned} \frac{\partial E_t}{\partial W_c} &= \frac{\partial E_t}{\partial \delta_t} \frac{\partial \delta_t}{\partial \Lambda_{t-1}} \frac{\partial \Lambda_{t-1}}{\partial W_c} \\ &= \delta_t \frac{\partial \Lambda_{t-1}}{\partial W_c} \end{aligned} \tag{6}$$

$$W_{c',t+1} = \tau W_{c,t} + (1 - \tau) W_{c',t} \tag{7}$$

The system model of IDHP is then used to identify the $\frac{\partial s_{t+1}}{\partial a_t}$ term from Eq. 2 and the $\frac{\partial s_t}{\partial s_{t-1}}$ term from Eq. 4. This model is also internal to the agent, it is used to improve the actions of the actor and to improve the value estimation of the critic. Treating the system in discrete time, an incremental discrete model of the states can be written as $\Delta s_{t+1} = F_t \Delta s_t + G_t \Delta a_t$. This results in the following definition for the two partial derivatives

$$\frac{\partial s_{t+1}}{\partial a_t} \approx G_t$$

$$\frac{\partial s_{t+1}}{\partial s_t} \approx F_t + G_t \frac{\partial a_t}{\partial s_t} \tag{8}$$

Using RLS, a linear model can be constructed by first defining the state increment $\delta s_{t+1} = s_{t+1} - s_t$ and action increment $\delta a_{t+1} = a_{t+1} - a_t$, then defining the linear model parameter matrix $\Theta_t = \begin{bmatrix} F_t & G_t \end{bmatrix}^\top \in \mathbb{R}^{(n+m)\times n}$ and variable vector $X_t = \begin{bmatrix} \delta s_{t+1} & \delta a_{t+1} \end{bmatrix} \in \mathbb{R}^{n+m}$. With the RLS algorithm, Θ_t can then be identified online according to Alg. 1.

Combining the actor, critic, and RLS model, the IDHP algorithm can then be summarized in the diagram presented in Fig 1.

Algorithm 1 exponentially weighted RLS algorithm.

1: **Initialize**. Parameter covariance $\Sigma_0 \in \mathbb{R}^{(n+m)\times(n+m)}$, parameter $\Theta_0 \in \mathbb{R}^{(n+m)\times n}$.

2: **Online Model Identification**. For each time step, $t = 1, 2, \cdots$, compute:

$$\begin{aligned}
\delta s_t &= s_t - s_{t-1} \\
\delta a_t &= a_t - a_{t-1} \\
X_t &= \begin{bmatrix} \delta s_t & \delta a_t \end{bmatrix}^\top \\
\kappa_t &= \frac{\Sigma_{t-1} X_t}{\rho + X_t^\top \Sigma_{t-1} X_t} \\
\epsilon_t &= \delta x_t - X_t^\top \Theta_{t-1} \\
\Theta_t &= \Theta_t + \kappa_t \epsilon_t \\
\Sigma_t &= \frac{1}{\rho}(\Sigma_{t-1} - \kappa_t X_t^\top \Sigma_{t-1})
\end{aligned}$$

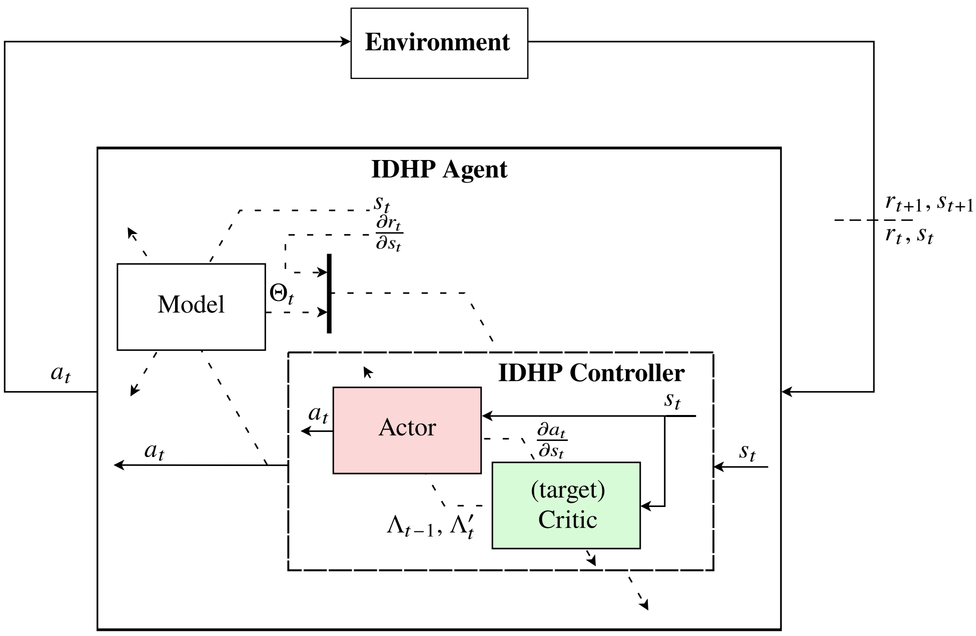

Fig. 1 MDP flow diagram representing the signal flows internal to the IDHP agent, dashed signals represent variables used to update the blocks which they cross.

C. Multi-step Updates and Eligibility Traces

The TD error computes the error between the value which the critic estimated and the value which is observed, this observed value is referred to as the TD target. In the case of Eq. 4, the TD target is composed of the terms $\frac{\partial r_{t-1}}{\partial s_{t-1}} + \gamma \Lambda_t' \frac{\partial s_t}{\partial s_{t-1}}$. It can be seen that the TD target is composed of an observed reward signal and an estimate made by the target critic. The idea of multi-step TD error is to use more observed reward signals to construct a more accurate TD target [26, 27].

For the IDHP's TD error, a multi-step version is expressed as follows:

$$\delta_{n,t} = \Lambda_{t-n} - \frac{\partial(\gamma^n J_t' + \sum_{m=0}^{n-1} \gamma^m r_{t-n+m})}{\partial s_{t-n}} \tag{9}$$

Instead of using the reward at one single time step to compute the TD error, it is possible to extend the error to include rewards from multiple time steps. This results in a new gradient descent term for the critic parameters update equation:

$$\frac{\partial E_t}{\partial W_c} = \delta_t \frac{\partial \Lambda_{t-n}}{\partial W_c} \tag{10}$$

An alternative and more general method for incorporating additional information to agent updates is the eligibility trace **E**, which keeps track of how eligible each function parameter is in each update step. This is done by storing previous function gradients and reusing them in the future at decaying magnitudes [28]. The function gradient in question is the derivative of the function output with respect to each function parameter, for the actor's case **E** would accumulate the $\frac{\partial a_t}{\partial W_a}$ term from Eq. 2, and for in the critic's case **E** would accumulate $\frac{\partial \Lambda_t}{\partial W_c}$ from Eq. 6. In implementation, the eligibility trace results in a similar algorithm as momentum gradient descent, which accumulates past function updates and also reuses them in the future at decaying magnitude. The difference between these two methods is in the variable being accumulated. Whereas momentum gradient descent accumulates the total parameter update, eligibility traces only accumulate the function's gradient.

To incorporate eligibility traces, the parameter update equations are changed to the form shown in the following equations:

$$W_t = W_{t-1} + \eta \frac{\partial M}{\partial O} \mathbf{E}_{t-1} \tag{11}$$

$$\mathbf{E}_t = \lambda\gamma \mathbf{E}_{t-1} + \nabla W_{t-1}, \quad \mathbf{E}_0 = \mathbf{0} \tag{12}$$

Where ∇W is the gradient of the network output with respect to network weights, $\frac{\partial M}{\partial O}$ is the gradient of the relevant metric, M, with respect to network output, O. For the critic, this partial derivative would be δ_t and for the actor this would be $\left(\frac{\partial r_t}{\partial s_{t+1}} + \Lambda_{t+1}\right)$; $\lambda \in [0, 1)$ is the trace decay rate which controls how quickly do prior gradients decay in the eligibility trace, $\lambda = 0$ decays previous gradients completely and results in the original update rules, while $\lambda \to 1$ means previous gradients decay according to γ.

A multi-step policy evaluation has been successfully augmented to the HDP algorithm [21] which yielded increased sample efficiency, an improvement further refined by an adaptive multi-step scheme [22]. An eligibility trace style update has also been applied successfully to ACD algorithms on several works [20, 29], such an augmentation similarly improved the agent's sample efficiency.

III. Methodology

Taking the idea of multi-step updates and eligibility traces from TD learning, it becomes possible to refine the method of updating the actor and the critic in the ACD algorithms. The methods for incorporating such ideas into the IDHP algorithm, and how the augmentations are to be evaluated, are outlined in the methodology presented in this section.

A. IDHP Augmentations

Multi-step updates and eligibility traces can be incorporated individually or together in the IDHP algorithm, with multi-step TD applied to the critic and eligibility traces applied to either the critic or the actor. However, from preliminary empirical testing, the option of applying eligibility traces to the critic was shown to negatively impact the learning performance of IDHP. Thus the three options present are to: apply multi-step updates to the critic, apply eligibility traces to the actor, or the two options combined.

For the critic, which is only augmented with the multi-step TD error, the gradient descent term of Eq. 6 used for updating the critic is reworked to include a multi-step TD error. While each algorithm or MDP being solved typically has a certain n which is optimal, the present paper only considers a 2-step TD for the sake of simplicity, which can be obtained by substituting $n = 2$ to Eq. 9, which yields $\delta_{2,t}$ expressed in Eq. 13. To incorporate the 2 step TD error into the critic update is to simply substitute δ_t with $\delta_{2,t}$ in Eq. 6.

$$
\begin{aligned}
\delta_{2,t} &= \Lambda_{t-2} - \frac{\partial(\gamma^2 J_t' + \sum_{m=0}^{1}\gamma^m r_{t-2+m})}{\partial s_{t-2}} \\
&= \Lambda_{t-2} - \frac{\partial(\gamma^2 V_t' + r_{t-2} + \gamma r_{t-1})}{\partial s_{t-2}} \\
&= \Lambda_{t-2} - \gamma^2 \Lambda_t' \left.\frac{\partial s_t}{\partial s_{t-1}}\right|_t \left.\frac{\partial s_{t-1}}{\partial s_{t-2}}\right|_{t-1} - \frac{\partial r_{t-2}}{\partial s_{t-2}} - \gamma \frac{\partial r_{t-1}}{\partial s_{t-1}} \left.\frac{\partial s_{t-1}}{\partial s_{t-2}}\right|_{t-1}
\end{aligned} \tag{13}
$$

Regarding the actor, the primary augmentation is in incorporating eligibility traces. To do so, the gradient descent term $\frac{\partial a_{t-1}}{\partial W_a}$ of Eq. 2 is replaced by $\mathbf{E}$, which is updated according to Eq. 14. A secondary augmentation is to add a Conditioning for Action Policy Smoothness (CAPS) parameter to mitigate the noisy actions commonly observed in RL agents [30]. This is done by adding L_{CAPS}, as defined in Eq. 15, to R_t. This term penalizes large variations in the actor policy and large temporal changes in the actor's actions, the weights of these penalties can be adjusted through the factors λ_S and λ_T respectively. Combining these two augmentations results in a new expression shown in Eq. 16 for the gradient descent term $\frac{\partial R_t}{\partial W_a}$ used in Eq. 1.

$$
\mathbf{E}_t = \lambda\gamma\mathbf{E}_{t-1} + \frac{\partial a_t}{\partial W_a} \tag{14}
$$

$$
L_{CAPS} = \lambda_T \|\pi(s_t) - \pi(\tilde{s})\|_2 + \lambda_S \|\pi(s_t) - \pi(s_{t-1})\|_2 \,, \quad \tilde{s} \sim \mathcal{N}(s_t, diag(\sigma)) \,, \quad \sigma \in \mathcal{R}^n \tag{15}
$$

$$
\frac{\partial R_t}{\partial W_a} = \left(\left[\frac{\partial r_t}{\partial s_t} + \Lambda_t \right] G_{t-1} - L_{CAPS} \right) \mathbf{E}_t \tag{16}
$$

Ultimately, this results in 3 augmented IDHP algorithms in addition to the baseline IDHP algorithm. The first augmented algorithm is IDHP(λ), which has the actor augmented with an eligibility trace update; the second is MIDHP, which has the critic augmented with a multi-step update; the third is MIDHP(λ), which has both the two augmentations simultaneously.

B. Aircraft Pitch Control as an MDP

The four algorithms are evaluated in their ability to control the pitching motion of an aircraft in a flight control task. This is done in simulation using CitAST, a high fidelity nonlinear 6 degrees of freedom dynamics model of a fixed-wing business jet running at 100 Hz or $dt = 0.01$ s is used [31]. The aircraft is modelled with engine and control surface dynamics, such as inertia in deflecting the control surfaces. Airspeed control is delegated to an auto-throttle controlling engine thrust settings. The aircraft model has been validated by flight test data onboard a Cessna Citation II research aircraft [32]. During the experiments conducted in this paper, the aircraft model's state and inputs are trimmed for an airspeed of 90 m/s at an altitude of 2000 m.

The pitch control task needs to first be framed in terms of an MDP before the IDHP algorithm is applied as a flight controller. The control scheme which the MDP will emulate is a simple feedback control scheme, which can be represented in the form of Figure 2.

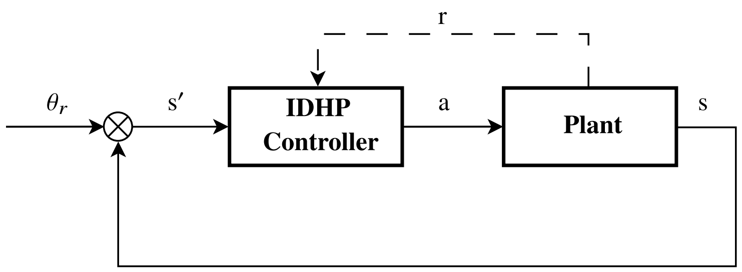

Fig. 2 Control diagram of the pitch control MDP.

The dynamics model of the aircraft already fulfils the role of the state transition function $\mathcal{P}(s_{t+1}, r_{t+1}|s_t, a_t)$, this model is the plant used in Fig 2. Thus, the only remaining variables to fully define the MDP are s, a, and r. In addition to these variables, $\frac{\partial r}{\partial s}$ also needs to be defined for the IDHP algorithm,

The aircraft model used has a state vector x as shown in Eq. 17, using the inertial and body frames as shown in Fig 3. To create s, only a subset of x states will be used, causing the resultant MDP to be only partially observable (POMDP). Specifically, s is made to include only a select number of longitudinal aircraft states, as shown in Eq. 18. In addition, to make the control task more explicit to the agent, the actor and critic functions are provided with the pitching error $\theta_e = \theta - \theta_r$. This addition requires a slight abuse of notation where the actor and critic inputs will be the augmented MDP state s' shown in Eq. 19, instead of only s.

$$x = \begin{bmatrix} p & q & r & V & \alpha & \beta & \theta & \phi & \psi & H & X_e & Y_e \end{bmatrix}^\top \tag{17}$$

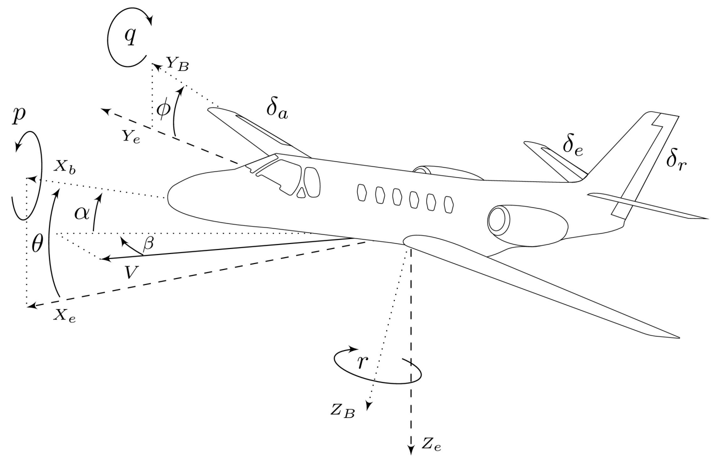

Fig. 3 Reference frames used for the definition of the various states of the Cessna-Citation II model, adopted from Seres [33].

$$s = \begin{bmatrix} \alpha & \theta & q \end{bmatrix}^\top \qquad s' = \begin{bmatrix} \alpha & \theta & q & \theta_e \end{bmatrix}^\top \tag{18, 19}$$

The full set of actuators modelled u is shown in Eq. 20. Just like for s, not all of the modelled variables will be used in creating a. The agents in this control task will only be in control over the elevator, specifically the elevator deflection from the trim angle δ_e', see Eq. 21. In addition, a symmetric deflection limit close to the realistic saturation limits of the PH-LAB is set on the elevator δ_e.

$$u = \begin{bmatrix} \delta_e & \delta_a & \delta_r & \text{tr}_e & \text{tr}_a & \text{tr}_r & \delta_f & \text{gear} & T_1 & T_2 \end{bmatrix}^\top \tag{20}$$

$$a = \begin{bmatrix} \delta_e' \end{bmatrix} , \quad -15\frac{\pi}{180} < \delta_e' < 15\frac{\pi}{180} \text{ [rad]} \tag{21}$$

The reward r is defined as the negative square of the pitch tracking error, as shown in Eq. 22, and it's derivative $\frac{\partial r}{\partial s}$ shown in the following:

$$r = -(\theta - \theta_r)^2 \qquad \frac{\partial r}{\partial s} = \begin{bmatrix} 0 & -2(\theta - \theta_r) & 0 \end{bmatrix} \tag{22, 23}$$

At initialization, the dynamics model states and inputs are set equal to the trim values, according to the values as follows:

$$x_0 = \begin{bmatrix} 0 & 0 & 0 & 90 \text{ m/s} & 0.0576 \text{ rad} & 0 & 0 & 0.0576 \text{ rad} & 0 & 2000 \text{ m} & 0 & 0 \end{bmatrix}^\top \tag{24}$$

$$u_0 = \begin{bmatrix} -0.02855 \text{ rad} & 0 & 0 & 0 & 0 & 0 & 0 & 0 & 55\ \% & 55\ \% \end{bmatrix}^\top \tag{25}$$

C. IDHP Algorithm Configuration

The constants and variables which need to be initialized for the IDHP algorithm, including the dynamic model state and inputs of the MDP, are tabulated in Tab. 1. The version of IDHP implemented uses varying learning rates and eligibility trace decay rates, starting at higher values to aid network weights convergence, and then decreasing to a lower value after 4 s. These high and low values are denoted by an h and l in the subscript respectively: $\eta_{\cdot,h}$, $\eta_{\cdot,l}$, λ_h, and λ_l. Starting from 4 s, the rates are smoothly transitioned from higher to lower values through multiplication with the factor k_t defined at every t as follows:

$$k_t = c + (1 - c)\frac{v_l}{v_t} , \quad c = 0.998 \tag{26}$$

Where v_t is the rate's value at t, and v_l is the lower value of the rate. The constant c changes how rapidly the rate drops, and is set to be 0.998 for the present study. Multiplying v_t by the factor k_t brings v_t asymptotically towards v_l, that is to say $\lim_{t\to\infty} v_h \prod_{i=0}^{t} k_i = v_l$.

Table 1 IDHP initialization variables and hyperparameters, η_a, η_c, and λ values are shown in Tab 2.

Hyperparameters		Variable initialization			
Actor learning rates:	$\eta_{a,h}$,$\eta_{a,l}$	Eligibility trace:	$\mathbf{E}_0$	=	$\mathbf{0}$
Critic learning rates:	$\eta_{c,h}$,$\eta_{c,l}$	RLS model parameter:	Θ_0	=	$\mathbf{0}$
Eligibility trace decay rates:	λ_h,λ_l	RLS model covariance:	Σ_0	=	$10^6 \cdot \mathbb{I}$
MDP reward discount factor:	$\gamma = 0.6$	Actor-network weights:	$W_{a,0}$	~	$\mathcal{N}(\mathbf{0}, 0.1^2\mathbb{I})$
RLS forgetting factor:	$\rho = 1$	Critic-network weights:	$W_{c,0}$	~	$\mathcal{N}(\mathbf{0}, 0.1^2\mathbb{I})$
Target critic mixing factor:	$\tau = 0.02$	Trim states:	x_0	=	Eq 24
CAPS weights:	$\lambda_T, \lambda_S = 0.012, 0.001$	Trim inputs:	u_0	=	Eq 25

For the function approximators of the actor and the critic, a single hidden layer neural network with 10 nodes in the hidden layer is used. This network size is a compromise struck between learning complexity and agent performance, as it was observed that this size is just before agent performance degrades, but not too big that the number of parameters to be optimized slows down learning. In both networks, there are no biases in any of the layers, the input layer takes s' and has four nodes, and the hidden layer uses a tanh activation function. The output layer of the two networks are different. For the actor, its output is elevator deflection from trim δ_e' and so only a single node in the output layer is required, a tanh activation function is also used in this layer with the upper and lower asymptotes being $15\pi/180$, the limits stated in Eq. 21. For the critic, its output layer estimates value function gradients over s and thus has 3 nodes, a simple linear activation function is used.

The IDHP algorithm is created by combining the three modules and defining the flow of variables from one module to another. This is depicted graphically in Figure 1, in addition to the r and s signals shown, the inputs of the IDHP agent are augmented by θ_r to allow for the construction of s', while the output is a. IDHP uses the inputs for two categories of computation, the first of which is to compute the control action, which is done simply by the actor, and the second category is to compute all the necessary internal updates, done by the critic and the RLS model. The order of update computations is clarified further in Alg. 2.

Algorithm 2 IDHP algorithm.

1: **Initialize**:
Set initial variable values and hyperparameters listed in Tab. 1.
2: **Online loop**:
For $t = 0$ **to** T/dt **do**

$a_t \leftarrow \pi(s_t'; W_{a,t})$ ▹ sample action from policy

$u_t = u_0 + a_t$ ▹ add commanded action to trim input

$s_{t+1}, r_{t+1}, \theta_{r,t+1} \leftarrow \text{Environment}(u_t)$ ▹ perform action to propagate dynamics

$\eta_{a,t}, \eta_{c,t}, \lambda_t \leftarrow \begin{cases} \eta_{\cdot,h}, \lambda_h & \text{if} \quad t < 4s \\ \eta_{\cdot,t-1} k_t, \lambda_{t-1} k_t & \text{otherwise} \end{cases}$ ▹ $k_t \leftarrow$ Eq. 26

If using multi-step IDHP **and** $t > 2$ **then**

$\delta_t = \Lambda(s_{t-2}') - \frac{\partial r_{t-2}}{\partial s_{t-2}} - \gamma \frac{\partial r_{t-1}}{\partial s_{t-1}} \frac{\partial s_{t-1}}{\partial s_{t-2}}\Big|_{t-1} - \gamma^2 \Lambda'(s_t') \frac{\partial s_t}{\partial s_{t-1}}\Big|_t \frac{\partial s_{t-1}}{\partial s_{t-2}}\Big|_{t-1}$ ▹ Eq. 13, $\frac{\partial s_t}{\partial s_{t-1}} \leftarrow$ Eq. 8

Else

$\delta_t = \Lambda(s_{t-1}') - \frac{\partial r_{t-1}}{\partial s_{t-1}} - \gamma \Lambda'(s_t') \frac{\partial s_t}{\partial s_{t-1}}\Big|_t$ ▹ Eq. 4, $\frac{\partial s_t}{\partial s_{t-1}} \leftarrow$ Eq. 8

End If

$\frac{\partial E_t}{\partial W_c} = \delta_t \frac{\partial \Lambda_t}{\partial W_c}$ ▹ Eq. 6

$W_{c,t+1} = W_{c,t} - \eta_{c,t} \frac{\partial E_t}{\partial W_c}$ ▹ Eq. 5

$W_{c',t+1} = \tau W_{c,t} + (1 - \tau) W_{c',t}$

$\mathbf{E}_{t+1} = \lambda_t \gamma \mathbf{E}_t + \frac{\partial \pi(s_t')}{\partial W_a}$ ▹ Eq. 14, $\lambda = 0$ if not using eligibility traces

$\frac{\partial R_t}{\partial W_a} = \left(\left[\frac{\partial r_t}{\partial s_t} + \Lambda(s_t) \right] G_{t-1} - L_{CAPS} \right) \mathbf{E}_t$ ▹ Eq. 16

$W_{a,t+1} = W_{a,t} + \eta_{a,t} \frac{\partial R_t}{\partial W_a}$ ▹ Eq. 1

$F_{t+1}, G_{t+1} \leftarrow$Algorithm 1

Implementation of the ∇W term in Eq. 12 differs based on the actor and critic function form used. In the case of the present IDHP, where eligibility traces are used only on the actor, whose function is a neural network, ∇W represents the derivative of the actor network with respect to its weights. Such a derivative is called the Jacobian matrix of the actor network, where the rows are the outputs of the network, and columns are the derivatives of the outputs with respect to each weight. For the actor, the Jacobian matrix is a 1 by 40 matrix, since in total the actor network has 1 output and $3 \cdot 10 + 10 \cdot 1$ weights, therefore $\nabla W = \frac{\partial \pi(s)}{\partial W_a} \in \mathcal{R}^{1\times 40}$.

Since the augmented IDHP algorithms are either algorithmically different from the baseline, have new hyperparameters, or both, each algorithm's hyperparameters are tuned individually through trial and error to maximize that algorithm's performance. This leads to each algorithm having its own set of learning and decay rates, which are reported in Tab. 2.

Table 2 Hyperparameters used for each of the four algorithms.

		IDHP	IDHP(λ)	MIDHP	MIDHP(λ)
$\eta_{a,h}, \eta_{a,l}$	:	$40, 10$	$25, 7.5$	$43, 6.5$	$30, 5.0$
$\eta_{c,h}, \eta_{c,l}$	:	$0.5, 0.25$	$0.5, 0.25$	$0.9, 0.05$	$0.7, 0.1$
λ_h, λ_l	:	N/A	$0.99, 0.8$	N/A	$0.99, 0.4$

D. Experiment Setup

A simple flight manoeuvre is designed to evaluate the performance of the various algorithms. During the flight manoeuvre, several sudden faults will be introduced to the aircraft to evaluate the fault tolerance behaviour of the agents.

The overall flight lasts 90 s, the first 55 s of flight is referred to as the *warmup* phase, while the remainder is referred to as the *manoeuvring* phase. As the agent is initialized randomly, the warmup phase is used to introduce the agent to the environment. This phase allows the agent's actor, critic, and model to explore their respective parameter space, and arrive at a local optimal. The manoeuvring phase is where the flight manoeuvre is performed to evaluate the controller's tracking performance, where a simple pitch-up pitch-down manoeuvre is done. Throughout the 90 s flight, the agents are to control the aircraft to follow a reference pitch signal θ_r which takes different shapes during the separate phases of flight. The warmup phase is designed to expose the agent to the aircraft dynamics, thus the reference signal is designed similarly to system identification manoeuvres, and the resemblance to typical aircraft manoeuvres is forgone. During the manoeuvring phase, a θ_r resembling what may be encountered during nominal aircraft operations is designed.

Thus, signal θ_r takes a sinusoidal form during warmup, a trapezoidal form during the pitch-up pitch-down manoeuvre, and remains equal to the θ_{trim} for all other times, this is described by Eq. 27. For convenience, the first 55 s of flight is referred to as the *warm up* phase, while the remainder is referred to as the *manoeuvring* phase.

$$\theta_{r,t} = \theta_{trim} + \frac{\pi}{180} \cdot \begin{cases} (10\sin(\frac{2\pi t}{15}) + 8\sin(\frac{2\pi t}{30}))(1 - \frac{t}{75}) & t < 45 \\ 1.5(t-55) & 55 \leq t < 65 \\ 15 & 65 \leq t < 75 \\ -1.5(t-85) & 75 \leq t < 85 \\ 0 & \text{otherwise} \end{cases} \quad \text{[rad]} \tag{27}$$

Three fault cases are designed based on this 90 flight manoeuvre. The four algorithms will perform 100 flights over the same 100 different random number generator seeds on each fault case. Since the only stochasticity in the experiment is the initial actor and critic network weights, that will be the only difference between each run. Ultimately, the 100 runs will provide a more accurate view of each algorithm than simply running the algorithms once. The cases all introduce the corresponding faults around the beginning of the manoeuvring phase, at the 60 s mark of the flight. The first fault is a shift in the Centre of Gravity (CG) of the aircraft, where the longitudinal location of the CG is shifted forward by 0.5 m. The second fault is to be a damaged elevator which is modelled by multiplying the δ_e by 0.3, modelling how a damaged elevator reduces its control effectiveness. The third fault is a combined damaged elevator and reduced elevator deflection limits, where δ_e is multiplied by 0.3 and the maximum and minimum δ_e are set to be $\pm 5\frac{\pi}{180}$ rad.

The full time trace of the reference signal is shown in Figure 4. During each run which concerns a flight with faults introduced, it will be introduced at 60 s, the time indicated by the red cross.

Five tests are compiled for the final evaluation and comparison of the algorithms, an overview of the tests are tabulated in Tab. 3. Test one studies the four algorithms during the warmup phase of the flight, while tests two, three, and four study how the four algorithms handle the nominal and faulty aircraft during the manoeuvering phase.

All five tests will use the same two metrics for algorithm evaluation, the first metric is the Root Squared Error (RSE) in θ_e, measuring the tracking accuracy of the controller and defined in Eq. 28. The second metric is a smoothness metric Sm, which measures controller action smoothness. It's definition is taken from [30] and presented in the following:

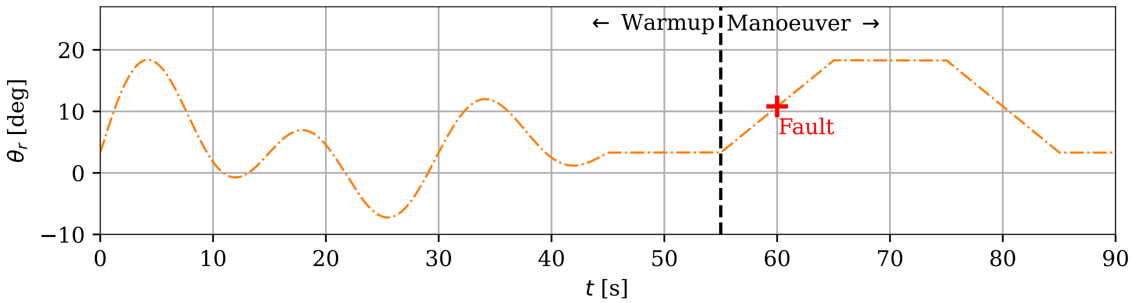

Fig. 4 Reference pitch signal θ_r, vertical black line at 55 s demarcates the end of the *warmup* phase and the start of the *manoeuvering* phase, red cross at 60 marks introduction of fault if any.

$$\text{RSE} = \sum_{t=0}^{T/dt} \sqrt{\theta_{e,t}^2} \qquad Sm = \frac{2}{n f_s} \sum_{i=1}^{n} M_i f_i \tag{28, 29}$$

Where M_i is the amplitude of the i-th frequency component f_i where $i \in [1, n]$, with n the number of frequency components sampled, and $f_s = 100$ being the sampling frequency in the time domain. Calculating Sm is done by first taking the Fourier transform of δ_e from the concerned flight phase, and then using the obtained spectrum in Eq. 29.

Table 3 The five tests used in evaluating the proposed augmentations on IDHP.

		Test 1	Test 2	Test 3	Test 4	Test 5
Phase	:	Warmup (0 to 55 s)	Manoeuvering (55 to 90 s)	Manoeuvering (55 to 90 s)	Manoeuvering (55 to 90 s)	Manoeuvering (55 to 90 s)
Faults	:	N/A	None	Shifted CG	Damaged Elevator	Damaged and saturated elevator
Metrics	:	RSE, Sm				

With the first test, the question of how the proposed augmentations affect the ability of IDHP to learn from tabular rasa may be answered. As the first test is concerned only with the performance of the controllers when learning from a randomly initialized state. The second to fifth tests will tell of the fault tolerance behaviours of the four controllers as well as how they may perform in flight once trained.

E. Statistical Interpretation of Results

The five tests in Tab. 3 will generate samples of metrics for the four algorithms. To systematically decide which algorithm's metrics were better than another, two statistical measures must be used to interpret these results: one measure for quantifying the *statistical significance* of any difference, and another measure to quantify the *substantive significance* of such observed differences [34]. The first measure is the t-statistic from Student's t-test, which can be used to decide whether the mean of two samples' underlying distribution is different from another [35], under the critical assumption that the samples are normally distributed. The second measure is the A-value from Vargha and Delaney's (VD) A-test, this value can be used to rank the underlying distribution of two samples [36]. The A-value is bounded to the interval $[0, 1]$ and measures the relative difference of two samples, $A = 0.5$ means that there are no relative differences in the samples, < 0.5 means that the the first sample is smaller than the second, and vice versa for > 0.5.

While the A-value could be used to quantify the absolute difference between samples, the present paper will only use this measure for ranking different samples. As an example, this ranking can be done if two A-tests are taken where one sample is used in both tests, allowing for an ordinal ranking of the three samples involved in the two tests.

These statistics will be taken between the clean samples of IDHP and the augmented algorithms, that is to say, the gathered metrics are cleaned of outliers before taking any statistical tests. In such a manner, the following questions can be answered 1) whether an augmented algorithm's metrics are significantly different from IDHP's metrics, by reading the comparison's t-statistic, with a p-value of 0.05 being used to decide for statistical significance; and 2) by what magnitude this augmented algorithm's metrics are different from IDHP's metrics, through reading the A-value. Since all A-values are taken between IDHP and the augmented algorithm metrics, it would be possible to ordinally rank the metrics of the four algorithms for each test in Tab. 3. Summarily, the proposed augmentations' effects on the flight controllers may be concluded.

IV. Results and Discussion

The three proposed algorithms of IDHP(λ), MIDHP, and MIDHP(λ) along with the baseline algorithm IDHP are evaluated through the experiments designed in the Methodology Sec. III.D. The results gathered from these Monte Carlo experiments are presented and discussed in this section.

Before diving into the metrics of the five tests, the flight performance of the controller created by the IDHP algorithm with no augmentations and no faults introduced is presented in Figure 5, to provide some frame of reference for the metrics shown hereafter. Figure 5 shows the flight of all 100 runs in translucent blue lines, with the aircraft pitch in the upper subplot and elevator deflection commanded by the IDHP controller in the lower subplot.

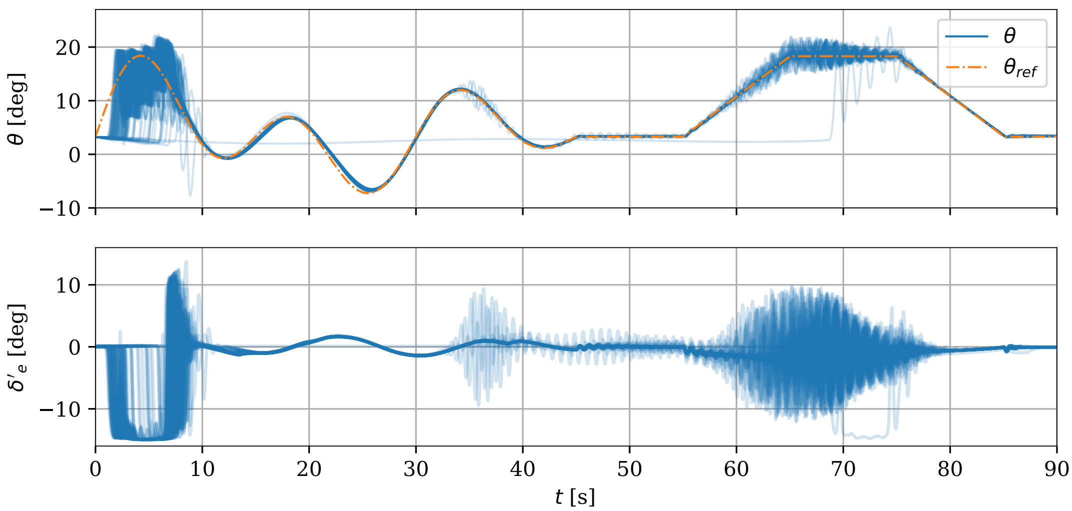

Fig. 5 Time trace of all 100 IDHP controller flights with no faults introduced to the aircraft.

Figure 5 shows how the IDHP agent starts out not knowing how to control the aircraft, but over the first 10 s comes to learn a stable controller which is able to follow the reference signal. The behaviour of this controller can be seen to stabilize over the remainder of the warmup phase, indicating that the actor-network weights have stabilized. Having warmed up the controller allowing it to learn a usable actor network, the aircraft is then commanded to trim for a short time before commencing the pitch-up pitch-down manoeuvre.

These samples of controllers can be seen to track the reference signal with good accuracy in portions of the flight. However, during the initial 10 s of the warmup and the maximum pitch-up segment of the manoeuvre, the controllers command a very oscillatory or noisy action. This occurs despite the CAPS parameter being incorporated into IDHP. Additionally, there are about 3 runs which exhibit oscillatory actions towards the end of the warmup phase around 35 s, which is symptomatic of a high gain controller. This issue becomes more stark during the manoeuvering phase, where at the high-pitch segment, many of the controllers become marginally stable, exhibiting highly oscillatory actions. Lastly, there is also one controller which did not manage to learn a stable controller during the warmup phase.

Taking a step back, the performances of the four algorithms over the five tests are presented in the following subsections using RSE and Sm metrics from the Monte Carlo experiments. These results are used to compare the augmented algorithms against the baseline IDHP.

A. Warmup Segment

The four algorithms' RSE and Sm metrics in Test 1, the test evaluating an algorithm's warmup performance, are shown in Figure 6. The statistical test results on the outlier-free or cleaned metric samples are summarized and presented in Tab. 4. From the figure, it appears that the tracking error and smoothness of all controllers are comparable, with the Inter-Quartile Range (IQR) being at similar values of around 5-6 $\times 10^3$ deg for RSE and 0.7-0.9 $\times 10^5$ for Sm.

The statistical testing results of Tab. 4 also tell a similar story. When it comes to RSE, there is no statistically significant difference between the four algorithms' controllers. However, a slightly smaller A-value is reported in all the comparisons between the augmented algorithms and the baseline IDHP, signifying a marginal yet statistically insignificant improvement in tracking performance by the augmentations during the warmup phase.

The Sm metric statistical tests show that there are statistically significant differences between the smoothness of the augmented algorithms of IDHP(λ), and MIDHP(λ), versus the baseline IDHP. Specifically, both these two augmented algorithms demonstrated a less smooth control action during warmup, signified by $A > 0.5$ which means the Sm of these augmented algorithms were higher than IDHP. For the MIDHP Sm, however, while the actions are less smooth than those of IDHP according to the A-value, this finding was not statistically significant.

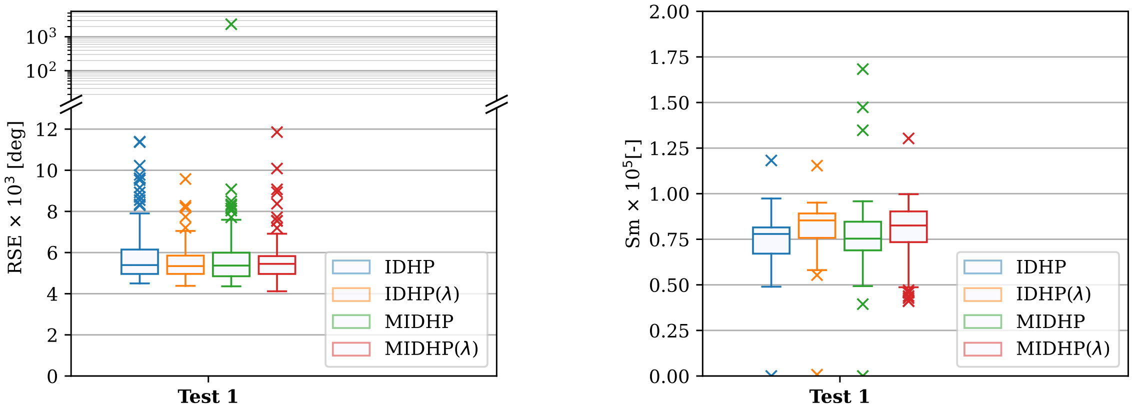

(a) RSE. (b) Sm.

Fig. 6 Test 1 RSE & Sm result boxplots.

Table 4 VD's A-values on the RSE & Sm results on the first test, red A-value indicates statistically insignificant result according to Student's t-test (p-value > 0.05), A-value < 0.5 indicate the augmented algorithm's metrics are smaller than IDHP's and vice versa.

		Test 1	
		RSE	*Sm*
IDHP(λ) vs IDHP	:	0.478	0.756
MIDHP vs IDHP	:	0.475	0.540
MIDHP(λ) vs IDHP	:	0.471	0.653

B. Manoeuvering Segment

In tests 2 to 5, the control performance of the four algorithms on the nominal aircraft and one which has some fault introduced, is evaluated. Figure 7 presents the boxplots that capture the distribution of RSE and Sm metrics, while

Tab. 5 tabulates the corresponding statistical test results on the cleaned samples. The distribution of metrics in the manoeuvring phase was more diverse than in the warmup phase, according to Figure 7. It is interesting to note that for all algorithms the introduction of faults seems to have a smoothening effect on the control action, this can be seen in Sub-figure 7b. It is as if the change in dynamics pressured or allowed the agents to learn a smoother policy.

Generally, the Multi-step augmented algorithms have improved tracking performance and much-improved action smoothness. However, this is not consistently observed, as the MIDHP algorithm had a dramatically larger spread of RSE and Sm during test 1: where no fault is introduced. From Figure 7, it is seen that the MIDHP(λ) controller has the lowest median and general RSE in all four tests, where 75 % of the runs had lower RSE than approximately 75 % of the runs from IDHP for three out of the four tests. For example, the RSE lower quartile for IDHP on test 4 was roughly 0.8×10^3 deg, while the RSE upper quartile for MIDHP(λ) was roughly 0.7×10^3 deg. The smallest improvement in RSE by MIDHP(λ) was found in test 3, which had a 30 % drop in median RSE. On the matter of action smoothness, MIDHP(λ) also consistently had some of the lowest overall Sm of the four algorithms. However, there were still a handful of runs from other algorithms which achieved lower Sm than any MIDHP(λ) runs.

Diving deeper into the flights themselves, Figure 8 shows all 100 flights of the IDHP and MIDHP(λ) controllers to give more insight into their control performances. Comparing Subfig. 8a to 8b, some differences can be noted. First, the action of MIDHP(λ) is generally smoother than IDHP, especially once the aircraft θ has reached up to the flat segment of θ_r, recovering better from the overshoot around 70 s. Second, the θ of MIDHP(λ) follows θ_r more closely, aside from during the pitch-up segment where one MIDHP(λ) controller is very oscillatory, which seems to be corrected once fault was introduced. Third, there is one controller in IDHP which does not manage to control the aircraft effectively during this manoeuvre.

Observing the statistical test results, it can be seen that most tests demonstrate a statistically significant improvement in RSE and Sm by the augmented algorithms. The two notable outliers of these improvements are first the MIDHP performance in test 1, which is deemed statistically significantly worse than that of IDHP; second the smoothness of the IDHP(λ) controller versus IDHP, where IDHP(λ) was deemed in general noisier but with three out of four tests showing a statistically insignificant change. Finally, the tests also show that MIDHP(λ) performs overall best out of all algorithms whether there are faults or not. Considering both the results of Tab. 4 and 5, the MIDHP(λ) RSE ranks best of all algorithms in three tests, ties for best in test 1, and ranks second in test 3. While there was little improvement in RSE during warmup, MIDHP(λ)'s improvement in median RSE during the manoeuvering phase ranged between 26% on Test 3 to 46% on Test 4. MIDHP(λ)'s Sm metrics similarly rank very high in all the tests, being the best in tests 2 to 5, and third in test 1.

Table 5 VD's A-values on the RSE & Sm results on the second to fifth tests, red A-value indicates statistically insignificant result according to Student's t-test (p-value = 0.05), A-value < 0.5 indicate the augmented algorithm's metrics are smaller than IDHP's and vice versa.

(a) RSE.

		Test 2	Test 3	Test 4	Test 5
IDHP(λ) vs IDHP	:	0.190	0.346	0.471	0.399
MIDHP vs IDHP	:	0.537	0.283	0.051	0.102
MIDHP(λ) vs IDHP	:	0.042	0.303	0.042	0.080

(b) Sm.

		Test 2	Test 3	Test 4	Test 5
IDHP(λ) vs IDHP	:	0.447	0.521	0.559	0.615
MIDHP vs IDHP	:	0.544	0.217	0.078	0.074
MIDHP(λ) vs IDHP	:	0.013	0.143	0.027	0.022

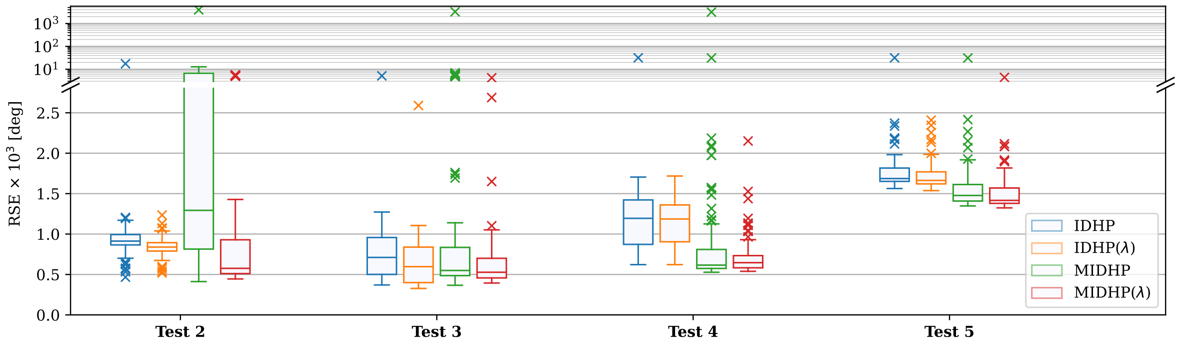

(a) RSE.

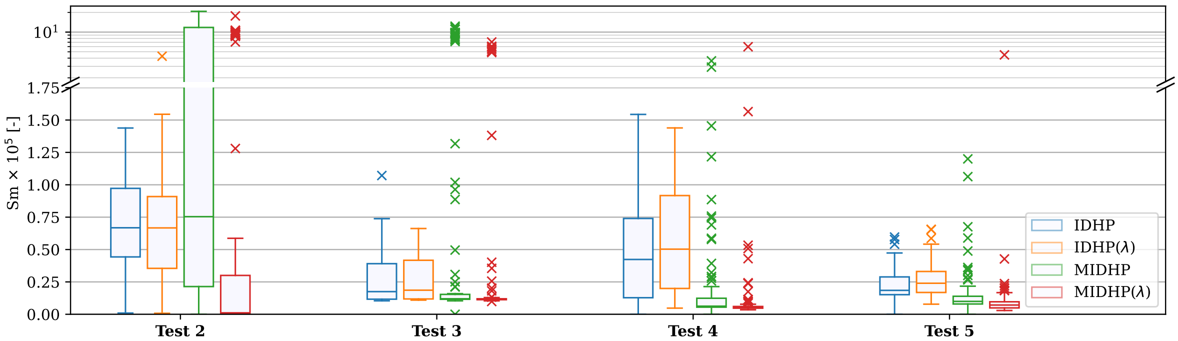

(b) Sm.

Fig. 7 Test 2, 3, 4, and 5 RSE & Sm result boxplots.

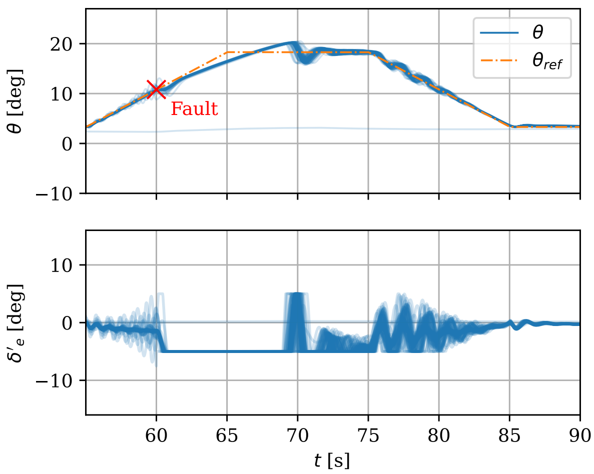

(a) IDHP.

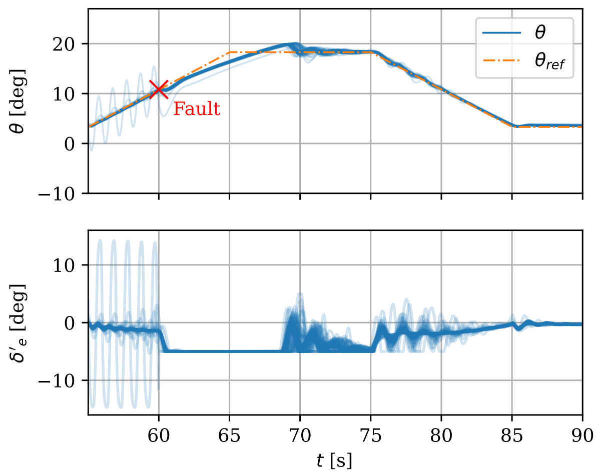

(b) MIDHP(λ).

Fig. 8 Comparing the Monte Carlo flights of IDHP and MIDHP(λ) in test 5: a damaged and saturated elevator fault introduced at 60 **s.**

V. Conclusion

Eligibility traces and Multi-step temporal difference errors have been long standing means of improving the sample efficiency and, on occasion, the asymptotic performance of RL agents in solving an MDP.

In this paper, the method by which these means can be incorporated into the ACD algorithm, IDHP, has been developed and implemented. Resulting in three augmented variants of IDHP. Simulated flight tests were then conducted, where a flight controller created from these RL algorithms was used to control the pitch attitude of a small business jet with various faults being introduced. Through observing the results of these tests, it was empirically shown that the proposed augmentations have the potential to improve the fault tolerance of a flight controller based on IDHP. In the face of faults such as an elevator control effectiveness reduction of 70% and its deflection angles limited to a third of the original range, these augmentations resulted in not only successful and improved tracking over IDHP, but also in control action smoothness - an issue that must be addressed if such controllers were to become a reality.

Out of all the augmentations, MIDHP(λ), which combines both eligibility traces and multi-step error, was shown to be the most promising algorithm with the best tracking performance in the face of faults, and the smoothest control actions.

The issue of success rate stands as an obstacle to the real-world online deployment of such controllers. Seeing as several runs result in highly oscillatory control actions in all the here-studied algorithms, it remains risky to give full control authority over to the IDHP based flight controller. Overcoming this issue will be an important step towards these algorithms' real-world deployment as intelligent and adaptive flight controllers. It is therefore worthwhile to investigate how the smoothening effect of changing aircraft dynamics or methods such as CAPS might be exploited more extensively.

References

[1] McDonald, R. A., German, B. J., Takahashi, T., Bil, C., Anemaat, W., Chaput, A., Vos, R., and Harrison, N., "Future aircraft concepts and design methods," *The Aeronautical Journal*, Vol. 126, No. 1295, 2022, pp. 92–124.

[2] Hodgkinson, D., and Johnston, R., *Aviation law and drones: Unmanned aircraft and the future of aviation*, Routledge, 2018.

[3] Yusaf, T., Fernandes, L., Abu Talib, A. R., Altarazi, Y. S., Alrefae, W., Kadirgama, K., Ramasamy, D., Jayasuriya, A., Brown, G., Mamat, R., et al., "Sustainable aviation—Hydrogen is the future," *Sustainability*, Vol. 14, No. 1, 2022, p. 548.

[4] Hanover, D., Loquercio, A., Bauersfeld, L., Romero, A., Penicka, R., Song, Y., Cioffi, G., Kaufmann, E., and Scaramuzza, D., "Autonomous drone racing: A survey," *IEEE Transactions on Robotics*, 2024.

[5] Balas, G. J., "Flight control law design: An industry perspective," *European Journal of Control*, Vol. 9, No. 2-3, 2003, pp. 207–226.

[6] Kwatny, H., Dongmo, J.-E., Chang, B.-C., Bajpai, G., Yasar, M., and Belcastro, C., "Aircraft accident prevention: Loss-of-control analysis," *AIAA guidance, navigation, and control conference*, 2009, p. 6256.

[7] Sonneveldt, L., Van Oort, E., Chu, Q., and Mulder, J., "Nonlinear adaptive trajectory control applied to an F-16 model," *Journal of Guidance, control, and Dynamics*, Vol. 32, No. 1, 2009, pp. 25–39.

[8] Johnson, E., Calise, A., and De Blauwe, H., "In flight validation of adaptive flight control methods," *AIAA Guidance, Navigation and Control Conference and Exhibit*, 2008, p. 6989.

[9] Bosworth, J., "Flight results of the NF-15B intelligent flight control system (IFCS) aircraft with adaptation to a longitudinally destabilized plant," *AIAA Guidance, Navigation and Control Conference and Exhibit*, 2008, p. 6985.

[10] Silver, D., Hubert, T., Schrittwieser, J., Antonoglou, I., Lai, M., Guez, A., Lanctot, M., Sifre, L., Kumaran, D., Graepel, T., Lillicrap, T. P., Simonyan, K., and Hassabis, D., "Mastering Chess and Shogi by Self-Play with a General Reinforcement Learning Algorithm," *CoRR*, Vol. abs/1712.01815, 2017. URL `http://arxiv.org/abs/1712.01815`.

[11] Mnih, V., Kavukcuoglu, K., Silver, D., Rusu, A. A., Veness, J., Bellemare, M. G., Graves, A., Riedmiller, M., Fidjeland, A. K., Ostrovski, G., Petersen, S., Beattie, C., Sadik, A., Antonoglou, I., King, H., Kumaran, D., Wierstra, D., Legg, S., and Hassabis, D., "Human-level control through deep reinforcement learning," *Nature*, Vol. 518, No. 7540, 2015, pp. 529–533. https://doi.org/10.1038/nature14236.

[12] Kiran, B. R., Sobh, I., Talpaert, V., Mannion, P., Al Sallab, A. A., Yogamani, S., and Pérez, P., "Deep reinforcement learning for autonomous driving: A survey," *IEEE Transactions on Intelligent Transportation Systems*, Vol. 23, No. 6, 2021, pp. 4909–4926.

[13] Kober, J., Bagnell, J. A., and Peters, J., “Reinforcement learning in robotics: A survey,” *The International Journal of Robotics Research*, Vol. 32, No. 11, 2013, pp. 1238–1274.

[14] Khan, S. G., Herrmann, G., Lewis, F. L., Pipe, T., and Melhuish, C., “Reinforcement learning and optimal adaptive control: An overview and implementation examples,” *Annual reviews in control*, Vol. 36, No. 1, 2012, pp. 42–59.

[15] Prokhorov, D. V., and Wunsch, D. C., “Adaptive critic designs,” *IEEE transactions on Neural Networks*, Vol. 8, No. 5, 1997, pp. 997–1007.

[16] Zhou, Y., Van Kampen, E.-J., and Chu, Q., “Incremental model based online dual heuristic programming for nonlinear adaptive control,” *Control Engineering Practice*, Vol. 73, 2018, pp. 13–25. https://doi.org/10.1016/j.conengprac.2017.12.011.

[17] Shayan, K., and Van Kampen, E.-J., “Online actor-critic-based adaptive control for a tailless aircraft with innovative control effectors,” *AIAA Scitech 2021 Forum*, 2021, p. 0884.

[18] Li, H., Sun, L., Tan, W., Liu, X., and Dang, W., “Incremental dual heuristic dynamic programming based hybrid approach for multi-channel control of unstable tailless aircraft,” *IEEE Access*, Vol. 10, 2022, pp. 31677–31691.

[19] Ferrari, S., and Stengel, R. F., “Online adaptive critic flight control,” *Journal of Guidance, Control, and Dynamics*, Vol. 27, No. 5, 2004, pp. 777–786.

[20] Li, T., Zhao, D., and Yi, J., “Heuristic Dynamic Programming strategy with eligibility traces,” *2008 American Control Conference*, 2008, pp. 4535–4540. https://doi.org/10.1109/ACC.2008.4587210.

[21] Luo, B., Liu, D., Huang, T., Yang, X., and Ma, H., “Multi-step heuristic dynamic programming for optimal control of nonlinear discrete-time systems,” *Information Sciences*, Vol. 411, 2017, pp. 66–83. https://doi.org/https://doi.org/10.1016/j.ins.2017.05.005.

[22] Wang, D., Wang, J., Zhao, M., Xin, P., and Qiao, J., “Adaptive Multi-Step Evaluation Design With Stability Guarantee for Discrete-Time Optimal Learning Control,” *IEEE/CAA Journal of Automatica Sinica*, Vol. 10, No. 9, 2023, pp. 1797–1809. https://doi.org/10.1109/JAS.2023.123684.

[23] Enns, R., and Si, J., “Helicopter trimming and tracking control using direct neural dynamic programming,” *IEEE Transactions on Neural networks*, Vol. 14, No. 4, 2003, pp. 929–939.

[24] van Kampen, E.-J., Chu, Q., and Mulder, J., “Continuous adaptive critic flight control aided with approximated plant dynamics,” *AIAA Guidance, Navigation, and Control Conference and Exhibit*, 2006, p. 6429.

[25] Heyer, S., Kroezen, D., and Van Kampen, E.-J., “Online Adaptive Incremental Reinforcement Learning Flight Control for a CS-25 Class Aircraft,” *AIAA SciTech 2022 Forum*, 2020, p. 1844. https://doi.org/10.2514/6.2020-1844.

[26] Watkins, C. J. C. H., “Learning from delayed rewards,” Ph.D. thesis, King’s College, Cambridge United Kingdom, 1989.

[27] Cichosz, P., “Truncating temporal differences: On the efficient implementation of TD (lambda) for reinforcement learning,” *Journal of Artificial Intelligence Research*, Vol. 2, 1994, pp. 287–318.

[28] Singh, S. P., and Sutton, R. S., “Reinforcement learning with replacing eligibility traces,” *Machine learning*, Vol. 22, No. 1, 1996, pp. 123–158.

[29] Ye, J., Bian, Y., Xu, B., Qin, Z., and Hu, M., “Online Optimal Control of Discrete-Time Systems Based on Globalized Dual Heuristic Programming with Eligibility Traces,” *2021 3rd International Conference on Industrial Artificial Intelligence (IAI)*, 2021, pp. 1–6. https://doi.org/10.1109/IAI53119.2021.9619346.

[30] Mysore, S., Mabsout, B., Mancuso, R., and Saenko, K., “Regularizing action policies for smooth control with reinforcement learning,” *2021 IEEE International Conference on Robotics and Automation (ICRA)*, IEEE, 2021, pp. 1810–1816.

[31] Van Der Linden, C., “DASMAT-Delft University aircraft simulation model and analysis tool: A Matlab/Simulink environment for flight dynamics and control analysis,” *Series 03: Control and Simulation 03*, 1998.

[32] Van den Hoek, M., de Visser, C., and Pool, D., "Identification of a Cessna Citation II model based on flight test data," *Advances in Aerospace Guidance, Navigation and Control: Selected Papers of the Fourth CEAS Specialist Conference on Guidance, Navigation and Control Held in Warsaw, Poland, April 2017*, Springer, 2018, pp. 259–277.

[33] Seres, P., "Distributional Reinforcement Learning for Flight Control," MSc thesis, Faculty of Aerospace Engineering, TU Delft, 2022.

[34] Sullivan, G. M., and Feinn, R., "Using effect size—or why the P value is not enough," *Journal of graduate medical education*, Vol. 4, No. 3, 2012, pp. 279–282.

[35] Student, "The probable error of a mean," *Biometrika*, 1908, pp. 1–25.

[36] Vargha, A., and Delaney, H. D., "A critique and improvement of the CL common language effect size statistics of McGraw and Wong," *Journal of Educational and Behavioral Statistics*, Vol. 25, No. 2, 2000, pp. 101–132.

Part II

Preliminary Results

2 Literature Study

The thesis project commences with a study of literature, this is intended to introduce the main concepts that will be used as the foundation of the methodologies used, as well as supplement the discussion of any results gathered. Literature studies are conducted in the fields related to the research project; for the present research, the main relevant research fields are reinforcement learning -constituted largely of approximate dynamic programming and deep reinforcement learning research-, and the field at the intersection of reinforcement learning with flight control.

This chapter is laid out as follows. Section 2.1 introduces the basic concepts to lay the theoretical understanding that underlines most reinforcement learning research. This is followed by two sections that discuss the two main research fields dominant in reinforcement learning for control applications: dynamic programming discussed in Section 2.2, and deep reinforcement learning discussed in Section 2.3. These two sections will start with touching on the earlier and more fundamental algorithms, shifting focus progressively to the respective state of the art. The problem of applying reinforcement learning to flight control is then discussed in Section 2.4, which will present various research efforts towards this goal and interesting directions for further study.

2.1. Reinforcement Learning Foundations

The basic idea of reinforcement learning is to have some agent associate rewards with actions that help realize a goal and promote the agent to take more of such actions by asking it to maximize the reward. The agent is not told what the goal is explicitly, its only interface with the world around it is through executing these actions, and observing that it has transitioned into some state and received some reward. Reinforcement learning can be thought of as a way in which theorists have attempted to codify and formulate algorithms for, the universal experience of learning through trial and error. Much like how a child learns to walk, or a dog learns to sit, it is through reinforcement learning that machines can learn how to perform tasks that might not be easily programmed. Through this codification, computer programs have been made that demonstrated impressive levels of learning; for example, programs can learn through reinforcement learning to play various high-dimensional board games to a level of expertise surpassing any living player [9], and a robotic arm can learn hand dexterity and mimic the hand movements of a human [10].

Understanding how the reinforcement learning algorithms work behind such examples and how they may be applied to flight control will require understanding the foundations first, thus this section will introduce the basic terminologies and ideas used to build these algorithms.

2.1.1. Markov Decision Process

The MDP is the mathematical framework that is used to model sequential decision processes such as how an agent interacts with an environment, and it is what contextualizes all the ideas in reinforcement learning, for instance, the basic notion that an agent performs an action and receives a reward.

In such a framework, there exist two entities: the agent and the environment, and information flows from one entity to another to model making decisions and their resulting consequences. In reinforcement learning the agent is sometimes also called the learner, it selects an action A_t which gets fed to the environment, and the environment will provide the corresponding state S_{t+1} which the agent has transitioned to as a result of action A_t and the reward associated to that state transition R_{t+1}, the agent can subsequently use S_{t+1} and R_{t+1} to decide on the next time step's action A_{t+1}. A graphical depiction of this agent-environment interface in the MDP is shown in Figure 2.1.

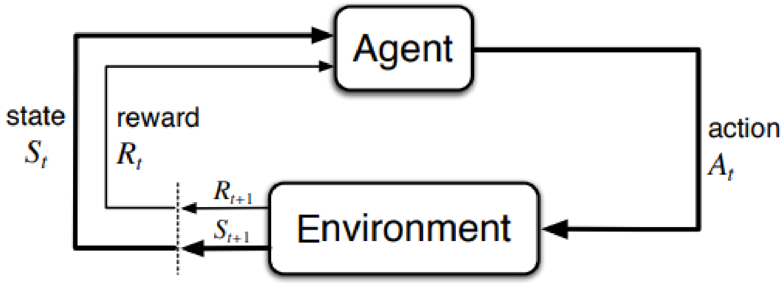

Figure 2.1: Flow diagram of the agent-environment interaction central to the MDP

This time trace of an agent-environment interaction is recorded in a so-called *trajectory* $\mathcal{T}$, which is a chain of state-action-reward-next state values for the entire duration of the decision process:

$$\mathcal{T} = S_0, A_0, R_1, S_1, A_1, R_2, \ldots, S_{T-1}, A_{T-1}, R_T, S_T, A_T \tag{2.1}$$

The state-action-reward-next state of one timestep is commonly collected into one tuple of variables, which can be referred to as a *transition tuple* or *experiences*:

$$(S_t, A_t, R_{t+1}, S_{t+1}) \tag{2.2}$$

One central component of MDPs is the dynamics of the environment. In the simpler case of finite and discrete processes, the dynamics of the environment can be considered to be a discrete conditional probability distribution $p(s', r|s, a)$ as shown in Equation 2.3. which returns the probability of transitioning to a state s' and obtaining a reward r given that the agent observed a previous state s and executed an action a.

$$p(s', r|s, a) \doteq Pr\{St = s', R_t = r|S_{t-1} = s, A_{t-1} = a\} \tag{2.3}$$

From Equation 2.3, it is possible to compute the expected reward for any state-action pairs $r(s, a)$:

$$r(s, a) \doteq \mathbb{E}\{R_t|S_{t-1} = s, A_{t-1} = a\} = \sum_r r \sum_{s'} p(s', r|s, a) \tag{2.4}$$

Modelling the environment dynamics, i.e. the MDP dynamics, can also be done using other modelling methods. For example, state space systems of equations are commonly used when creating control systems, and as such are also used to serve as the dynamics model in the MDPs [11]–[13]. In both cases, one important property that the models possess is the *Markov property*, also referred to as the memoryless property. This property states that to predict the system in the next time step, only information from the current time step is necessary, which means that having any information from previous time steps does not influence the outcome of the prediction. This property is captured by the equation below:

$$Pr\{S_t, R_t|S_{t-1}, A_{t-1}\} = Pr\{S_t, R_t|S_1, \ldots, S_{t-1}, A_1, \ldots, A_{t-1}\} \tag{2.5}$$

In reinforcement learning, having the dynamics of the environment possess the Markov property is useful. Many algorithms assume that the evolution of the system can be perfectly predicted by only using information from the current time step [14], which implies that for a learner to decide what actions to take to enter into a trajectory which maximizes its rewards, it is sufficient to only know of the current state of the MDP.

In the context of flight control, the MDP can be conveniently formulated using state space systems. For example, the action, state, and reward in Figure 2.1 can be considered equivalent to the control vector, the state vector, and an output vector in the state space formulation respectively.

2.1.2. Rewards and Returns

How learners in a reinforcement learning problem gauge their performance is through reward signals, this reward signal is made to be representative of the goal of the reinforcement learning problem.

Reward signals are central to the *reinforcement* in reinforcement learning, as they are made to be associated with states and actions that get the agent closer to the goal, thus incentivizing the learner to repeat more of such actions with the ultimate effect of the agent becoming more proficient in the posed task. Strong parallels can be drawn between an agent in the reinforcement learning context becoming better at obtaining higher reward signals, and that of animal behaviour adapting to receive more desirable stimuli in the context of domestic animal training, a so-called “Law of Effect”[15]. This parallel arises from the strong connections between reinforcement learning as a computer science and mathematical theory, and reinforcement learning as a field of psychology, and shows how ideas in reinforcement learning are often grounded in ideas from nature.

In reinforcement learning nomenclature, a distinction in terminology exists between the reward being received every time step, and the cumulative reward that an agent receives over many time steps. While rewards are received every time step, when they are summed up over time, they are then referred to as the *return*. For example, an episodic return refers to how much cumulative reward an agent has received throughout an episode. Formally, returns are defined by Equation 2.6 as the sum of all future discounted rewards, where the discount factor $\gamma \in [0, 1]$ is introduced which allows for returns to be computed even when a task is not episodic but continuing, i.e. $T = \infty$. Increasing γ from 0 to 1 increases the weight of rewards received later in time, which makes the agent more “far-sighted”, the opposite case of decreasing γ causes the agent to be more “myopic”.

$$G_t \doteq R_{t+1} + \gamma R_{t+2} + \cdots + \gamma^{T-t-1} R_T = \sum_{k=t+1}^{T} \gamma^{k-t-1} R_k \tag{2.6}$$

The goal of a learner in reinforcement learning is to maximize the return G_t, this return serves as one of the main metrics for evaluating the success of an agent. Moreover, the task of designing appropriate reward signals is one of the most important when posing a reinforcement learning problem. If the desired outcome is not associated explicitly with rewards, an agent would likely not learn to reach such an outcome.

2.1.3. Policy

A policy is what an agent follows to decide on what action to choose. Formally, a policy π is defined as a functional mapping from state s to the probability of choosing an action a, i.e. probability of action a conditioned on state s:

$$\pi(a|s) \doteq Pr\{A_t = a | S_t = s\} \tag{2.7}$$

The specific formulation of $\pi(a|s)$ differs greatly from algorithm to algorithm, in fact, there is no restriction on the form of the probability distribution that $\pi(a|s)$ takes. For instance, it is permissible that $\pi(a|s)$ is deterministic, i.e. if the state is s_1, then action is a_1. The overarching theme is that an agent should follow a policy that will maximize its returns.

2.1.4. Value Function

Value functions predict how much return an agent will receive in expectation if it were to follow a policy π. Two types of value functions are commonly used in reinforcement learning, the state-value function $v_\pi(s)$ and the action-value function $q_\pi(s, a)$. The state-value function is the expected return from being in any single state, mathematically this is defined as:

$$V_\pi(s) \doteq \mathbb{E}_\pi\{G_t|S_t = s\} \tag{2.8}$$

Where $V_\pi(s)$ is the value of state s, and G_t is the return from time t onwards when following the policy π. Notation of the expectation operator is slightly abused to include the π to indicate that the agent is following policy π. The state-value function can be intuitively understood as how worthwhile it is to be in a certain state. The action-value function is defined as the expected return of a particular state-action pair, this can again be mathematically stated as follows:

$$Q_\pi(s,a) \doteq \mathbb{E}_\pi\{G_t|S_t = s, A_t = a\} \tag{2.9}$$

Where $Q_\pi(s,a)$ is the value of taking action a in state s, and G_t is the return from time t onwards when following the policy π. The action-value function can be intuitively understood as how worthwhile it is to take a certain action in a certain state.

2.1.5. Bellman Equation

The equation commonly referred to as *the* Bellman equation is the Bellman equation for the state-value function, presented in Equation 2.10, which is derived starting from the definition of the state-value function Equation 2.8:

$$\begin{aligned}
V_\pi(s) &\doteq \mathbb{E}_\pi\{G_t|S_t = s\} \\
&= \mathbb{E}_\pi\{R_{t+1} + \gamma G_{t+1}|S_t = s\} \\
&= \sum_{r,g_t} p(r, g_t|s)[r + \gamma g_t] \\
&= \sum_{a,s'} \sum_{r,g_t} p(a, s', r, g_t|s)[r + \gamma g_t] \\
&= \sum_{a} \sum_{s',r} \sum_{g_t} \underbrace{p(a|s)}_{=\pi(a|s)} p(s', r|s, a) \underbrace{p(g_t|s', r, s, a)}_{=p(g_t|s'),\ \text{Markov}}[r + \gamma g_t] \\
&= \sum_{a} \pi(a|s) \sum_{s',r} p(s', r|s, a)[r + \gamma \sum_{g_t} p(g_t|s')g_t] \\
&= \sum_{a} \pi(a|s) \sum_{s',r} p(s', r|s, a)[r + \gamma V_\pi(s')]
\end{aligned} \tag{2.10}$$

This equation defines an analytical relationship between the value function of successive states, suggesting that the value of a previous state can be calculated once the subsequent state's value function, the environment dynamics, and the followed policy are known.

Notice that the value function in Equation 2.10 is recursively defined. This recursive formulation lends itself readily to dynamic programming techniques, which simply means that Equation 2.10 is adopted as an update equation for estimates of the state value function, whereby iteratively applying this update the estimate converges towards the true value. The Bellman equation of Equation 2.10 was first derived by Richard Bellman and is associated with the basic foundations of the field of dynamic programming [16].

There also exists a Bellman equation for the action-value function, which is presented in Equation 2.11.

$$Q_\pi(s,a) \doteq \sum_{s',r} p(s', r|s, a)[r + \gamma V_\pi(s')] \tag{2.11}$$

2.1.6. Distinguishing Algorithm Characteristics

There exist many ways to characterize what exactly a reinforcement learning algorithm is. In this subsection, three of the most basic characteristics which have the biggest implications on the performance of an algorithm are identified and described, and are useful when explaining the observed behaviour of certain algorithms.

On-Policy vs Off-Policy

One basic distinguishing characteristic of reinforcement learning algorithms by being on-policy or off-policy. To be on-policy means to optimize for an estimated variable while simultaneously using the same variable to dictate the agent's actions, such a variable is often the policy function of an agent, hence the terminology, but can also be the value function of an agent.

In the case of the variable being a policy, an off-policy algorithm would be interacting with the environment using one policy and consequently generate transition tuples which are used as samples for training a second policy. The first policy which generates the transition tuples is called the *behaviour policy*, while the policy using the generated tuples as training samples is called the *target policy* [17].

Separating the sample generating and training policies can be desirable when considering the issue of exploration versus exploitation. When the two policies are separate, it is easier to direct the behaviour policy to be more exploratory, allowing transition tuples to cover a wider region of the state and action space and thus providing the target policy with greater generalization power. However, adopting an on-policy approach can result in a simpler algorithm, which converges to a stable policy much quicker albeit with a slightly less optimal agent [18].

Model-Based vs Model-Free

The second characteristic is model-based versus model-free, which is whether an algorithm uses some model of the environment's dynamics or not. For standard benchmarking of algorithms, it is possible to use the model of the benchmark environments, which are made with the intent of easy modelling, such as the inverted pendulum environment, the mountain car environment, or the lunar lander environment from the Farama foundation [19]. When such models are readily usable, an algorithm can leverage this model to efficiently learn the optimal value function and policy of the MDP.

However, in the real world, obtaining models of systems can be complicated. This is true in the aerospace industry where time and cost-intensive system identification campaigns are required to obtain a mathematical model describing the dynamics of a vehicle. To add further, novel aircraft designs which do not follow the traditional tube-and-wing design scheme, will not be able to directly leverage the wealth of developed tools or knowledge on flight dynamics for creating dynamic models. This traditional aircraft design scheme is very well known in the aviation industry, to the point where many well-established textbooks on the design of such aircraft and their flight dynamic properties are available, for instance: Torenbeek [20] on the synthesis of subsonic aircraft design, or Nelson [21] on flight stability and automatic control, amongst others. Such knowledge can, to some extent, be applied to the modelling and research of innovative aircraft designs, such as blended wing-body designs or distributed propulsion designs. However, the development of high-fidelity models for such aircraft designs is in itself a research area, where model developments have to stray away from familiar territories of tube-and-wing modelling, and is still being actively studied [22], [23].

In short, developing flight dynamic models for aircraft can be a drawn-out procedure, and potentially result in low-fidelity models in the case of innovative aircraft, which complicates obtaining MDP environment models for flight control problems. When models of the environment are not at hand, a reinforcement learning algorithm can be designed in the following two ways:

1. Use some function approximator or pre-defined model structure and estimate the environment dynamics by updating this model, adding complexity in what model structure to use and steps for estimating the model.
2. To be model-free and only optimize value and policy functions based solely on sampled experiences, which is less efficient at learning than a model-based approach.

Value-Based vs Policy-Based

The distinction between value and policy-based is what the algorithm is designed to estimate. When the algorithm is value-based, it trains an estimate of the optimal value function from which the actions are inferred; versus in the policy-based case, where an estimate of the optimal policy function is trained from which actions are directly obtained.

In the case when function approximators are used in an algorithm, they are additionally distinguished by where the function approximator is used. Where value-based and policy-based algorithms use the approximator in the value function and the policy function respectively.

The main benefits and drawbacks of each approach are in how they handle high dimensional states or action spaces, where value-based methods can handle a large number of states better and policy-based methods can handle a large number of actions better.

2.1.7. Basic Reinforcement Learning Algorithms

The goal of reinforcement learning algorithms is to teach an agent to behave optimally in some MDP. This is done by incrementally improving the value function estimate of a process, as well as the policy used to guide the agent. Three basic approaches can be identified to achieve this goal, these are *Monte Carlo Learning*, *Temporal Difference Learning*, and *Dynamic Programming*. The first two of these approaches are described in this subsection, while the last of these approaches is elaborated in more depth under Section 2.2.

In general, updating a value estimate involves using *targets*, which is the value that an estimate is moved towards, the most important distinction between Monte Carlo (MC) and Temporal Difference (TD) learning is in how this target is formulated.

Monte Carlo Learning

MC learning uses the *sampled episodes* from an agent interacting with an environment to improve its estimation of the value function. For illustrative purposes, the MC algorithm described here learns the action-value $Q(s_t, a_t) = Q_\pi(s_t, a_t)$ of the process.

Here, an agent initialized with a complete but random table of action-values along with an arbitrary policy is placed in a MDP and begins executing actions. With each action it takes, the environment transitions to a different state and the agent observes this new state along with the new reward. To allow the agent to learn, the action-value table is improved by summing up the rewards observed from each state-action pair that the agent comes across until this trajectory reaches a terminal state, and using this sum as a *monte carlo* estimate of the return G for the state action pair at the root of that trajectory.

$$Q(s_t, s_t) = Q(s_t, a_t) + \alpha[G_t - Q(s_t, a_t)] \tag{2.12}$$

Where α is a learning step size. This type of learning does not depend on the Markov property for convergence and the use of sampled experience as opposed to using modeled dynamics to estimate values makes MC learning appealing methods.

Temporal Difference Learning

TD learning also uses *sampled transitions* to improve an agent's action and value estimates. Unlike MC learning, it does not use sample episodes, thus it does not need to wait for the sum of rewards to reach a terminal state for a return's estimate to be defined, it updates the action-value of a state-action pair the instant which the agent receives the reward for that pair:

$$Q(s_t, a_t) = Q(s_t, a_t) + \alpha[R_{t+1} + \gamma Q(s_{t+1}, a_{s+1}) - Q(s_t, a_t)] \tag{2.13}$$

Updating value estimates at every transition is known as *bootstrapping*, which is to improve the accuracy of an estimate by basing it on other estimates. Bootstrapping and temporal difference are widely applied methods in reinforcement learning because of their simplicity, and their minimal computation needs [17]. As opposed to MC methods, their wall clock time -real time needed- for training is often lower since they do not need to wait until the end of an episode for estimates to be updated.

2.2. Dynamic Programming

One major field of reinforcement learning research focuses on the use of *Dynamic Programming* techniques with an emphasis on tackling optimal control problems[24]. Dynamic programming is a term coined by Richard Bellman, it has roots in the field of optimization and is used to refer to the problem-solving approach of divide and conquer, where a more complicated problem is broken into sub-problems for which recursive algorithms can be devised to come up with their solutions[16]. In the context of reinforcement learning, classical applications of dynamic programming revolve around the

Bellman equation stated in Equation 2.10 and results in the method known as *Policy Iteration*, which is used to obtain the optimal value function and policy for *finite* MDPes, processes whose state s and action a variables belong to countable sets denoted $\mathcal{S}$ and $\mathcal{A}$ respectively. This method will be described in Section 2.2.1 and Section 2.2.2. Modern applications of dynamic programming extend the method of policy iteration to make it more computationally tractable and is described in Section 2.2.3.

The classes of algorithms that are branched off from dynamic programming methods are summarized in Figure 2.2.

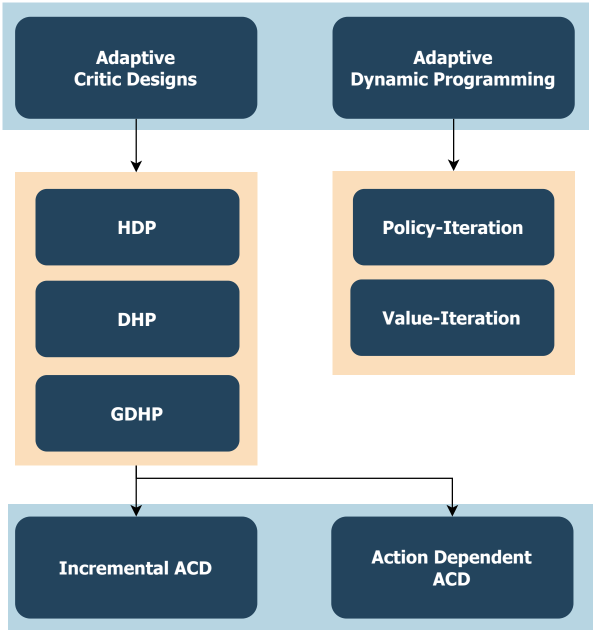

Figure 2.2: Overview of Approximate Dynamic Programming and Adaptive Critic Design algorithms, light blue box presents the class of algorithms, light orange box presents reinforcement learning algorithms.

2.2.1. Policy Iteration

This method iteratively applies two steps to find the optimal value function and policy, these steps are *policy evaluation* and *policy improvement*. The method is graphically depicted in Figure 2.3 and is outlined as follows:

1. Initialize $\pi(a|s)$ and $V_{\pi'}(s)$ arbitrarily.
2. Perform Policy Evaluation to compute the value function of π
3. Perform Policy Improvement to find a more optimal policy
4. Repeat from Step 2 until π and $V_\pi(s)$ stop varying, i.e. converge.

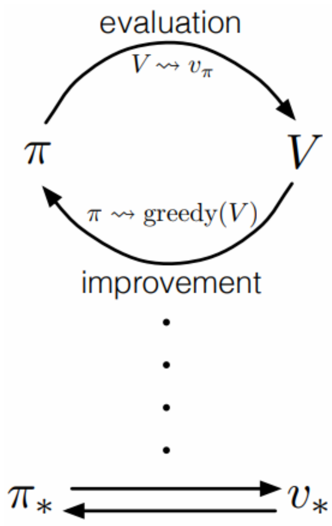

Figure 2.3: The method of policy iteration, by iteratively evaluation a policy's value function, and subsequently determining the greedy policy for that value function, the policy and value function eventually converges to a fixed iteration point when they are optimal for the given MDP, adopted from Sutton and Barto [17].

This algorithm is proven to converge toward the optimal value function and policy[17] under certain conditions. Namely, it assumes a perfect environment model is available for use. Nonetheless, the theoretical guarantee for optimality makes it an important foundation method in reinforcement learning and is detailed further.

Policy Evaluation

For a given policy π, the value function of this policy V_π is computed by starting with an initial estimate $V_{\pi,0}$ and recursively applying the Bellman equation on all s as an update rule as shown in Equation 2.14. This update will be applied until the value function has converged, where convergence can be defined in several ways, the simplest of which is when the norm of the difference between subsequent value functions is smaller than a small constant ϵ.

$$V_{\pi,k+1} = \sum_a \pi(a|s) \sum_{s',r} p(s',r|s,a)[r + \gamma V_{\pi,k}(s')] \quad \forall s \in \mathcal{S} \tag{2.14}$$

Note that to compute the update formulated in Equation 2.14, the environment dynamics $p(s',r|s,a)$ needs to be known and defined, which is an assumption made during the policy evaluation step.

By inspection of Equation 2.10, it can be concluded that the update equation Equation 2.14 will only converge when the estimation v_k is equal to the true value function v_π.

Policy Improvement

For any given value function v_π, an improved policy π' is obtained by making π' deterministic and greedy with respect to v_π. This is done by defining π' to choose the action that has the highest action value in each state s:

$$\pi'(a|s) = \begin{cases} 1, & \text{if } a = \underset{a}{\operatorname{argmax}}\ q_\pi(s,a) \\ 0, & \text{otherwise} \end{cases} \tag{2.15}$$

The policy improvement step is guaranteed to find a policy that is at least as good as the previous policy, and in the case of a finite MDP, the policy improvement step is guaranteed to find the optimal policy [16]. After finding a greedy policy on the given value function, the previous value function will no longer be accurate for the new policy *if it is suboptimal for the given MDP*. This means that when a policy evaluation step is subsequently performed, a sub-optimal policy will cause the evaluation step to yield a different value function, but an optimal policy will yield the same value function. In other words, this algorithm only converges when the optimal policy and its corresponding value function are determined[17].

2.2.2. Generalized Policy Iteration

In the policy iteration method just described, the policy evaluation and improvement steps are carried out with the specific update rules in Equation 2.14 and Equation 2.15. However, the idea behind policy iteration: evaluating and improving upon some estimated policy or value function, is very useful and can be used to describe on a high level the idea behind many reinforcement learning algorithms as stated by Sutton and Barto [17], who use the term *generalized policy iteration* to capture this idea.

For example, instead of iterating the policy evaluation step until the value function converges, it is possible to only take one or a few policy evaluation iterations, and proceed with policy improvement thereafter. This is the idea behind Value Iteration algorithms, which is applied to optimal control problems without using Bellman equations[25], [26].

Another example comes from outside of the dynamic programming field, the class of actor-critic can be described using the idea of generalized policy iteration, wherein an estimate of the critic function (the value function) is improved based on sampled transitions from the MDP, and the policy function (the actor) is improved using information from the critic.

2.2.3. Approximate Dynamic Programming

Finite MDP are characterized by their discrete and small number of states and actions that are possible, this makes it possible to use dynamic programming to solve for the optimal value function and policy using the equations from Section 2.2.1. However, many systems that are interesting to model and find solutions for have many states and actions possible, and real-life processes frequently have continuous variables instead of discrete ones. Such circumstances can cause a combinatorial explosion in the number of state-action pairs describing the system, which means having a value and an action probability distribution defined for each state becomes impractical. This is the so-called *curse of dimensionality*, alluded to in Section 2.2.1. Moreover, evaluation of the Bellman equations also requires a known transition probability distribution of the environment. Not only does this suffer from the curse of dimensionality in the case of large and/or continuous state spaces, but knowledge of such distribution might not be available for some systems, or at the very least inconvenient or difficult to identify.

One solution to circumvent these issues is to use function approximators for the value function, policy function, and environment model, which leads to the class of dynamic programming based reinforcement learning algorithms called Approximate Dynamic Programming (ADP). In this class, it is common to refer to value functions as *cost-to-go* or *cost* functions instead. Two basic methods exist in this class, the first is the ADP version of the Policy Iteration (PI) algorithm, its high-level algorithm is outlined in Algorithm 1.

Algorithm 1 Policy iteration, adapted from [27]

1: **Initialize**. Define a policy $\pi_0(s_k)$ which is admissible, i.e. stabilizing, and an arbitrary initial value function $V_0(s)$.

2: **Policy Evaluation**. Determine the value function of the current policy using the Hamilton-Jacobi-Bellman Equation:

$$V_{i+1}(s_t) = r(s_t, \pi_i(s_t)) + \gamma V_{i+1}(s_{t+1}) \tag{2.16}$$

3: **Policy Improvement**. Determine an improved policy.

$$\pi_{i+1}(s_t) = \underset{\pi(s_t)}{\operatorname{argmin}}[r(s_t, \pi_i(s_t)) + \gamma V_i(s_{t+1})] \tag{2.17}$$

4: If $V_i(s) \equiv V_{i-1}(s)$ then terminate, else $i = i + 1$ and return to step 2

Algorithm 1 fits into the mould of generalized policy iteration, which incorporates certain aspects of optimal control theory and has some note-worthy aspects. Firstly, the policy evaluation step Equation 2.14 of this algorithm is not formulated in the MDP framework, and instead is the Hamilton-Jacobi-Bellman (HJB) equation which is generally difficult to evaluate especially online [28]. But, it can be solved approximately by methods such as least squares approximation using environment observations [29], or by iteratively evaluating the equation until convergence [27]. Secondly, the policy in such algorithms is deterministic instead of stochastic as in the original formulation of PI. Thirdly, if the system dynamics can be formulated as Equation 2.18 with n and m being the number of state and control variables respectively, and the reward of the system is formulated in an Linear Quadratic Regulator (LQR) manner as shown in Equation 2.19, then it is known that the policy improvement step takes the form of Equation 2.20 [30].

$$x_{t+1} = f(x_t) + g(x_t)u_t \tag{2.18}$$

$$r(x_t, u_t) = x_t^\top Q x_t + u_t^\top R u_t \tag{2.19}$$

$$\text{Where} \quad \{x, f(x)\} \in \mathbb{R}^n,\ g(x) \in \mathbb{R}^{n\times m},\ u \in \mathbb{R}^m,\ Q \in \mathbb{R}^{n\times n},\ R \in \mathbb{R}^{m\times m}$$

$$\pi_{i+1}(s_t) = -\frac{\gamma}{2} R^{-1} g^\top(s_t) \frac{\partial V_i(s_{t+1})}{\partial s_{t+1}} \tag{2.20}$$

The second basic algorithm of the ADP class is Value Iteration (VI), whose high-level algorithm is shown in Algorithm 2.

Algorithm 2 Value iteration, adapted from [27]

1: **Initialize**. Define an arbitrary policy $\pi_0(s_k)$, and an arbitrary initial value function $V_0(s)$.
2: **Policy Evaluation**. Determine the value function of the current policy using the Hamilton-Jacobi-Bellman Equation:

$$V_{i+1}(s_t) = r(s_t, \pi_i(s_t)) + \gamma V_i(s_{t+1}) \tag{2.21}$$

3: **Policy Improvement**. Determine an improved policy.

$$\pi_{i+1}(s_t) = \underset{\pi(s_t)}{\operatorname{argmin}}[r(s_t, \pi_i(s_t)) + \gamma V_i(s_{t+1})] \tag{2.22}$$

4: If $V_i(s) \equiv V_{i-1}(s)$ then terminate, else $i = i + 1$ and return to step 2

Here the same method of policy evaluation and reduction of policy improvement in the LQR case holds. The difference between PI in Algorithm 1 and VI in Algorithm 2 is that the policy evaluation step in Algorithm 2 involves only one evaluation of Equation 2.21, this is distinguished by the LHS value function having the subscript $i + 1$ and the RHS having i. Furthermore, VI do not require the initial policy to be admissible, which means that to use VI algorithms it is not necessary to perform any a priori step on the control policy.

Various forms of these algorithms have been developed further and shown a convergence rate that could allow them to be applied to online control of systems. For instance, Wei et al. [31] present an optimal control algorithm based on the framework of ADP using neural networks as function approximations. They demonstrate via simulation of an inverted pendulum control problem that even though their solution of the HJB equation is only approximately optimal, by iteratively performing the police evaluation and improvement steps, their ADP method can converge to the optimal control law within 5 s or 10 iteration steps. A similar method based on action-value or Q function is proposed by Lin et al. [32] and demonstrates similar convergence speeds.

By linearizing a nonlinear system's dynamics, it is possible to perform the policy evaluation and improvement steps in a much more efficient manner. This approach is adopted by Zhou et al. [33], [34] who used Recursive Least Squares (RLS) regression to identify a linear model at each time step, thus obtaining a time-varying linear model, which reduced the control problem to an LQR like problem. Note that this approach relies on a sufficiently high sensor sampling rate, in the order of 10^2 Hz, which is needed for the assumption of linear dynamics to hold, as any smooth nonlinear function can be approximated locally by linear functions.

Multi-step and Eligibility Trace Extensions of ADP Methods

One trade-off that ADP methods have to face is between adopting a more policy iteration or a more value iteration approach. In the former approach, algorithms developed generally see faster convergence in their estimates, naturally a desirable characteristic. However, such algorithms require the initial policies to be admissible, otherwise, the control policy would drive the system towards instability, causing the iterative HJB equation to grow unbounded. This issue is not faced by the latter approach, as VI algorithms do not seek to fully converge towards the optimal solution of the HJB equation, instead VI only require the value function estimation to be iterated by one step, instead of a large or infinite number of steps.

This dichotomy can be reframed into a spectrum of algorithms by considering the idea of *multi-step* iterations or updates, which is to take multiple transitions or timesteps worth of information while updating estimates in a reinforcement learning algorithm [17].

With the incorporation of a multi-step augmentation to the policy evaluation update rule, this dichotomy is turned into a spectrum of algorithms, where an ADP method can select how many steps should a policy evaluation iteration take. At the extreme of taking infinite steps, a multi-step ADP method is simply the PI algorithm, on the other extreme, a single-step ADP method is the VI algorithm [35].

A high-level view of the multi-step ADP algorithm is shown in Algorithm 3, with n being the number of steps. To automate the choice of n, Wang et al. [36] derived a criterion for switching n from a low number during the initial iterations of the algorithm, where the initial arbitrary policy is not guaranteed to be admissible, to a high number during the latter iterations when the policy is verified to be admissible under the proposed criterion.

Algorithm 3 Multi-step value iteration, known as multi-step heuristic dynamic programming in and adapted from [35].

1: **Initialize**. Define an arbitrary policy $\pi_0(s_k)$, and an arbitrary initial value function $V_0(s)$.

2: **Policy Evaluation**. Determine the value function of the current policy using the multi-step approximation of the Hamilton-Jacobi-Bellman Equation:

$$V_{i+1}(s_t) = \gamma^n V_i(s_{t+1}) + \sum_{l=t}^{t+n-1} \gamma^{l-t} r(s_l, \pi_i(s_l)) \tag{2.23}$$

3: **Policy Improvement**. Determine an improved policy.

$$\pi_{i+1}(s_t) = \underset{\pi(s_t)}{\operatorname{argmin}}[r(s_t, \pi_i(s_t)) + \gamma V_i(s_{t+1})] \tag{2.24}$$

4: If $V_i(s) \equiv V_{i-1}(s)$ then terminate, else $i = i + 1$ and return to step 2

In a similar vein of leveraging the loose policy condition which Heuristic Dynamic Programming (HDP) has, and finding ways of increasing the convergence rate of HDP, eligibility traces can also be employed [37], [38]. Eligibility traces are an alternative method of incorporating additional samples from past timesteps for updating estimates, the objective here is again to improve convergence rates of algorithms, however, the algorithm behind this method is different than multi-step ideas.

Instead of explicitly retrieving samples from certain time steps, eligibility traces simply store the past updates made to the critic or actor, and persistently but at a decaying rate add such updates to the critic or actor for subsequent timesteps. This method is illustrated in Equation 2.25, where $\theta(t)$ is the set or vector of parameters for a certain function approximator at time t, this approximator could be the critic or the actor, $\mathbf{E}(t)$ is the eligibility trace at time t, and $\Delta\theta(t)$ is the update made to the function approximator at time t.

$$\begin{aligned} \theta(t+1) &= \theta(t) + \eta \mathbf{E}(t) \\ \mathbf{E}(t+1) &= \mathbf{E}(t) + \nabla \boldsymbol{\theta}(t), \quad \mathbf{E}(0) = 0 \end{aligned} \tag{2.25}$$

2.2.4. Actor Critic Designs

Alongside adaptive dynamic programming, there is a class of algorithms called Actor-Critic Design (ACD) [39]. In this class of algorithms, the estimate of value functions is referred to as the *critic*, the critic is thus "responsible" for policy evaluation; while the estimate of the policy functions is referred to as the *actor*, which is thus "responsible" for policy improvement. It should be noted that in literature, the terms ADP and ACD can be found to be used interchangeably [39]–[41], notably with the progenitor of ACD, Paul Werbos, also using these terms and reinforcement learning interchangeably [25]. Algorithmically, practical implementations of some ADP and ACD algorithms are very much alike, as will be stated later during the description of HDP. However, in this literature study, the distinction between ADP being dynamic programming algorithms which are more optimal control-oriented, and ACD being dynamic programming algorithms which are more reinforcement learning-oriented is made.

Adaptive critic designs can be considered to be reinforcement learning algorithms developed from generalized dynamic programming algorithms [39] whose algorithms are structured similarly to the PI Algorithm 1 or the VI Algorithm 2. Just like ADP, ACD algorithms are sample efficient enough for entirely online trained controllers to be implemented, which can converge towards a stable controller within a short period of time [35], [40], [42].

Several main algorithms form the basis of this class: the first and simplest algorithm is HDP, the second and slightly more complicated algorithm is Dual Heuristic Programming (DHP), and the third but most complicated algorithm is Globalized Dual Heuristic Programming (GDHP) [39]. The increase in complexity comes from what the critics of each algorithm estimate, where HDP only estimates the value function, DHP estimates the gradient of the value function, and GDHP estimates both the value and gradient of the value functions. Two extensions of all three of these basic algorithms exist, the first kind of extension makes the critic function Action-Dependent (AD), which changes the critic from being an estimate of the state-value function to an estimate of the action-value function [43]. The second kind of extension changes how the model estimate is obtained, where an RLS regressor is used to identify linear systems for the immediate time steps, as opposed to using online supervised learning with neural networks or with offline identified models.

In the ACD context, the value function is often called the cost-to-go function, but its definition remains the same as the return expected from a given state; the rewards also have a different name, and are sometimes called the one-step costs.

$$V(s_t) = r_t + \gamma V(s_{t+1}) \tag{2.26}$$

Heuristic Dynamic Programming

HDP is characterized by using the critic to estimate the value function $V(s_t)$ itself [39].

This critic is evaluated by the critic TD error $e_c(t)$ defined in Equation 2.27, and is trained to minimize the critic error function Equation 2.28. To perform training, the function approximator of the critic is updated using a gradient descent method to minimize the error function, meaning the parameters $\theta(t)$ are updated according to Equation 2.29.

$$e_{1,c}(t) = V(s_t) - r_t - \gamma V(s_{t+1}) \tag{2.27}$$

$$E_c(t) = \frac{1}{2} e_{1,c}(t)^\top e_{1,c}(t) \tag{2.28}$$

$$\theta_c(t+1) = \theta_c(t) - \nabla\theta_c(t) \tag{2.29}$$

$$\text{Where} \quad \nabla\theta_c(t) = \eta_c \frac{\partial E_c(T)}{\partial \theta_c(t)} = \eta_c \frac{\partial E_c(T)}{\partial e_{1,c}(t)} \frac{\partial e_{1,c}(t)}{\partial V(s_t)} \frac{\partial V(s_t)}{\partial \theta_c(t)}$$

Correspondingly, there is also the actor loss, the actor error function, and the actor update rule that are expressed in the following equations:

$$e_a(t) = V(s_t) - V_{true}(s_t) \tag{2.30}$$

$$E_a(t) = \frac{1}{2} e_a(t)^\top e_a(t) \tag{2.31}$$

$$\theta_a(t+1) = \theta_a(t) - \nabla\theta_a(t) \tag{2.32}$$

$$\text{Where} \quad \nabla\theta_a(t) = \frac{\partial E_a(t+1)}{\partial \theta_a(t)} = \frac{\partial E_a(t+1)}{\partial e_a(t+1)} \frac{\partial e_a(t+1)}{\partial V(s_{t+1})} \frac{\partial V(s_{t+1})}{\partial s_{t+1}} \frac{\partial x_{t+1}}{\partial u_t} \frac{\partial u_t}{\partial \theta_a(t)} \tag{2.33}$$

Observing the formulation of HDP thus far presented, an interesting note can be made of the close resemblance in the practical implementation of HDP and PI or VI algorithms or even the interchangeable use of ADP with HDP [35], [44], [45].

Observing the update equations, it can be seen that the actor update contains the partial derivative $\frac{\partial x_{t+1}}{\partial u_t}$, this is a derivative that needs to be obtained using a system model which would define the relation between the state x_{t+1} and the action u_t. As a result, this makes the HDP algorithm model-dependent. However, this dependency can be removed if HDP is made AD, in which case the value function would be a function of both state and action $V(s_t, u_t)$, this allows the chain rule expansion in Equation 2.33 to reduce the term $\frac{\partial V(s_{t+1})}{\partial s_{t+1}} \frac{\partial s_{t+1}}{\partial u_t}$ to only $\frac{\partial V(s_{t+1})}{\partial u_t}$ since V would be an explicit function of u_t, thus eliminating the system dynamics $\frac{\partial x_{t+1}}{\partial u_t}$.

An alternative way of alleviating model dependency is to use the incremental method of Zhou et al., who developed the Incremental Heuristic Dual Programming (IHDP) algorithm and successfully applied it to several tasks, including a flight control task [46], and a launch vehicle control task [47]. In this case, the partial $\frac{\partial x_{t+1}}{\partial u_t}$ can be replaced by a control effectiveness matrix from an online identified linear system. Note that this does not make the algorithm entirely model free, since the formulation of the update rules still involves using system dynamics, i.e requires environment modeling.

This algorithm performs relatively poorly compared to DHP and GDHP in terms of control performance and disturbance rejection [39], [48], but nonetheless have been deployed successfully [49]–[51].

Dual Heuristic Programming

DHP is characterized by the critic estimating the gradient of the value function $\lambda(s_t)$, instead of the value function directly [39]. This gradient can also be referred to as the *costate* [27]:

$$\lambda(s_t) = \frac{\partial V(s_t)}{\partial s_t} \tag{2.34}$$

Here, the actor formulation is identical to the HDP algorithm, and only the critic formulations are changed. The critic TD error is now defined using gradients of the value function, as shown in Equation 2.35, with the critic error function and function parameter update remaining unchanged.

$$e_{2,c}(t) = \lambda(s_t) - \frac{\partial r_t}{\partial x_t} - \gamma\lambda(s_{t+1}) \frac{\partial x_{t+1}}{\partial x_t} \tag{2.35}$$

$$E_c(t) = \frac{1}{2} e_{2,c}(t)^\top e_{2,c}(t) \tag{2.36}$$

$$\theta_c(t+1) = \theta_c(t) - \nabla\theta_c(t) \tag{2.37}$$

$$\text{Where} \quad \nabla\theta_c(t) = \eta_c \frac{\partial E_c(t)}{\partial \theta_c(t)} = \eta_c \frac{\partial E_c(t)}{\partial e_{2,c}(t)} \frac{\partial e_{2,c}(t)}{\partial \lambda(s_t)} \frac{\partial \lambda(s_t)}{\partial w_c(t)}$$

With this variation, the model-dependency of the algorithm has increased, as the critic TD error also uses the system dynamics in the form of $\frac{\partial x_{t+1}}{\partial x_t}$ in its formulation. Here, introducing an AD variant will not remove the model dependence from the algorithm entirely, only from the actor component.

Because the critic function in DHP directly outputs value function gradients, which are needed in actor updates, there are no additional numerical errors that get injected into the actor function parameter update, which cannot be said for the HDP algorithm.

This algorithm is extended to an incremental model identification version, resulting in IDHP. Application of IDHP to the task of flight control demonstrated improved reference tracking performance and fault tolerance than a pure DHP algorithm [4], [52], wherein the IDHP controller was able to recover control of the simulated aircraft even after the flight dynamics were reversed mid-flight.

Globalized Dual Heuristic Programming

GDHP is characterized by the critic estimating the value and gradient of the value function simultaneously [39], thus the critic can be treated as returning a vector of value function variables $\begin{bmatrix} V(s_t) & \lambda(s_t) \end{bmatrix}^\top$. This results in the GDHP critic error function being composed of two terms, a HDP and a DHP td error:

$$E_c(t) = \frac{1}{2} e_{1,c}(t)^\top e_{1,c}(t) + \frac{1}{2} e_{2,c}(t)^\top e_{2,c}(t) \tag{2.38}$$

$$\theta_c(t+1) = \theta_c(t) - \nabla\theta_c(t) \tag{2.39}$$

$$\text{Where} \quad \nabla\theta_c(t) = \eta_c \frac{\partial E_c(t)}{\partial \theta_c(t)} = \eta_c \left(\frac{\partial E_c(t)}{\partial e_{1,c}(t)} \frac{\partial e_{1,c}(t)}{\partial V(s_t)} \frac{\partial V(s_t)}{\partial \theta_c(t)} + \frac{\partial E_c(t)}{\partial e_{2,c}(t)} \frac{\partial e_{2,c}(t)}{\partial \lambda(x_t)} \frac{\partial \lambda(s_t)}{\partial \theta_c(t)} \right) \tag{2.40}$$

GDHP are theoretically superior to both HDP and DHP since its critic estimates both the outputs of their respective critics, but the two common implementations of GDHP both have practical issues. In the first common implementation, the GDHP critic only outputs the value function [53], [54] and the partial derivative $\frac{\partial \lambda(s_t)}{\partial w_c(t)}$ from Equation 2.40 is then computed by replacing it with the partial derivative $\frac{\partial^2 V(s_t)}{\partial s_t \partial w_c(t)}$, which is computationally expensive and practically complicated to implement. The second common implementation of GDHP involves using one function approximator for the critic, which outputs both the value function and its gradient [55]–[57], just as stated at the beginning of this subsection. However, in such implementations, the gradient of the value function is not guaranteed to be an accurate estimate of the gradient.

Reconciling the two issues of computational complexity and analytical accuracy, Zhou [58] proposed the idea of building the critic as two function approximations but with a novelty of formulating the $\lambda(s_t)$ approximator based explicitly on the $V(s_t)$ approximator, which was applied to a longitudinal flight control task, and shows promising capacity in being able to reap the simultaneous benefit of efficiency and accuracy.

2.3. Deep Reinforcement Learning

Besides Adaptive Dynamic Programming, the other major field of reinforcement learning research is Deep Reinforcement Learning (DRL). Both of these fields revolve around using function approximators [59] to address the curse of dimensionality which hinders the deployment of reinforcement learning algorithms to real-life problems, which often contain many continuous variables. A big distinction between these fields is how DRL stems largely from deep learning methods, where deep neural networks are used as the function approximator or incorporated in any other way into algorithms. The types of algorithms belonging to this class are summarized in Figure 2.4. As can be seen, DRL is separated into various classes of algorithms and this section will describe each one of these classes, in addition to presenting notable algorithms from each class.

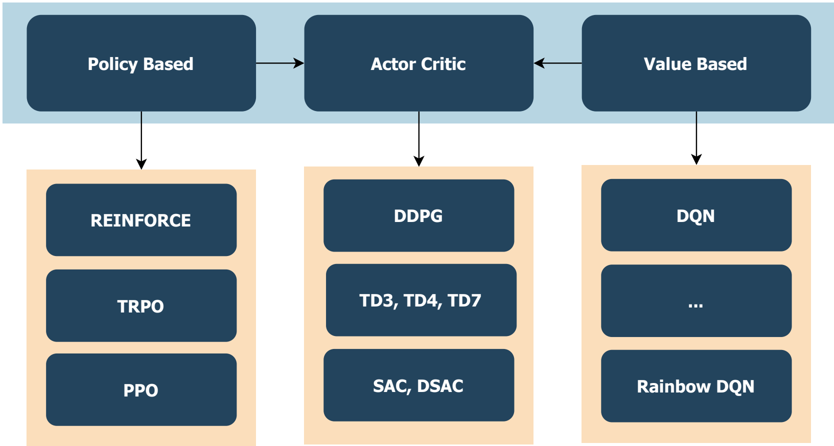

Figure 2.4: Overview of deep reinforcement learning algorithms, light blue box presents the class of algorithms, light orange box presents reinforcement learning algorithms.

This section is laid out as follows, first a description of deep learning is given in Section 2.3.1, then value-based methods are discussed in Section 2.3.2, followed by policy-based methods in Section 2.3.3, and lastly a discussion on the combination of policy and value-based methods called actor-critic methods in Section 2.3.4.

2.3.1. Deep Learning

Deep learning refers to the subfield of machine learning which studies deep neural networks and their applications. This field has its origins in the ideas of artificial neural networks and is a scientific effort that has dramatically changed the idea of what an artificial neural network is and what it might be capable of. Deep neural networks fundamentally are an expansion of artificial neural networks, they use the same basic architecture of a neural network, with layers of interconnected neurons between a surface or input layer and a final output layer. One distinction between deep and artificial neural networks is that deep neural networks use many more layers and nodes than are typical in artificial networks. In addition to deep neural networks, deep learning also encompasses many other types of neural networks, a short list of some network types under deep learning and their descriptions are listed below.

1. **Deep Neural Network (DNN)**. Neural networks with a large number of neurons and hidden layers. From the *Universal Approximation Theorem*, it is known that neural networks are capable function approximators, and were pioneered to do as such [60]. The large network structure of DNNs allows them to be trained more efficiently to approximate a given function [61], in addition to allowing them to approximate more nonlinearities.
2. **Convolutional Neural Network (CNN)**. Neural networks which contain convolutional layers that process the input into a map of features detected. Pioneered in handwritten number detection [62], incorporating convolution into neural networks allows for detecting and utilizing patterns that may exist in the input data.
3. **Recurrent Neural Network (RNN)**. Neural networks that feed their output back as input, or have some form of memory component. Their architecture makes them more applicable to temporal data than other network architectures and is popular for generative predictive sequences in for example text writing [63] and language modelling [64].

Deep learning had several groundbreaking results before practitioners of reinforcement learning managed to apply some of the advances into their own algorithms, such as in the area of computer vision [65], [66], speech recognition [67], [68], and in handwriting generation [63]. These results demonstrated that deep neural networks had the power to use the same raw data which humans perceive, and interpret useful information out of them, or even generate new information. So it seemed only natural to see if it was possible to combine the learning emulation of reinforcement learning, with the world processing emulation of deep learning, to produce machines that could perceive *and* learn from the world just as humans do. This ethos is notably different from that of ADP or ACD, as here the emphasis is on recreating the way in which humans and animals interact with an environment, rather than on extending mathematical theory.

DNNs for Function Approximation

A generic neural network layer can be denoted as a vector function $f(x)$ in the following manner:

$$f(x) = g(\theta x + b) \tag{2.41}$$

With $\boldsymbol{\theta}$ a square weight matrix, b a vector of biases, and $g(\cdot)$ an arbitrary activation function, preferably differentiable. To build a full network such as a DNN, one simply has to use the output of one layer as the input of a subsequent layer:

$$y = h(x) = f_1(f_2(\ldots(f_k(x)))) \tag{2.42}$$

Just as the case in ADP and ACD, when a DNN is being used as the function approximator, the weights and biases parameterizing the network are the values that need to be updated during training. These updates are done in such a way that improvements in estimate accuracy are observed, which can be done by gradient descent.

The specific gradient descent method used to optimize parameters in neural networks is called *back-propagation*, which is the name given to the broad method of determining the derivative of the entire set of parameters. This method uses, the gradient of the network's *loss function* J, which measures the accuracy of the network's prediction, with respect to all the weight and biases of the network, to provide the increment on each parameter that would result in the lowest loss. When $g_k(\cdot)$ is differentiable everywhere, this gradient will always be defined, when that is not the case, numerical errors may propagate through the network update thus differentiability for $g(\cdot)$ is generally desired.

This partial derivative in practice can be calculated very efficiently, as all the information needed is present during one feedforward step of the network.

For the main step of optimizing values of weights and biases, this gradient is used with an optimizer to determine the increment applied to each parameter [69]. A popular option in DRL is Stochastic Gradient Descent (SGD), the stochastic in this optimizer's name refers to the fact that this optimizer uses one training sample to determine a gradient, which is stochastic as the training sample is essentially one realisation of a random process. This single sample gradient is then scaled by a learning rate η SGD is an easy-to-understand and implement optimizer, but is rudimentary in comparison to other optimizers. SGD nonetheless forms the basis for many gradient optimizer algorithms, and the parameter update rule using SGD is shown as follows:

$$\theta_{t+1} = \theta_t - \eta \nabla J(\theta_t) \tag{2.43}$$

One improved optimizer is the Adagrad optimizer, which is based on SGD but features a variable η which adapts to each parameter, such that the size of a parameter's update is based on the frequency that the parameter is updated; these changes make Adagrad particularly suitable when training data is sparse [69].

Finally, when it comes to using DNNs as function approximators, one should keep in mind that they break many of the proven convergence properties that reinforcement learning algorithms would otherwise possess with a linear function approximator, or no function approximation at all [17], [70]. In addition, the optimization problem of finding the optimal function approximator parameters becomes more difficult to solve when using DNNs. For example, the optimization problem is typically multi-modal which means that it is possible for optimization algorithms to be stuck at local optimum. This does not necessarily mean it is infeasible to use DNNs for function approximation, as long as proper hyperparameter tuning and addition of convergence/stability aiding measures are used, as will be made evident in subsequent sections.

2.3.2. Value Based Deep Reinforcement Learning

Value-based DRL algorithms focus on the estimation of the optimal value function $Q^*(s, a)$ using DNNs as function approximators, resulting in an approximate value function $Q(s, a, \theta_c)$ parameterized by some parameters θ_c, and have a relatively simple policy component that picks the action which has the maximum value according to the value estimates, i.e. picks the greedy action. It is sometimes desirable to not always act greedily, and to instead pick the actions estimated to be suboptimal with some small probability ϵ in order to facilitate exploration, a so-called ϵ greedy strategy:

$$\pi'(a|s) = \begin{cases} 1-\epsilon, & \text{if } a = \underset{a}{\text{argmax}}\ Q_\pi(s,a) \\ \epsilon, & \text{otherwise} \end{cases}, \quad 0 < \epsilon < 1 \tag{2.44}$$

Deep Q Network

The first successful DRL algorithm came from the value-based approach, and it was the Deep Q Network (DQN) algorithm [71]. It was a model-free algorithm that managed to successfully use pixel-based sensory input to learn control policies for a series of Atari games. The algorithm is based on Q-learning, in the tabular case this would mean using either the temporal difference learning method or the MC learning method to iteratively update an estimate for the action-value function of all state-action pairs. Here, the dimension of the state space was immense, because frames of gameplay footage are used as pixel-based sensory information. Thus it is logical to use a CNN as a function approximator for the action-value function, called the *Q-network*, instead of discretely recording the action value for every combination. This algorithm had two features that contributed largely to its success, they were: *Expereience Replay* and *Target Network*.

- **Experience Replay** [71]. Deep learning typically assumes samples to be independent, which is untrue for samples in reinforcement learning problems and can result in biases introduced to the Q-network estimates. To reduce the correlation between samples, the agent's experienced transition tuples (s_t, a_t, r_t, s_{t+1}) are stored in a queue memory buffer with a limited size n; and training of the Q-network is done by sampling a transition randomly from this queue, and updating the value estimate associated with the state transition of this sample with the recorded reward.
- **Target Network** [71]. The target here is the value that a value estimate is moved towards, as described in Section 2.1.7. Learning instability can arise when targets change too rapidly, which can be the case if the targets are taken from the estimated Q-network. Hence, a separate *target* Q-network is stored, from which the update targets are retrieved and whose weights are only periodically synchronized with the estimated Q-network. Thus ensuring the targets do not vary drastically from update to update.

The problems that these two features aim to tackle are universal in reinforcement learning, and while other techniques to address these challenges of sample correlation and learning stability exist, the two features augmented to DQN can be useful in other algorithms as well.

Rainbow DQN and other improvements

Many independent experiments and improvements were made to the architecture of DQN and other reinforcement learning algorithms, each of which addressed an issue separate from the other, van Hasselt et al. compiled a list of such ingredients for an algorithm and combined them into one single DQN value based algorithm called Rainbow DQN [72]. These various modules are compiled in the following list:

- **Double Learning** [73]. Originally proposed in the tabular setting, the idea of double learning is to keep and learn two estimates of the value function at the same time, with either one of the two networks being randomly chosen to be trained for any given experience sample. Doing so reduces the value estimates, which are overly optimistic due to the bias arising from the usage of the argmax operator [74].
- **Prioritized Experience Replay** [75]. When learning under the experience replay framework, the transitions from the memory buffer are sampled with uniform probability. This can be suboptimal considering that some transitions do not contain significant information on the environment, and thus do not train the agent as well as it would have been trained if another transition was sampled. By assuming transitions that result in a higher TD error as being more important for learning, and

sampling such transitions with higher probability, it has been shown that an agent's rate of learning improves, i.e. sample efficiency can be raised.

- **Duelling Network Architecture** [76]. A novel neural network architecture, named *duelling architecture*, is adopted to approximate the value function estimates. The duelling architecture is distinguished by the output layer being preceded by two streams of separate hidden layers, the first stream being used to estimate state-value functions, while the second is used to estimate action advantages -a similar variable to the action value-. Preceding these two streams is one common convolutional network, laid out in a similar manner as the convolutional layers in the original DQN algorithm. By utilizing this duelling architecture, the complexity of learning for the neural network is reduced, which contributes towards higher sample efficiency and better agent performance.
- **Multi-step Bootstrapping** [17], [77]. The basic approach in bootstrap learning algorithms and thus in most value-based methods is to use the reward from a single transition as the learning target. As suggested by Sutton [78] and corroborated in ADP research [35], taking multiple timesteps worth of transitions to form a learning target can produce faster learning rate, as it allows rewards to be propagated throughout the domain of the estimate faster [78]. This variation was used on four standard algorithms by Mnih et al. [77], where the idea was brought further to using transitions from several asynchronously trained agents, which defined a class of asynchronous algorithms with agents trained on separate computing units.
- **Distributional Learning** [79], [80]. Whereas the traditional reinforcement learning paradigm is concerned with *expected* values, there is also a view that studying the distribution of values can be incorporated into learners, which should allow for more risk-aware behaviours, and intuitively allow agents to make use of more information than merely the expectation of a random variable. A commonly used analogy is that distributional learning is to treat the environment observations as fully coloured pictures, while expectational learning is to treat them as black-and-white pictures. To make use of distributional reinforcement learning, an estimate for the distribution of returns and thus of the state or action-values are learned, specifically the first and second moments of the distribution [79].
- **Noisy networks** [81]. The problem of exploration vs exploitation is important for algorithms to address, noisey networks seek to provide a means of finetuning the degree of exploration built into an algorithm. A noisy network is made by adding random values to the weights and biases to any neural network, which can be done to any given network as well as other forms of function approximators. The advantage that such an augmentation brings to algorithms is by allowing estimates to escape local optima, increasing the likelihood of encountering the global optimum by traversing the domain more broadly.

2.3.3. Policy Based Deep Reinforcement Learning

Policy-based methods, also known as policy search methods, primarily optimize the policy of an agent as opposed to the value function, and can select actions without the need to consult value functions, but can reap benefits by simultaneously estimating values as will be discussed in Section 2.3.4. The policy $\pi(a|s, \theta_a)$ in such methods is approximated with a DNN parameterized with the parameters θ_a. By training for an optimal policy directly, instead of training a value function on which a policy will be inferred, one layer of complexity is removed from the training task.

The foundation of policy-based methods is based upon the *policy gradient theorem*, which is an analytical expression derived from the Bellman equations of Equation 2.10 which defines the gradient of a policy's performance or optimality with respect to the policy parameters, this gradient is called the *policy gradient*. According to this theorem, the following proportionality for the gradient of a policy's loss holds true:

$$\nabla J(\theta_a) \propto \sum_s \mu(s) \sum_a q_\pi(s,a) \nabla \pi(a|s,\theta_a) \tag{2.45}$$

Where $\mu(s)$ is the state distribution which describes the importance of each state, which is related to how often a state is visited, and thus is theoretically a function of the policy parameters since the policy decides what action and thus what states might be visited. The Important result of this theorem is that this expression shows that policy gradient does not require taking the gradient of $\mu(s)$, despite it being technically a function of policy parameters, which makes it much easier to implement gradient descent routines to optimize a policy [17].

REINFORCE

The simplest form of policy-based method is called REINFORCE, which is an acronym for the form of the algorithm: REward Increment = Nonnegative Factor $\times$ Offset Reinforcement $\times$ Characteristic Eligibility [82]. REINFORCE uses the MC learning approach to train its policy network, where the parameter updates to the policy are only performed at the end of each episode. The parameter update rule of REINFORCE is expressed as follows [17]:

$$\theta_{t+1} = \theta_t + \eta G_t \nabla \ln(\pi(A_t|S_t, \theta_t)) \tag{2.46}$$

In this update rule, every parameter update is proportional to the return observed G_t for each state-action pair $S_t A_t$., and it is in the direction of the vector represented by $\nabla\ln()$, which is the direction in parameter space that contains policies which have a higher likelihood of repeating action A_t when in state S_t. This update is thus logical since if a state action pair has a high return, it would be beneficial to update the policy to enact such actions more, which is exactly what the update term in Equation 2.46 does.

Trust Region-policy Optimization

The theoretical convergence properties of REINFORCE are very positive, in the expectation this algorithm is guaranteed to improve the policy [17], [82]. In practice, algorithms revolving around the REINFORCE framework have very low sample efficiency and thus are slow to converge, in addition to high variance in learning rate. One way of circumventing these deficiencies is to incorporate baselines that modulate the magnitude of policy parameter updates, thus reducing learning variance. An extension of this idea is the TRPO algorithm proposed by Schulman et al.

TRPO effectively reduces the variance of policy updates through constraining update steps when the parameter updates are too aggressive [83], this aggressiveness is determined by measuring the distance between the original policy and the updated policy. Since a policy function is a probability distribution, measuring the distance between policies thus requires using probability distance measures, in the case of TRPO this distance measure is the Kullback-Leibler (KL) divergence; returning a scalar value representing how different the two probability distributions are [84].

This algorithm casts the policy-gradient method as an optimization problem, which is formulated as follows:

$$\begin{aligned} &\underset{\theta_a}{\text{maximize}} \ \mathbb{E}\left[\frac{\pi(a|s,\theta_a)}{\pi(a|s,\theta_{a,old})} Q_{\pi_{old}}(s,a)\right] \\ &\text{subject to} \ \mathbb{E}\big[D_{KL}\big(\pi(\cdot|s,\theta_a)||\pi(\cdot|s,\theta_{a,old})\big)\big] \leq \delta \end{aligned} \tag{2.47}$$

Being a policy-based method, no function is used to approximate the action-values $Q_\pi(s,a)$. Instead, π is executed over some number of time steps generating a trajectory, and these values are estimated using samples from the trajectory.

Formulating the policy learning problem as an optimization problem is noticeably divergent from all algorithms thus far presented, indeed this approach of addressing the reinforcement learning problem is a field of research in itself, such as in the DRL subfield of policy search [85] and evolutionary reinforcement learning [86]. The optimization problem from Equation 2.47 is then solved using conjugate gradient optimization algorithms. The specific optimization algorithm proposed by Schulman et al to solve the TRPO problem uses Hessian matrices and thus can be considered to be a second-order algorithm.

Despite the reduced learning variance benefits that this algorithm has over REINFORCE, TRPO remains complicated to implement, uses the KL divergence measure which is computationally expensive due to the optimization algorithm posed, while suffering from slow learning rates [87]. Hence, more augmentations were proposed.

Proximal Policy Optimization

When the policy-gradient algorithms were cast into an optimization problem, as done by Schulman et al. through TRPO, this opened up new possibilities for making changes to policy-gradient algorithms. For one, instead of posing a constrained optimization problem as done in Equation 2.47, an unconstrained optimization problem can be formulated by stating the optimization constraints as penalties in the objective function being maximized, resulting in the optimization problem posed by Equation 2.48 with a tunable parameter β.

$$\underset{\theta_a}{\text{maximize}} \ \mathbb{E}\left[\frac{\pi(a|s,\theta_a)}{\pi(a|s,\theta_{a,old})}A_{\pi_{old}}(s,a) - \beta D_{KL}[\pi(\cdot|s,\theta_a)||\pi(\cdot|s,\theta_{a,old})]\right] \tag{2.48}$$

In fact, Equation 2.48 is the optimization problem suggested by the theory which justifies TRPO [87]. However, the presence of β makes this objective function difficult to define, thus surrogate objective functions are formulated to pose essentially the same optimization problem as Equation 2.48. Such a surrogate objective function $J_{CLIP}(\boldsymbol{\theta}_a)$ is defined in Equation 2.49, it has a tunable parameter ϵ and uses the *advantage function* $A_\pi(s,a)$, and is the loss function that creates the PPO algorithm.

$$\underset{\theta_a}{\text{maximize}} \ J_{CLIP}(\theta_a) = \mathbb{E}\left[\min\Big(r(\theta_a), \text{clip}\big(r(\theta_a); 1-\epsilon, 1+\epsilon\big)\Big)A_{\pi_{old}}(s,a)\right] \tag{2.49}$$

$$\text{Where} \quad r(\theta_a) = \frac{\pi(a|s,\theta_a)}{\pi(a|s,\theta_{a,old})}, \quad A_\pi(s,a) = Q_\pi(s,a) - V_\pi(s)$$

Just like TRPO, PPO uses samples from generated trajectories to estimate the advantage function values. By using $J_{CLIP}(\theta_a)$, first-order optimization techniques such as SGD can be adopted, which are much more computationally efficient than second-order techniques. It is with such an objective function that PPO can have the variance reduction of TRPO but with better computational complexity and empirically better sample efficiency as shown in Figure 2.5.

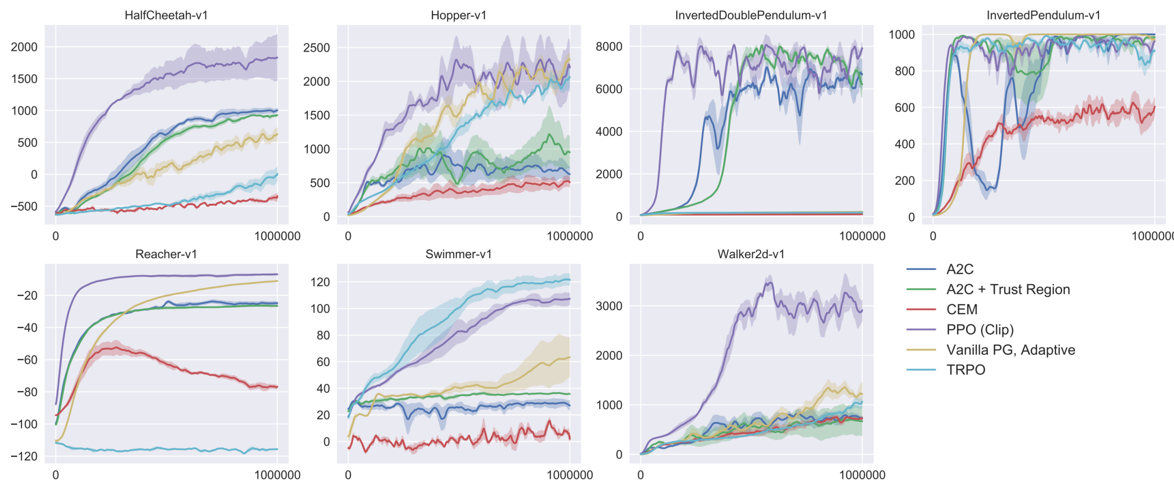

Figure 2.5: Comparison of PPO with TRPO and various other algorithms on several benchmark environments, taken from [87]

2.3.4. Actor Critic Deep Reinforcement Learning

With both value-based and policy-based methods introduced, the backdrop is set for actor-critic methods. In both these predecessor methods, either the value function or the policy is being approximated by a DNN, this has the big disadvantage of still being ham-strung by the curse of dimensionality when either action or state space is large. Specifically, value-based methods can perform well when the state space is large and the action space is small, while policy-based methods perform well when the action space is large and the state space is small.

For continuous control problems with continuous state and action spaces, both cases are true. The logical solution is, therefore, to use function approximators for both value and policy functions, with DNN being a popular approximator candidate. This architecture is called *actor-critic*, where the *actor* refers to the policy or the DNN approximating the policy, and *critic* refers to the value function or the approximating DNN. When neural networks are used, the actor or critic is also referred to as the actor-network or critic-network.

Moreover, because the actor-critic method models both value and policy functions, such methods typically involve improving one function after the other. This structure is reminiscent of the generalized policy iteration idea from dynamic programming, mentioned in Section 2.2.2, showing that interestingly many ideas within reinforcement learning build upon and are related to one another.

Deep Deterministic Policy Gradient

Lillicrap et al. identified many of the same problems stated in this subsection's introduction, and combined the experience replay and target network ideas of DQN for value function training, along with the ability of policy-based algorithm to handle continuous action spaces, to build the actor-critic algorithm known as DDPG [88].

The core algorithm of DDPG is based on Deterministic Policy Gradient (DPG), this algorithm is already an actor-critic algorithm but does not use deep neural networks for any function approximation, hence the lack of *deep* in DPG. DPG uses a deterministic policy as opposed to a stochastic policy, this results in more efficient gradient determinations as the gradient of deterministic policies only requires integrating over the state-space, rather than over the state-*action*-space which is required for gradients of stochastic policies [70]. An intuitive explanation behind this difference is that stochastic policies have a non-zero probability of taking each action in the action-space, thus to evaluate the change in optimality of such a policy, it is necessary to consider the entire action space, the same is not true for deterministic policies since they can only take one action for any given state.

DPG in its original form is incompatible with using DNN for function approximation, as using such approximations results in the applied gradient computations becoming incorrect estimations of the true policy gradient [70]. However, by applying the tricks of experience replay and target networks from DQN, DDPG is able to extend DPG to employ DNN for function approximation as well. Specifically, Lilicrap et al. used replay buffers to train their actor and critic-networks, in addition to creating target networks for both the critic and actor thus stabilizing learning.

The crux of DDPG algorithm is in how it trains the actor and critic. This is done by sampling a minibatch of N transition tuples $(s_i, a_i, s_{i+1}, r_i)$from the replay buffer, and using this minibatch of samples to determine the loss function of Equation 2.50 which the critic is trained to minimize, and the policy gradient Equation 2.52 used to update the actor.

$$J_c = \frac{1}{N}\sum_i (y_i - Q(s_i, a_i, \theta_c))^2 \tag{2.50}$$

$$y_i = r_i + \gamma Q(s_i, \pi(s_{i+1}, \theta_a^T), \theta_c^T) \tag{2.51}$$

$$\nabla_{\theta_a} J_a = \frac{1}{N}\sum_i \nabla_a Q\big(s_i, \pi(s_i, \theta_a), \theta_c\big)\nabla_{\theta_a}\pi(s_i, \theta_a) \tag{2.52}$$

$$\text{Where} \quad \theta^T = \text{ target network parameters}$$

A noteworthy achievement of the DDPG algorithm is that it was able to yield a useful reinforcement learning agent despite being prone to the deadly triad; DDPG uses function approximations, it updates the critic-network through a TD like method, and it is an off-policy method due to using experience replay for training. Demonstrating superior performance than DPG on which it was based [88].

Twin Delayed DDPG

One problem with DDPG is shown to be inherited from value-based methods by Fujimoto et al. [89], and this is the over-optimism of value function estimates in the critic-network. Within the realm of value-based research, this issue has already been addressed through the introduction of double learning by van

Hasselt [74], with duplicate value networks. This is not to be confused with the duplicate networks of the target-network solution which deliberately slows down training of the target network, while double training randomly selects one of the duplicate networks for training.

Fujimoto et al. thus introduced double learning to DDPG by training two critic-networks at the same time, resulting in the Twin Delayed Deep Deterministic policy gradient (TD3) algorithm [89]. In addition to using double learning, TD3 also improved over DDPG in two more ways. Firstly, the updates to the actor and critic are made asynchronous, with the value estimates of the critic being updated at a higher rate than the actor's policy, which mitigated the occurrence of divergent updates to policy parameters and constitutes the *delayed* part in the name of TD3.

The second improvement is to add a bit of noise to the critic learning. In DDPG the critic is trained using a TD learning approach with a learning target being obtained using the deterministic actor, introducing this determinism into the learning target can cause value-learning to suffer from high variance. Thus to combat this variance, the learning target for the critic is instead not picked using only the deterministic action from the actor, but with some noise added to the action before the learning target is retrieved from the critic. Which can be done by changing the formulation of Equation 2.51 to add some clipped random variable ϵ, which for example can be distributed normally $\epsilon \sim clip(\mathcal{N}(0, 0.1), -c, c)$, resulting in the reformulated learning target y_i being:

$$y_i = r_i + \gamma Q\big(s_i, \pi(s_{i+1}, \theta_a^T) + \epsilon, \theta_c^T\big) \tag{2.53}$$

Soft Actor Critic

Around the same time but independent of the efforts of Fujimoto et al., Haarnoja et al. [90] posed an alternative set of improvements to DDPG which culminated in the Soft Actor Critic (SAC) algorithm.

As opposed to the algorithms discussed thus far, SAC uses the unique goal maximizing return and randomness simultaneously, which is an approach called *maximum entropy reinforcement learning* [91]. In this framework, the optimality of a policy is measured not solely by the expected return, but by an expectation over the sum of return and entropy:

$$J(\pi) = \sum_t \mathbb{E}[r_t + \underbrace{\alpha\mathcal{H}(\pi(s_t))}_{\text{entropy of policy}}] \tag{2.54}$$

Where α is a temperature parameter that weighs how important being random is, and the entropy function $\mathcal{H}$ measures how random a policy is. Formulating such a loss function leads to the agent seeking to learn the most rewarding policy which is also most stochastic, Such a policy is crucial in the early stages of training, as it allows an agent to explore state and actions more widely thanks to the loss function favouring random actions, which can increase the odds of finding a near-globally optimal policy. Logically, if a deterministic policy was used, then this improvement would not have contributed to any changes in the algorithm's behaviour. Thus, Haarnoja et al. returned to using stochastic policies for the actor-network, in SAC the policy is modelled as a multivariate but diagonal Gaussian, with the actor-network outputs being the Gaussian's mean and covariance.

In addition to adopting a maximum entropy framework to evaluate its policy, SAC also uses several of the improvements present in TD3. This includes the double action-value learning trick introduced by van Hasselt [74], where just like in TD3 two action values are trained simultaneously, and a less optimistic value estimate is taken by sampling the minimum action value from the two critics when calculating the learning target for a given state-action pair.

Just like Rainbow DQN, SAC can be extended to a distributional version, known as Distributional SAC (DSAC), which was shown to provide better sample efficiency over SAC on benchmark problems [92].

2.4. Flight Control by Reinforcement Learning

In recent years, various deep reinforcement learning algorithms have been applied to the task of flight control. These algorithms have been used to train flight controllers for several aircraft types, including fixed-wing aircraft, quadcopters, and helicopters.

2.4.1. Flight Control as an MDP

The goal of this thesis is to develop an intelligent flight control system for the PH-LAB, thus it is important to understand how the flight control problem is formulated, and how that can be translated into a problem that a reinforcement learning agent can handle.

Formulating the MDP

The flight control environment is constituted of two components: the flight dynamics, and the reference trajectory. The flight dynamics component receives the action from the agent and computes how the aircraft states evolved, and then the target state that the aircraft should have is obtained from the reference trajectory. To arrive at the states and rewards of the MDP, this target and actual state are combined to produce the process's states and rewards. The specific way in which they are combined depends on the design of the MDP.

As an example, in Dally and van Kampen's work [3], the states x of the aircraft are shown in Equation 2.55, and the reference trajectory adopted defines targets for the sideslip, pitch, and roll states, as shown in Equation 2.56. In this work, two reinforcement learning controllers are implemented, meaning there are two MDPs to be defined here, for simplicity's sake this explanation will concern itself with only one controller: the attitude controller. To define the MDP states for this agent, the aircraft states x and reference trajectory x_{ref} are first combined to produce an error vector e, defined in Equation 2.57. This error vector is then weighted producing e_w, and concatenated with the aircraft's current control surface deflections and aircraft attitude rates, to produce the MDP states s shown in Equation 2.58. The inclusion of the control surface deflections may seem redundant, however, it was necessary in the case of this controller due to the agent only providing *increments* to the control surface deflections; thus providing the agent with knowledge of what current deflections are, gave more context on what increments should be fed back to the aircraft. The reward r of this MDP is then created by using e_w, which is clipped to $[-1, 0]$, the norm of it taken and scaled, as shown in Equation 2.59.

$$x = \begin{bmatrix} p & q & r & V & \alpha & \beta & \theta & \phi & \psi & h \end{bmatrix}^\top \tag{2.55}$$

$$x_{ref} = \begin{bmatrix} \beta_{ref} & \theta_{ref} & \psi_{ref} \end{bmatrix}^\top \tag{2.56}$$

$$e = \begin{bmatrix} \beta_{ref} - \beta & \theta_{ref} - \theta & \psi_{ref} - \psi \end{bmatrix}^\top \tag{2.57}$$

$$s = \begin{bmatrix} e_w^\top & \delta_a & \delta_e & \delta_r & p & q & r \end{bmatrix}^\top \tag{2.58}$$

$$r = -\frac{1}{3}\|\text{clip}(e_w, -1, 0)\| \tag{2.59}$$

Modelling Flight Dynamics

A flight dynamics model in its general form is modelled as two systems of ordinary differential equations which are functions of a vector of states x and a vector of inputs u. The first system models the derivative of the states $\dot{x}$ at any given time for the given state and inputs using the state transition functions $f(\cdot)$, whereas the second system models observations y using the observation equations $g(\cdot)$, which is how states are observed from the aircraft in a real-life system where the states are not necessarily directly known. Such a representation is shown in Equation 2.60

$$\begin{aligned} \dot{x} &= f(x, u) \\ y &= g(x, u) \end{aligned} \tag{2.60}$$

These differential equations describe the motion of an aircraft in three-dimensional continuous space, but the motion has six degrees of freedom where three degrees belong to the translational motions and the remainder for rotational motions. The states of these equations typically consist of the aircraft's position p, velocity v, attitude a, and attitude rates $\mathbf{\Omega}$:

$$x = \begin{bmatrix} pos & v & a & \Omega \end{bmatrix}^T$$

$$\text{Where} \quad pos = \begin{bmatrix} x & y & z \end{bmatrix}^\top \quad v = \begin{bmatrix} u & v & w \end{bmatrix}^\top \quad a = \begin{bmatrix} \phi & \theta & \psi \end{bmatrix}^\top \quad \Omega = \begin{bmatrix} p & q & r \end{bmatrix}^\top$$

The inputs vector u typically consists of the control surface deflections $\delta_a, \delta_e, \delta_r$, thrust settings T. They are typically bounded by physical limits, which are referred to as saturation limits:

$$\begin{aligned} & u = \begin{bmatrix} \delta_a & \delta_e & \delta_r & T \end{bmatrix}^\top \\ \text{Subject to} \quad & u_{min} \leq u \leq u_{max} \end{aligned}$$

This way of modelling system dynamics is called a *state-space* representation, which is signified by the use of first-order differential equations to model the evolution of states over time. The state-space representation of an aircraft can be formulated using nonlinear dynamics, which is implied when the state transition functions are denoted using lowercase f and are a function of states and/or inputs. It can also be modelled using fully linear dynamics, which is referred to as a Linear Time-invariant (LTI) model when the model parameters stay fixed over time, where the system is denoted in the following manner:

$$\begin{aligned} \dot{x} &= Ax + Bu \\ y &= Cx + Du \end{aligned} \tag{2.61}$$

Where A, B, C, D are referred to as the state transition matrix, the input matrix, the output matrix, and the feedforward matrix respectively. LTI serves as a very useful tool, as it allows for many standard flight control design and evaluation practices to be employed. For example, they allow robust control techniques to be readily applied as the theory of $\mathcal{H}_\infty$ synthesis is founded on theory applicable only to linear systems, they allow for feedback gains to be readily calculated and thus for feedback controllers to be quickly developed, and they allow for the stability of the aircraft to be quickly analyzed by simple computation of the eigenvalues of the system [93]. A time-varying version of the linear state-space model is used in the incremental ACD case, where the A, B matrices would have different parameters over time.

To make these models useful for computing the states of the aircraft needed for an MDP, system state derivatives are integrated to compute the states in the next time step. This procedure can be simplified and a discrete version of Equation 2.60 obtained, defining the states and observations of the next time step:

$$\begin{aligned} x_{t+1} &= f(x_t, u_t) \\ y_t &= g(x_t, u_t) \end{aligned} \tag{2.62}$$

Finally, the deterministic form shown in Equation 2.62 is Markovian, as the states and inputs from the current timestep t are enough to predict the states and observations for the next timestep $t + 1$. The Markovian property remains even when stochasticity is introduced as long as no time correlation is present in this noise, methods do nonetheless exist that allow pseudo-time-correlated noise to be introduced to the model while remaining Markovian [94].

2.4.2. Learning to Fly

Flight control poses a formidable environment for reinforcement learning agents to excel in. The level of difficulty varies between aircraft designs, in agile aircraft such as fighter planes, the dynamics of such vehicles are designed to be highly unstable [95]–[97] to allow for performing fast manoeuvres with the least amount of control input, but as a result, such aircraft are demanding to control for pilots. In contrast, commercial airliners are designed to be stable and easy to control [98], [99], and thus offer a less harsh learning environment for an agent. Additionally, the coupled nature between control actions in one axis and state changes in a separate axis makes the control problem a high-dimensional and non-linear one, which adds to the challenge for reinforcement learning agents to learn to control an aircraft.

DRL Focused Research in RL for Flight Control

One of the earliest works to apply reinforcement learning to flight control was by Abbeel et al. [100], who formulated an LQR problem for the task of acrobatic helicopter flights and used a specific instance of reinforcement learning named differential dynamic programming to solve for the posed LQR's optimal policy. The result was a controller which can perform acrobatic manoeuvres such as flips and rolls, manoeuvres that are challenging even for human pilots.

DDPG appears to be a popular DRL algorithm applied to flight control. Fei et al. [101] managed to apply DDPG, specifically a benchmark implementation by Duan et al. [102][1], to the flight control of a flapping wing robot. This DDPG agent was trained to copy the extreme manoeuvre which hummingbirds can execute during fast escapes and managed to replicate the manoeuvre. DDPG was also adopted by De Marco et al. [103] in their research into flight control for an F-16 in a flight simulation, here the agent is trained to successfully fly an F-16 in a sequence of agile turns and manoeuvres with highly coupled dynamics, under the presence of sensor noise. The trained agent was duplicated and placed in a simulation of a prey-chaser scenario, where a prey agent was given a sequence of waypoints to follow, and a chaser agent was given the task of catching up to the prey, showing an interesting case of multi-agent interaction. Screenshots of this scenario are shown in Figure 2.6.

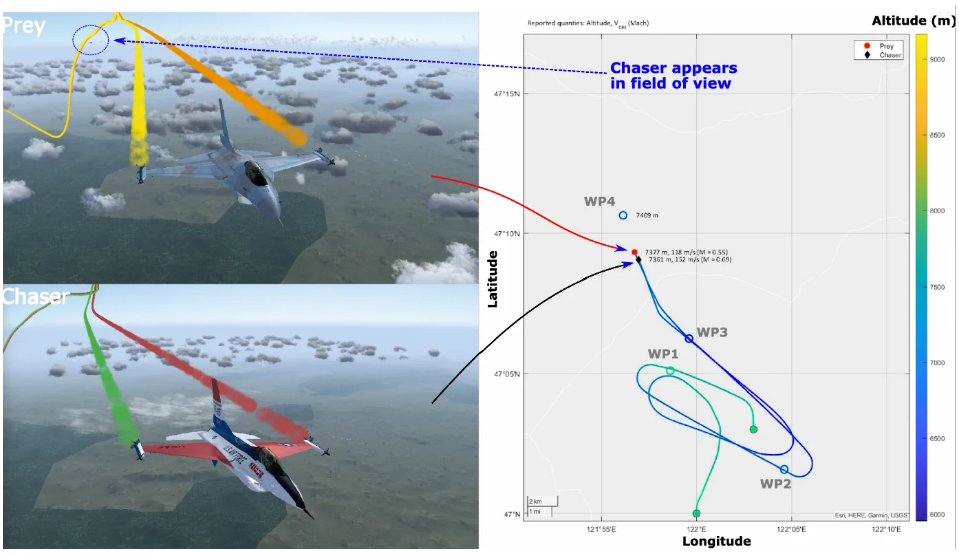

Figure 2.6: F-16 chaser simulation with DDPG pilots, screenshots of the jets in flight and their flight paths. Taken from [103]

This algorithm was also applied to the autonomous landing of fixed-wing aircraft in [104] and longitudinal control augmentation in [105].

The improved version of DDPG, namely SAC, also demonstrated success when applied to flight control. Dally and van Kampen developed a flight controller for a Cessna Citation 500 aircraft trained using SAC, alluded to in Section 2.4.1. The control structure used in this research was cascaded, while the overall controller controlled the aircraft's altitude, roll, and sideslip angle, the task was delegated to an inner and outer controller. The outer SAC controller handled altitude control by taking in reference altitude and providing a reference pitch angle for the subsequent inner SAC controller, which handled attitude control by taking in the reference pitch, roll, and sideslip, and providing control surface deflection increment commands to the aircraft. The SAC controller proved to be robust and fault-tolerant, wherein it remained performant in the face of gust disturbances, jammed or reduced effectiveness control surfaces, and loss of the horizontal tailplane. This research was followed by various efforts further supporting the ability of DRL based controllers at flight control. Such as the works of Seres et al. [106] on a DSAC based controller, which is the distributional extension of an SAC algorithm. This algorithm remedied some of the obstacles that were observed by Dally and van Kampen in the training of an SAC flight controller. Specifically, SAC was found to provide much better training stability than SAC, showing that during training DSAC produced lower variance across different training runs at an earlier point than SAC.

The main focus of this present research is on studying how to improve the fault tolerance of flight controllers through reinforcement learning methods. To this end, the works of Dally and van Kampen [3] show promise for continuing the development of SAC. Interestingly, research from Zahmatkesh et al.

[1] Implementations available at `https://github.com/rlworkgroup/garage`

[107] shows that some degree of fault tolerance can also be achieved when coupling a discrete Q-learning algorithm with fuzzy logic, a solution which was proposed to overcome the curse of dimensionality and bridge the gap between continuous state-action space and discrete Q function domain.

ADP Focused Research in RL for Flight Control

Parallel to DRL approaches, there are also many efforts focusing on the use of ADP and ACD algorithms for the task of flight control, which possess a distinct difference in how they handle control than DRL algorithms. As mentioned in Section 2.2.4, ACD algorithms are sample efficient enough for their parameters to converge within one training episode, this is notably true for incremental-ACD algorithms such as the IDHP [52].

Enns and Si [108] produced work on using neural dynamic methods for control of a helicopter and trimming of its dynamics. This work is likely to be the first work where ADP was applied to continuous time-uncertain systems, and demonstrated that it is feasible to apply ADP techniques to flight control of realistic systems in realistic control problems. In the following year, Stengel and Ferrari [109] presented a method for training an ADP based controller using gain scheduled PID controllers obtained a-priori in an offline phase, in addition to continually training the controller in an online phase using DHP. This work leveraged optimal control theory heavily to produce an algorithm which does has less reliance on more heuristic methods such as neural network optimization with gradient descent, and brings more theoretical guarantees to the optimality of the critic function in the offline trained controller.

Li et al. [110] demonstrated that a combination of IDHP and nonlinear dynamic inversion techniques to control a tailless aircraft's attitude can quickly adapt its critic and actor parameters after a sudden deformation of the wings and damage to elevators, maintaining high accuracy in its tracking performance before and after the onset of faults. In purely IDHP implementations, the performance of the algorithm is promising in simple systems, for example in Zhou et al. [52] where a nonlinear short-period longitudinal model of an aircraft is used as the MDP environment, here IDHP was able to continue tracking a sinusoidal reference angle of attack despite the dynamic coefficients of the system changing signs during testing, which represents an effective inversion of the aircraft dynamics.

When a pure IDHP controller is applied to more complicated systems such as a full six degrees of freedom simulation and a more difficult control task such as altitude tracking, where delays between actuator input and state response are more delayed, the actor and critic would at times diverge resulting in erratic control of the aircraft. Such observations were demonstrated by Lee and van Kampen [111], where an IDHP agent served as both the outer and inner loop controller in an altitude tracking task. This occasional non-convergence can be tackled through the use of target training networks, a concept borrowed from DQN which allows the learning of actor and critic-networks parameters to stabilize, and has been implemented by Heyer et al. [4] to significantly improve convergence rate. The implementation from Heyer et al. is, however, not purely IDHP, as outer loop control is performed with a PID controller instead, thus it remains a question as to how well target networks may help stabilize a pure IDHP controller. Besides improving stability of the online ACD controller, Teirlinck and van Kampen [112] showed that it is possible to merge the DRL and ACD approaches in one controller, where the DRL algorithm in the form of SAC provided a robust controller on which IDHP could be augmented, to reap the benefits of both the high generalization power of DRL control and online adaptive power of ACD. This resulted in a hybrid controller that demonstrated improved fault tolerance over a purely SAC based controller and lowered divergence than a pure IDHP controller.

For simpler tasks such as rate control, where state response exhibits a much quicker reaction to actuator inputs, ADP based controllers can provide very good tracking accuracy even in the presence of noise and imperfect observations [113]. This controller was further developed and evaluated in flight tests on a Cessna Citation aircraft, where it was able to successfully perform roll and pitch rate tracking.

Research Gaps

Regarding the topic of fault tolerance. Much work has been dedicated to improving and demonstrating the robust flight qualities which DRL can provide, a consequence of being able to train the agents in an offline and safe environment for extended durations. For instance, the SAC based altitude, pitch, and sideslip tracking controller by Dally and van Kampen were given approximately 10^6 timesteps of training each at a step size of $0.01s$ before controller evaluation, corresponding to roughly 2.8 hours of flight experience or 500 training episodes each containing $20s$ of flight time. Whereas ADP based flight controllers can converge towards an optimal control policy well within the duration of a $60s$ flight [4]. Furthermore, there remain unexplored ideas for extending ACD algorithms. In early reinforcement learning algorithms such as the TD(λ) by Sutton [78], and in more recent ADP research [35], [36], [38], [114], [115], the idea of using more than one transition or timestep's worth of information to perform actor or critic optimization allowed algorithms to be created which spanned the spectrum of using TD-like learning targets, or using MC-like learning targets, resulting in a degree of freedom that gave designers more ability to optimize performance of algorithms. Such ideas revolved around either explicitly using multiple timesteps of information to perform network updates, such as in multi-step ADP methods [35], [36], or eligibility trace updates [114], [115]. These ideas have not been applied to the case of IDHP algorithms just yet, and it remains an open but interesting question whether they can work under the incremental ACD framework, or better yet yield more optimal algorithms.

2.5. Synopsis

This chapter presented the literature and ideas that will form the basis of the present research and helped to answer the first of the research questions posed: **Q1**.

To understand the field of reinforcement learning, this chapter surveyed the various classes of algorithms that are present in reinforcement learning, such as incremental-ACD algorithms and actor-critic algorithms, as well as the techniques developed to push the performance of algorithms further. For instance, one of the main issues related to reinforcement learning algorithms, in both DRL and ADP cases is learning stability of actor and or critic-networks, and a solution that is effective in both is the use of target networks. Furthermore, algorithms can be made more advanced by combining previously developed algorithms with novel augmentations, as is done in the case of Rainbow DQN. A tree diagram summarizing various reinforcement learning algorithms, from the basic to state-of-the-art is summarized in Figure 2.7. With these findings, *Q1.1* of the stated research questions is answered.

From the works of Dally and van Kampen, Teirlinck and van Kampen, amongst others, inspiration for how fault tolerance is defined and tested can be gathered. For instance, a controller may be tested for fault tolerance by observing the tracking performance after the onset of faults, which can be done quantitatively by measuring some error between reference and actual aircraft states. To introduce faults, the dynamics model of the aircraft may be adjusted to reflect a corresponding failure mode, such as reducing the magnitude of the control derivative of ailerons to reduce damaged aileron surfaces. Thus, *Q1.2* is answered.

A survey of the same research also provided insight into how various algorithms perform when it comes to fault tolerance and tracking performance. While it's difficult to definitively say what algorithm has the absolute best fault tolerance, it is noted that SAC controllers are shown to have handled a wider array of faults than IDHP controllers, but IDHP showed that the ability to vary controller parameters mid-flight is an invaluable advantage in providing fault tolerance, while both classes of algorithms overall demonstrating comparable tracking accuracy in complex control tasks. These findings help answer *Q1.3, Q1.4*.

Finally, several potential avenues for augmenting reinforcement learning algorithms were discovered. The two main augmentations were eligibility traces and multi-step updates. From literature, it was identified that incorporating existing algorithms with such augmentations can improve the sample efficiency and rate at which agents converge to good policies and value functions. Therefore, these two augmentations will be further researched and incorporated into IDHP, thus answering *Q1.5*.

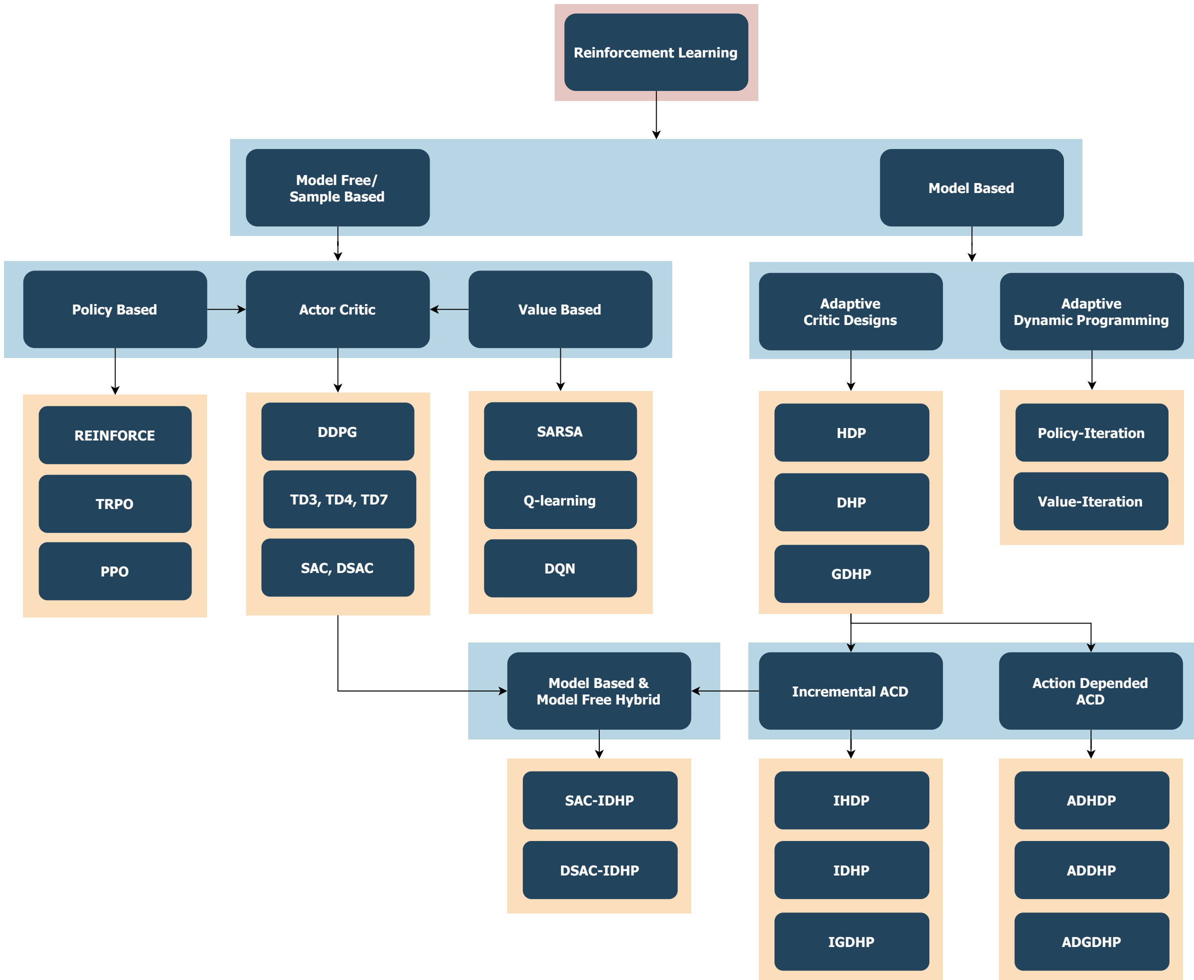

Figure 2.7: Overview of various reinforcement learning algorithms that have been encountered when compiling this literature study, light blue box presents the class of algorithms, light orange box presents reinforcement learning algorithms.

3

Preliminary Results

This thesis proposes two main augmentations to be made to the IDHP reinforcement learning algorithm and presents results on how they influence the behaviour of a IDHP based flight controller, in terms of its fault tolerance characteristics and tracking performance.

First, the MDP on which experiments are conducted is introduced and defined in Section 3.1. Second, the IDHP algorithm which was presented in Chapter 2 will be elaborated on and described in detail in Section 3.2. Third, the augmentations proposed to be made to the IDHP algorithm are to be explained in Section 3.3. These two sections are followed by Section 3.4 which defines the IDHP algorithm itself through Algorithm 5. The chapter is then concluded by Section 3.6 which presents the results gathered from experimenting with the proposed augmentations, in addition to discussions on note-worthy results; then Section 3.7 will succeed the results and discussion section to provide a conclusion of the observed results from the experiments.

3.1. Markov Decision Process Definition

The reinforcement learning agents will be tested on a simple MDP which has few states, few actions, and simple dynamics to evaluate and compare their performances. By choosing a simpler MDP, the runtime of simulations can be shorter. But more importantly, the difficulty of implementing a minimal working example of the agents will be minimized, as more developmental effort can be diverted away from implementing the environment: which would be less demanding due to its simplicity. This is beneficial for rapid prototyping and fine-tuning, making it easier to make preliminary judgements. This MDP is centred around a flight control problem, and its details will be explained in the remainder of this section.

3.1.1. Aircraft Model and Control Task

The system on which the algorithms are to be applied is the TUDelft NLR research aircraft PH-LAB, a Cessna Citation II single-aisle business jet modified for flight testing and research purposes. The Control and Simulations group of TUDelft has carried out dynamics modelling of this aircraft. Subsequently, these dynamics are linearized and reduced into an LTI model of the short-period motion of the aircraft.

While there are many ways in which aircraft flight dynamics can be simplified each resulting in different models, the short-period motion simplifications are chosen primarily for consistency with other research done on reinforcement learning for flight control within the Control and Simulations group.

To obtain this model, the nonlinear 6-DOF flight dynamics are first linearized and decoupled into the asymmetric and symmetric motions, under the assumption that the dynamics of the states in one motion are unaffected by the second motion and vice-versa. The asymmetric motions are discarded, and the symmetric motions are further simplified to capture only the short-period eigenmotion of an aircraft. This is done using the following two assumptions:

- Airspeed remains constant throughout the eigenmotion, hence airspeed dynamics and thrust input can be omitted.
- Flight path of the aircraft remains level throughout the eigenmotion, hence pitch dynamics θ can be omitted.

This results in a simplified model containing only α and q states with elevator deflection δ_e as sole input. This LTI model is shown in Equation 3.1, and the definitions of the coefficients are shown in Equation 3.2. To obtain the value of these coefficients, a nonlinear model of the Cessna Citation is first linearized around a chosen operating point, which allows the values of these relevant control and stability derivatives to be determined. This procedure was carried out by the Control & Simulations group at TU Delft [116]. The operating point which the nonlinear model is linearized around is at steady cruising condition, and the values of the resulting coefficients are presented in Table 3.1.

$$\begin{aligned} \dot{x} &= Ax + Ba \\ \Rightarrow \begin{bmatrix} \dot{\alpha} \\ \dot{q} \end{bmatrix} &= \begin{bmatrix} z_\alpha & z_q \\ m_\alpha & m_q \end{bmatrix} \begin{bmatrix} \alpha \\ q \end{bmatrix} + \begin{bmatrix} z_{\delta_e} \\ m_{\delta_e} \end{bmatrix} \delta_e \end{aligned} \tag{3.1}$$

$$\begin{aligned} z_\alpha &= \frac{V}{\bar{c}} \frac{C_{Z_\alpha}}{2\mu_c - C_{Z_{\dot{\alpha}}}} & m_\alpha &= \frac{V^2}{\bar{c}^2} \frac{C_{m_\alpha} + C_{Z_\alpha} \frac{C_{m_{\dot{\alpha}}}}{2\mu_C - C_{Z_{\dot{\alpha}}}}}{2\mu_c K_Y^2} \\ z_q &= \frac{2\mu_c + C_{Z_q}}{2\mu_c - C_{Z_{\dot{\alpha}}}} & m_q &= \frac{V}{\bar{c}} \frac{C_{m_q} + C_{m_{\dot{\alpha}}} \frac{2\mu_c + C_{Z_q}}{2\mu_C - C_{Z_{\dot{\alpha}}}}}{2\mu_c K_Y^2} \\ z_{\delta_e} &= \frac{V}{\bar{c}} \frac{C_{Z_{\delta_e}}}{2\mu_c - C_{Z_{\dot{\alpha}}}} & m_{\delta_e} &= \frac{V^2}{\bar{c}^2} \frac{C_{m_{\delta_e}} + C_{Z_{\delta_e}} \frac{C_{m_{\dot{\alpha}}}}{2\mu_C - C_{Z_{\dot{\alpha}}}}}{2\mu_c K_Y^2} \end{aligned} \tag{3.2}$$

Table 3.1: Stability and control derivatives for the PH-LAB at cruise condition, obtained by TU Delft [116].

V	$=$	$59.9m/s$	C_{Z_α}	$=$	-5.16	C_{m_α}	$=$	-0.43
$\bar{c}$	$=$	$2.022m$	$C_{Z_{\dot{\alpha}}}$	$=$	-1.43	$C_{m_{\dot{\alpha}}}$	$=$	-3.7
μ_c	$=$	102.7	C_Z	$=$	-3.86	C_{m_q}	$=$	-7.04
K_Y^2	$=$	0.98	$C_{Z_{\delta_e}}$	$=$	-0.6238	$C_{m_{\delta_e}}$	$=$	-1.553

This short period model's dynamics are considered representative for relatively short durations of simulations, since the model is derived based on the assumptions of the short-period response. Over longer simulation durations, the match between this model's states and the nonlinear or a real PH-LAB's states will begin to diverge, as the phugoid motion of the real aircraft will not manifest in the simulations. Nonetheless, this model is considered sufficient to provide the reinforcement learning agents with an environment which is adequately realistic, striking a good balance between fidelity and simplicity.

Lastly, the control task of this problem is to be an Angle of Attack (AoA) reference tracking task, where the IDHP agent has to learn to control the aircraft's AoA to follow a reference AoA signal. The design of this reference signal will be detailed in Section 3.5.

3.1.2. MDP Environment Specification

While the aircraft is what the agents ultimately control, they are to only interface with the MDP environment. The consequence of this is that the state and action space of the environment are not necessarily equivalent to those of the aircraft model, in this case, the short-period LTI. The MDP environment will be specified in this subsection, this entails defining the environment state s, action a, and reward r spaces.

For the LTI, the state and action spaces are denoted x and u, with their definitions given in Equation 3.3, from where it can be seen that the model state space is two dimensional and the input space is one dimensional.

$$x = \begin{bmatrix} \alpha \\ q \end{bmatrix} \qquad\qquad u = \delta_e \tag{3.3}$$

For the MDP environment, the state and action space definitions are design variables, they can be freely defined as long as they are related to the control problem at hand. Logically, the goal in these design decisions is to allow for the best-performing agents to be achieved, which involves consideration of several factors. For example, the state space should be designed such that the MDP is Markov, this theoretically gives the agents sufficient information about the environment to provide ideal performance. Luckily in the case of the short-period LTI, finding a Markov MDP environment is trivial as LTI state space models are, by definition, Markov. Furthermore, the scale of variables in s deserves consideration, as it is generally desirable for inputs to neural networks to belong in the same orders of magnitude if not entirely normalized [117].

Regarding s for the present MDP, some options are presented in the following:

$$s = \begin{cases} \text{Option 1:} & \alpha_{ref} - \alpha \\ \text{Option 2:} & \begin{bmatrix} \alpha & \alpha_{ref} \end{bmatrix}^\top \\ \text{Option 3:} & \begin{bmatrix} q & \alpha & \alpha_{ref} \end{bmatrix}^\top \\ \text{Option 4:} & \begin{bmatrix} q & \alpha & \alpha_{ref} - \alpha \end{bmatrix}^\top \end{cases} \tag{3.4}$$

These options are evaluated in an initial testing phase by running a Monte Carlo simulation, where the IDHP agent is run on each of the 4 options on 15 episodes, with the same IDHP hyperparameters used across all options. Using the “eye norm” [118] on the tracking performance in these simulations, it was determined that **Option 1** of a single dimensional MDP state space with the tracking error being the state variable, gave the best result.

For a, two possible options are to directly control the elevator deflection, or to control the increments to the elevator deflection:

$$a = \begin{cases} \text{Option 1:} & \delta_e \\ \text{Option 2:} & \Delta\delta_e \end{cases} \tag{3.5}$$

Similar to the state options, these two options are evaluated through Monte Carlo simulations to see which one allows for better tracking performance, where it was found that **Option 1** of a single dimensional MDP action space with the variable being elevator deflection angle gave the best results.

The reward signal is defined as the negative squared tracking error multiplied by a reward scaling factor κ, as shown in Equation 3.6. An associated reward gradient is defined as well, in Equation 3.7.

$$r = -\frac{\kappa}{2}(\alpha - \alpha_{ref})^2 \tag{3.6}$$

$$\frac{\partial r}{\partial x} = -\kappa \begin{bmatrix} \alpha - \alpha_{ref} & 0 \end{bmatrix}^\top \tag{3.7}$$

Lastly, one episode will last 60 s of simulation time, with a time step duration of 0.02 s.

3.1.3. Fault Scenarios

Several flight scenarios are designed to test the fault tolerance of the agent during some of the experiments. This is done by testing the agent on three different events: shifted centre of gravity, decrease in elevator effectiveness, and reversed elevator controls. The first two cases emulate faults which can be realistically expected to happen. For instance, a shift in the centre of gravity can occur if payloads are moved around in the aircraft. A decrease in elevator effectiveness can occur on catastrophic events, such as shrapnels from engine explosion, or perhaps excessive nose-up during takeoff damaging the tail. The last of the scenarios is not expected to be realistic, as there are unlikely to be events that cause elevator controls to suddenly be reversed; nonetheless, this fault can demonstrate the adaptiveness of the implemented agents to dramatic changes in system dynamics, which in turn implies fault tolerance.

Shifted Centre of Gravity

In this scenario, the centre of gravity is shifted from the nominal position towards the aircraft nose by half a metre. To model this, the stability and control derivatives can be recomputed based on their definitions [116], whereupon the LTI matrices can be redefined. The affected derivatives are denoted by an asterisk in the exponent and updated according to the following equations, they are functions of Δx which is positive towards the tail and in metres, and are defined in the following:

$$\begin{aligned}
C^*_{m_\alpha} &= C_{m_\alpha} - C_{Z_\alpha}\frac{\Delta x_{c.g}}{\bar{c}} \\
C^*_{m_{\dot{\alpha}}} &= C_{m_{\dot{\alpha}}} - C_{Z_{\dot{\alpha}}}\frac{\Delta x_{c.g}}{\bar{c}} \\
C^*_{Z_q} &= C_{m_q} - C_{Z_\alpha}\frac{\Delta x_{c.g}}{\bar{c}} \\
C^*_{m_q} &= C_{m_q} - (C_{Z_\alpha} + C_{m_\alpha})\frac{\Delta x_{c.g}}{\bar{c}} + C_{Z_\alpha}(\frac{\Delta x_{c.g}}{\bar{c}})^2 \\
C^*_{m_{\delta_e}} &= C_{m_{\delta_e}} - C_{Z_{\delta_e}}\frac{\Delta x_{c.g}}{\bar{c}}
\end{aligned}$$

Damaged Elevator

In this scenario, the control authority of the elevator is to be reduced by half. This can be modelled relatively easily, by dividing the input matrix of the short-period LTI by two, which halves the elevators' control effectiveness. The faulty input matrix B^* is defined according to Equation 3.8.

$$B^* = \frac{B}{2} \tag{3.8}$$

Reversed Elevator

In the last scenario, the mechanics on the ground accidentally rewired the flight control computer, which meant that at some point in the flight, the elevators would suddenly reverse the control commands it received. This is modelled by multiplying the input matrix of the LTI by -1, resulting in the faulty input matrix B^* shown in Equation 3.9.

$$B^* = -B \tag{3.9}$$

3.1.4. MDP Summary

The MDP on which the agents are tested revolves around AoA control on a simple model of an aircraft. The agent will provide the elevator deflection angles at each time step to the MDP environment, which will use this input to determine the subsequent time step's state and rewards which in turn is fed back to the agent.

When the environment receives action a from the agent, it feeds a as the input u to the short-period LTI model, which returns the next time step's model states. The model states and the reference AoA are used to calculate the subsequent time step's MDP state and reward.

The MDP environment variables are summarized in Table 3.2, and the flow of MDP variables is visualized in Figure 3.1.

Table 3.2: MDP environment summary.

Model state: x_t	$=$	$\begin{bmatrix}\alpha_t \\ q_t\end{bmatrix}$	MDP state: s_t	$=$	$\alpha_t - \alpha_{ref,t}$
Model or MDP action: u_t, a_t	$=$	$\delta_{e,t}$	MDP reward gradient: $\frac{\partial r_t}{\partial x_t}$	$=$	$-\kappa \begin{bmatrix}\alpha - \alpha_{ref} \\ 0\end{bmatrix}$
MDP reward: r_t	$=$	$-\frac{\kappa}{2}(\alpha_t - \alpha_{ref,t})^2$			
No. model states: n	$=$	2	No. model inputs: m	$=$	1
Time step: dt	$=$	0.02 s	Episode duration: T	$=$	60 s

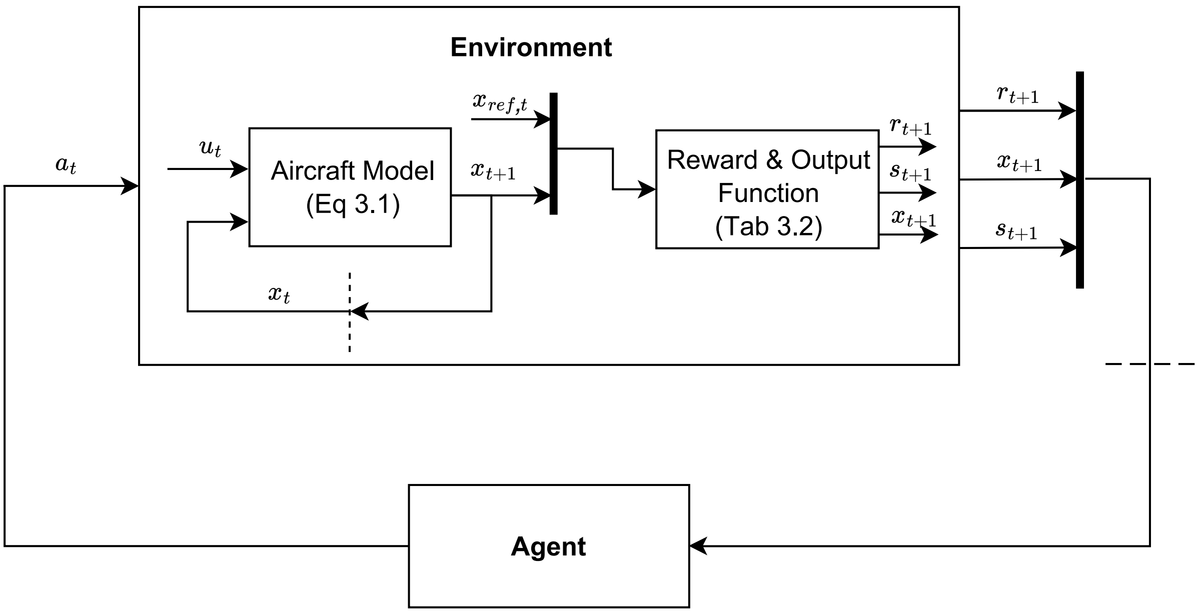

Figure 3.1: MDP environment flow diagram.

3.2. IDHP Agent

In answering research question **Q1**, it was identified that IDHP has the most promising fault tolerance potential. This section will introduce the details and the structure behind this reinforcement learning algorithm.

The overall algorithm consists of three components; the model, the critic, and the actor. These components are explained in Section 3.2.1, Section 3.2.2, and Section 3.2.3 respectively. The update rules thus written for the IDHP algorithm are taken from Zhou [52], with some nomenclature changes where variable names are swapped with reinforcement learning vocabulary; e.g. the use of reward instead of cost-to-go, and return function instead of loss function for the actor.

3.2.1. Model

The IDHP's model is meant to represent the system dynamics within the MDP environment, allowing it to update actor and critic parameters more efficiently. The model structure used is a discrete-time

Linear Time-Varying (LTV) model, which takes in one time step's state and actions and outputs the next time step's states. This model structure can be written as Equation 3.10.

$$\delta x_t = F_t \delta x_{t-1} + G_t \delta u_{t-1} \tag{3.10}$$

In IDHP, this model is identified using a RLS algorithm, specifically an exponentially weighted variant, which offers a computationally more efficient estimator than naive linear estimation for recursive estimation theoretically without numerical instability issues through using the matrix inversion lemma, a long-standing problem solved by Slock and Kailath [119]. With this algorithm, it became possible to estimate linear system models online assuming a sufficiently high sample rate, which to some degree ensures the observed dynamics are linear even when the dynamics are nonlinear over a large time scale. This advantage is leveraged to make DHP incrementally identify the system model, thus yielding the IDHP algorithm [120]. To understand and implement RLS, Haykin's work on Adaptive Filter Theory was used [121].

In RLS, the model parameters and model variables are grouped into Θ_t and X_t according to Equation 3.11 and Equation 3.12 respectively.

$$\Theta_t = \begin{bmatrix} F_t^\top \\ G_t^\top \end{bmatrix} \tag{3.11}$$

$$X_t = \begin{bmatrix} \delta x_t \\ \delta a_t \end{bmatrix} \tag{3.12}$$

$$\delta x_t = x_t - x_{t-1}$$

$$\delta a_t = a_t - a_{t-1}$$

To perform model estimation, an RLS covariance matrix Σ_t, an RLS gain k_t, an RLS prediction $\delta \hat{x}_t$, and an RLS error or innovation ϵ_t are defined according to the following definitions:

$$\begin{aligned} \Sigma_t &\in \mathbb{R}^{n+m} \\ k_t &= \frac{\Sigma_{t-1} X_t}{\rho + X_t^\top \Sigma_{t-1} X_t} \\ \delta \hat{x}_t &= X_t^\top \Theta_{t-1} \\ \epsilon_t &= \delta x_t - \delta \hat{x}_t \end{aligned}$$

Where ρ is the RLS forgetting factor. The two RLS variables which are directly related to model estimation, Θ and Σ, are updated according to Equation 3.13 and Equation 3.14 respectively.

$$\Theta_t = \Theta_t + k_t \epsilon_t \tag{3.13}$$

$$\Sigma_t = \frac{1}{\rho}(\Sigma_{t-1} - k_t X_t^\top \Sigma_{t-1}) \tag{3.14}$$

One possible option for initializing these two variables is to use Equation 3.15 with σ a large number.

$$\Theta_0 = \begin{bmatrix} 1 & 0 \\ 0 & 1 \\ 0 & 0 \end{bmatrix} \qquad \Sigma_0 = \sigma \begin{bmatrix} 1 & 0 & 0 \\ 0 & 1 & 0 \\ 0 & 0 & 1 \end{bmatrix} \tag{3.15}$$

Such an initialization offers a good initial guess of what the system dynamics may be, since the discrete state transition matrix approaches the identity matrix as the sample rate approaches infinity, and the discrete state input matrix approaches zero under likewise conditions; while directing the algorithm to perform big updates on the parameter matrix through initializing the covariance matrix to be large:

$$F_t = \mathbb{I} + dtA \Rightarrow \lim_{dt \to 0} F_t = \mathbb{I}$$
$$G_t = dtB \Rightarrow \lim_{dt \to 0} G_t = \mathbf{0}$$

Where A and B are the continuous state transition and input matrices respectively, and dt is the time step size in unit time. That being said, it was observed that initializing Θ with a null matrix also provides satisfactory results.

Finally, the RLS algorithm can be found summarized in Algorithm 4.

Algorithm 4 RLS algorithm.

1: **Initialize**. Parameter covariance $\Sigma_0 \in \mathbb{R}^{(n+m)\times(n+m)}$, parameter $\Theta_0 \in \mathbb{R}^{(n+m)\times n}$.
2: **Online Model Identification**. For each time step, $t = 1, 2, \cdots$, compute:

$$\begin{aligned}
\delta x_t &= x_t - x_{t-1} \\
\delta a_t &= a_t - a_{t-1} \\
X_t &= \begin{bmatrix} \delta x_t & \delta a_t \end{bmatrix}^\top \\
k_t &= \frac{\Sigma_{t-1} X_t}{\rho + X_t^\top \Sigma_{t-1} X_t} \\
\epsilon_t &= \delta x_t - X_t^\top \Theta_{t-1} \\
\Theta_t &= \Theta_t + k_t \epsilon_t \\
\Sigma_t &= \frac{1}{\rho}(\Sigma_{t-1} - k_t X_t^\top \Sigma_{t-1})
\end{aligned}$$

3.2.2. Critic

The critic of IDHP is a value gradient function, meaning it outputs the gradient of the value function. This function uses a single-layer neural network function approximator:

$$\lambda(s; W_c) = \frac{\partial V(s)}{\partial x}$$

Where W_c are the network weights parametrizing the critic-network, the semicolon delimiter denotes that the critic is parameterized by W_c.

This network has an input layer, one hidden layer, and an output layer. The domain of the critic-network spans the MDP state space which only has the single variable s, as defined in Table 3.2. Thus the input layer has a single neuron, it uses a linear activation function and has no output bias. The hidden layer consists of four neurons all using the $\tanh$ activation function and no output bias term. The number of neurons in the hidden layer was decided through preliminary testing of algorithm performance using a varying number of hidden neurons, where it was found that a small number of neurons had slightly poorer but very similar performance than higher numbers, and it was decided that a small hidden layer would be interesting to investigate to see the limit of network sizes for a usable flight controller. For the output layer, since the critic outputs the gradient of a state's value w.r.t. the model states x, the output layer thus has two output neurons, one neuron for the derivative w.r.t. each model state. The output neurons use a linear activation function with no output bias. The network can also be expressed as a vector function, as done in Equation 3.16.

$$\lambda(s; W_c) = W_{c,2} \tanh(W_{c,1} s) \tag{3.16}$$
$$\lambda(\cdot) \in \mathbb{R}^2 \quad W_{c,1} \in \mathbb{R}^{4\times 1} \quad W_{c,2} \in \mathbb{R}^{2\times 4}$$

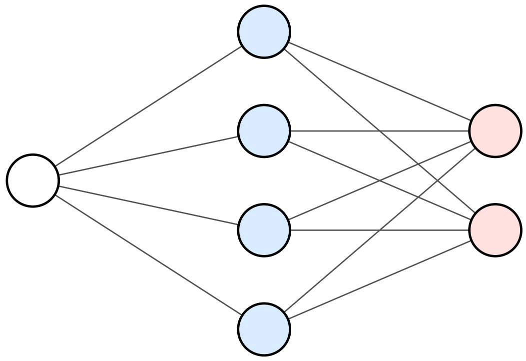

Input Nodes $= 1$ Hidden Nodes $= 4$ Output Nodes $= 2$

Activation $= linear$ Activation $= tanh$ Activation $= linear$

Bias $=$ None Bias $=$ None Bias $=$ None

Figure 3.2: IDHP critic-network.

Where the n in $W_{c,n}$ denote the layer number, counting from the input layer. A graphical depiction is also shown in Figure 3.3.

The critic-network is trained using temporal difference learning, by using previous estimates and current observations to improve its future estimation accuracy. This is done by defining a temporal difference error δ which quantifies the critic's accuracy, and then continuously updating critic parameters W_c to minimize the squared temporal difference error E through stochastic gradient descent. While theoretically, more advanced gradient descent algorithms such as AdaGrad or Adam can be used instead of simple stochastic gradient descent, experiments have shown that such optimizers can slow down learning of temporal difference methods, this is discussed by Gupta [122] and Nichols [123], and will be elaborated on in Section 3.3.2.

The IDHP critic δ and the quadratic temporal difference error E are formulated in Equation 3.18 and Equation 3.17 respectively.

$$E_t = \frac{1}{2}\delta_t^\top \delta_t \tag{3.17}$$

$$\delta_t = \lambda_{t-1} - \frac{\partial r_{t-1}}{\partial x_{t-1}} - \gamma \lambda'_t \left.\frac{\partial x_t}{\partial x_{t-1}}\right|_t \tag{3.18}$$

$$\lambda_{t-1} = \lambda(s_{t-1}; W_c(t-1)) \qquad \lambda'_t = \lambda'(s_t; W_{c'}(t-1))$$

$$\left.\frac{\partial x_t}{\partial x_{t-1}}\right|_t = F_t + G_t \frac{\partial a_{t-1}}{\partial x_{t-1}} \tag{3.19}$$

Where the vertical bar in $\left.\frac{\partial x_t}{\partial x_{t-1}}\right|_t$ denotes the time step for which this term is evaluated, i.e. the model matrices F_t and G_t are to be found at timestep t.

Note that in formulating δ_t, a target critic λ' is used to calculate the value gradient of the s_{t+1}. This target critic is identical to the critic, however, it is not trained but simply updated at a slower rate than the critic, and serves to stabilize the learning process of the critic-network by reducing the variance of target value gradients [124] [4].

The gradient descent equation used to optimize the critic for minimal E involves determining the gradient of E w.r.t. critic-network weights and incrementing critic weights by some fraction η_c of the negative of that gradient, the negative here is necessary as this is a minimization problem. This procedure can be summarized by Equation 3.20. To update the target critic, a moving average filter is used to trickle the latest critic weights into the target critic, shown in Equation 3.21.

$$W_{c,t} = W_{c,t-1} - \eta_c \frac{\partial E_{t-1}}{\partial W_c} \tag{3.20}$$

$$W_{c',t} = \tau W_{c,t-1} + (1-\tau) W_{c',t-1} \tag{3.21}$$

With the t subscript in $W_{c,t}$ denoting the time step which the weights are taken, and where η_c is the learning rate of the critic, $\tau \ll 1$ is a mixing factor typically made a very small positive number. To be able to implement Equation 3.20 and train the critic-network, it is necessary to expand the term $\frac{\partial E(t)}{\partial W_c}$:

$$\begin{aligned} E_t &= \frac{1}{2}\delta_t^\top \delta_t \\ \frac{\partial E_t}{\partial W_c} &= \frac{\partial E_t}{\partial \delta_t} \frac{\partial \delta_t}{\partial \lambda_{t-1}(\cdot)} \frac{\partial \lambda_{t-1}(\cdot)}{\partial W_c} \\ \frac{\partial E_t}{\partial W_c} &= \delta_t \frac{\partial \lambda_{t-1}(\cdot)}{\partial W_c} \end{aligned}$$

Thus, the critic weights are incremented by a product of δ_t and the gradient of the critic output w.r.t. the weights. The latter partial derivative term is defined since a neural network is analytically differentiable, the most common practice of calculating this derivative is through backpropagation algorithms, which efficiently evaluates this derivative thanks to the storage of intermediate variable during a feedforward operation of a network [125].

3.2.3. Actor

The actor of IDHP is a policy function which uses a single-layer neural network as a function approximator. This network comprises an input layer, one hidden layer, and an output layer. Just like the critic, the domain of the actor-network spans the MDP state space which only has the single variable s, thus the input layer has a single neuron. The input layer uses a linear activation function with no output bias. The hidden layer consists of four neurons all using the $\tanh$ activation function and no output bias term. The number of neurons in the hidden layer was once again decided upon based on preliminary testing, where it was found four neurons gave satisfactory algorithm performance. Lastly, for the output layer, the range of the policy function is the MDP action space which only has a single action a as defined in Table 3.2, thus the output layer has a single output neuron, which uses a $\tanh$ activation function and has no output bias. The network can be expressed as a scalar function, as done in Equation 3.22, where $W_{a,n}$ are the network weights parametrizing the actor-network with n being the layer number, counting from the input layer. The actor-network is also depicted graphically in Figure 3.3.

$$\begin{gathered} \pi(s; W_a) = \tanh(W_{a,2}\tanh(W_{a,1}s)) \\ \pi(\cdot) \in \mathbb{R} \quad W_{a,1} \in \mathbb{R}^{4\times 1} \quad W_{a,2} \in \mathbb{R}^{1\times 4} \end{gathered} \tag{3.22}$$

Note that since the output of the actor-network passes through a $tanh$, this means the output value is bound to the range $(-1, 1)$. Since the elevator deflection limit on the Cessna Citation II is from $[-20, 20]$ deg, it is thus necessary to scale the actor output by a factor of 20 before it can be used as the input value to the aircraft model. After this scaling, the actor's action a_t is retrieved.

To train the actor, its weights are updated to maximize the return function Equation 3.23 using stochastic gradient ascent Equation 3.24.

$$R_t = r_t + \gamma J(s_{t+1}) \tag{3.23}$$

$$W_{a,t} = W_{a,t-1} + \eta_a \frac{\partial R_{t-1}}{\partial W_a} \tag{3.24}$$

With t in the subscript of $W_{a,t}$ denoting time step, η_a is the learning rate of the actor. It can be observed that the return function utilizes the state value function $J(s)$, which is not estimated in the present

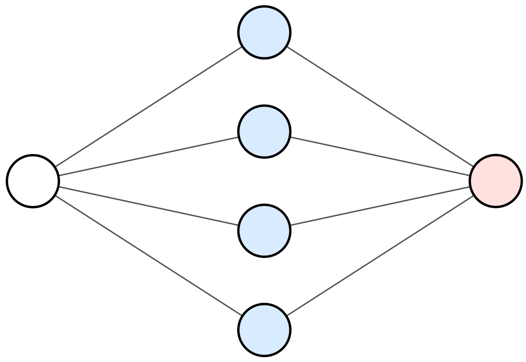

Input Nodes	$= 1$	Hidden Nodes	$= 4$	Output Nodes	$= 1$
Activation	$= linear$	Activation	$= tanh$	Activation	$= tanh$
Bias	= None	Bias	= None	Bias	= None

Figure 3.3: IDHP actor-network.

algorithm. This will prove to be a non-issue, as ultimately what is needed to perform actor weight updates are derivatives of $J(s)$. So, to further demonstrate this point, and for implementation of the gradient ascent update, the partial derivative $\frac{\partial R_{t-1}}{\partial W_a}$ is expanded:

$$\begin{aligned}\frac{\partial R_{t-1}}{\partial W_a} &= \frac{\partial R_{t-1}}{\partial x_t}\frac{\partial x_t}{\partial a_{t-1}}\frac{\partial a_{t-1}}{\partial W_a}\\ &= \left[\frac{\partial r_{t-1}}{\partial x_t} + \gamma\lambda'(s_t)\right]\left.\frac{\partial x_t}{\partial a_{t-1}}\right|_t\frac{\partial a_{t-1}}{\partial W_a}\\ \text{Where}\quad \left.\frac{\partial x_t}{\partial a_{t-1}}\right|_t &= G_t\end{aligned}$$

Observe that $J(s)$ disappears from the equation, and is replaced by $\lambda(s)$, which *is* estimated by the algorithm in the form of the critic.

Strictly speaking, the term $\frac{\partial r_{t-1}}{\partial x_t}$ is undefined, as it relates the derivative of past reward to a future model state. However, under the assumption of smooth system dynamics and high sampling rate, it is possible to replace this term with $\frac{\partial r_t}{\partial x_t}$. This re-expression is adopted in the present implementation.

3.2.4. Adaptive Learning

The actor and critic are tweaked to be more and less adaptive depending on the situation. During a warmup period and when a fault is detected in the aircraft, the agents will use a higher learning rate to be more adaptive. When the aircraft is functioning without anomaly and past the warmup period, the agents adopt a low learning rate.

The high and low learning rates are to be active under the conditions specified by Equation 3.25.

$$\eta = \begin{cases}\eta_{\cdot,h} & \text{if}\quad t < 3 \text{ or } ||e_{[t-2,t]}|| > 1\\ \eta_{\cdot,l} & \text{otherwise}\end{cases} \tag{3.25}$$

Where t is in seconds, and $e_{[t-2,t]}$ denotes the AoA tracking error in degrees between $t-2$ and t. In words, the learning setting is set to adaptive if the simulation time is less than 3 s or if the tracking error at any point in the past 2 s is greater than 1 deg. Otherwise, the learning setting is set to normal.

When it comes to the RLS model, a known problem associated with exponentially increasing covariance occurs when the system is not persistently excited [120], resulting in dramatic changes to parameter estimates once the system is excited. To counter this, the RLS forgetting factor ρ is set to 1, meaning that the latest parameters are estimated using all previous measurements, similar to ordinary least squares. This can be troublesome since the model parameters will vary less as time goes on, hampering adaptiveness. When the simulation time has proceeded past the warmup phase, if the RLS ϵ norm exceeds 9×10^{-5}, then Σ is re-initialized to a high variance matrix identical to the initial Σ_0, and the matrix will not be reset for the next 3 s, see Equation 3.26. The same reinitialization is done for the model parameter matrix Θ, see Equation 3.27.

$$\Sigma_{t+1} = \begin{cases} \text{Reset to } \Sigma_0 & \text{if} \quad ||\epsilon_t|| > 9 \times 10^{-5} \\ \text{Update using Equation 3.14} & \text{otherwise} \end{cases} \tag{3.26}$$

$$\Theta_{t+1} = \begin{cases} \text{Reset to } \Theta_0 & \text{if} \quad ||\epsilon_t|| > 9 \times 10^{-5} \\ \text{Update using Equation 3.13} & \text{otherwise} \end{cases} \tag{3.27}$$

3.2.5. IDHP Agent Summary

The reinforcement learning agent used to solve this MDP problem is an IDHP agent. This agent receives the MDP state, MDP reward, and model state at every time step. It then uses these signals to both compute that time step's action, as well as to update it's internal variables, namely the RLS model, the actor, and the critic. A flow chart of the IDHP agent is given in Figure 3.4.

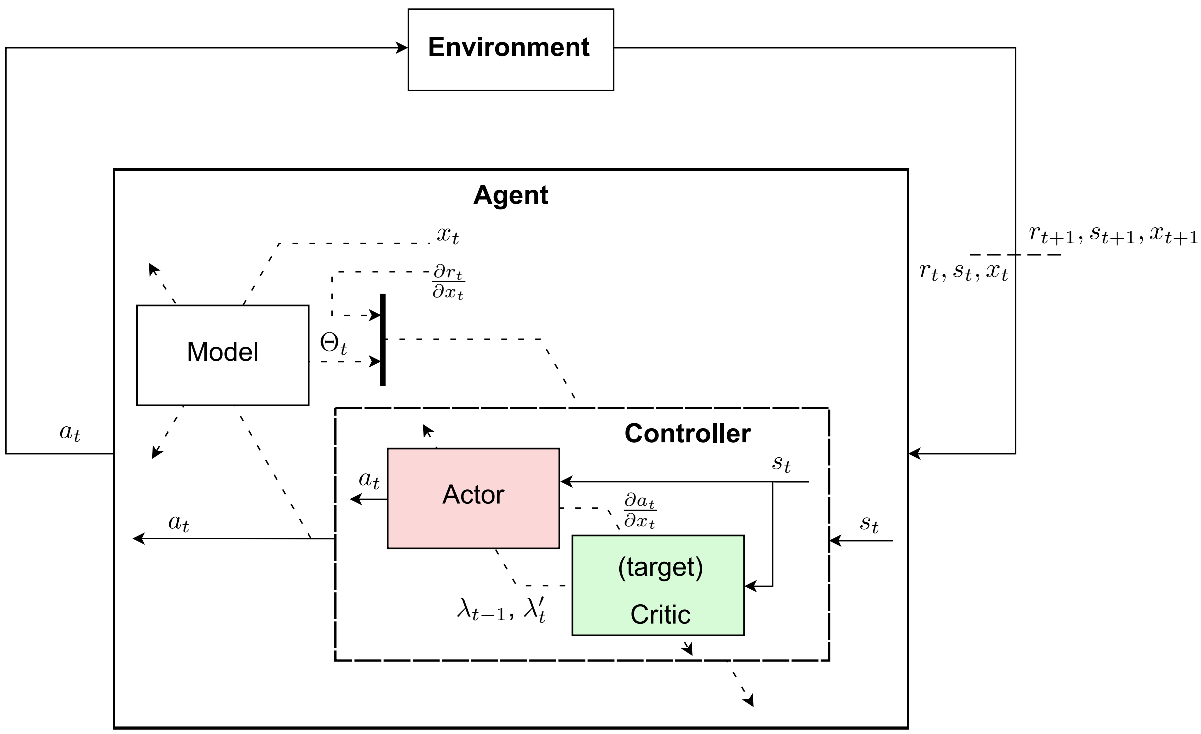

Figure 3.4: MDP agent flow diagram, dashed signals represent variables used to update the blocks which they cross.

3.3. IDHP augmentations

The IDHP algorithm is to be researched further to explore possibilities of improving it's fault tolerance and tracking performance. Potential augmentations that IDHP can leverage have been identified during the literature study phase, and they were briefly introduced in Chapter 2. The first of such augmentation is the multi-step update, explained in Section 3.3.1, and the second augmentation is the eligibility trace, explained in Section 3.3.2

3.3.1. Multistep Temporal Difference

IDHP uses a temporal difference approach in training the critic. Temporal difference methods use observed MDP state-reward pairs to compute a temporal difference target, this target constitutes the second and third term in the δ definition introduced in Equation 3.18, repeated below for clarity:

$$\delta_t = \lambda_{t-1} - \underbrace{(\frac{\partial r_{t-1}}{\partial x_{t-1}} + \gamma \lambda'_t \frac{\partial x_t}{\partial x_{t-1}})}_{\text{IDHP TD Target}}$$

The TD target is what a value function, or in the IDHP case the value gradient function, is trained to approximate. This target is an empirical estimation of what the true value/value gradient is for the current state. Thus, in theory, the more accurate this target is the faster the estimated value function approaches the true value function.

With the works of Watkins [126] and Cichosz [127] the idea of multi-step or truncating TD was introduced and demonstrated to improve learning rates of TD algorithms. Multi-step TD, also known as n-step TD, uses state-reward pairs observed over multiple time steps to reduce bias in the TD target, this generally takes the form of Equation 3.28.

$$\text{n-step TD Target} : \gamma^n V(s_n) + \sum_{m=0}^{n-1} \gamma^m r_m \tag{3.28}$$

Where it can be seen that more than one reward observation and the $n\text{-}th$ state value estimate are used to construct the TD target.

Precedence of n-step TD returns yielding improved agent learning rates can be found for simple TD algorithms in the textbook by Sutton and Barto [17], as well as for HDP in the works by Luo et al. [35] and Wang et al. [36], who proposed a different flavour of multi-step augmentation where policy evaluation is performed for several steps as opposed to gathering state-reward over multiple time steps.

The present research will extend the multi-step idea to the IDHP algorithm. To this end, a multi-step target can be constructed and the multi-step TD error δ_n can be constructed:

$$\delta_{n,t} = \lambda_{t-n} - \frac{\partial(\gamma^n V(s_t) + \sum_{m=0}^{n-1} \gamma^m r_{t-n+m})}{\partial x_{t-n}} \tag{3.29}$$

For the sake of simplicity, the present thesis will only consider the 2-step TD error, where the TD error for the critic takes the form of Equation 3.30.

$$\delta_{2,t} = \lambda_{t-2} - \left(\frac{\partial r_{t-2}}{\partial x_{t-2}} + \gamma \frac{\partial r_{t-1}}{\partial x_{t-1}} \frac{\partial x_{t-1}}{\partial x_{t-2}}\bigg|_{t-1} + \gamma^2 \lambda'_t \frac{\partial x_t}{\partial x_{t-1}}\bigg|_t \frac{\partial x_{t-1}}{\partial x_{t-2}}\bigg|_{t-1} \right) \tag{3.30}$$

With the state transition terms $\frac{\partial x_{t-1}}{\partial x_{t-2}}\big|_{t-1}$ and $\frac{\partial x_t}{\partial x_{t-1}}\big|_t$ calculated according to Equation 3.19.

3.3.2. Eligibility Traces

Eligibility traces are an alternative method for incorporating more prior information to agent training, this is achieved by storing the past neural network updates in an eligibility trace $\mathbf{E}$, and using them for several subsequent updates at decaying magnitudes. This results in a new set of equations used to update the network parameters.

$$\begin{aligned} W_{t+1} &= W_t + \eta \delta_t \mathbf{E}_t \\ \mathbf{E}_{t+1} &= \lambda \gamma \mathbf{E}_t + \nabla W_t, \quad \mathbf{E}_0 = 0 \end{aligned} \tag{3.31}$$

Where ∇W is the gradient of the network output w.r.t network weights, δ_t is the gradient of the relevant metric w.r.t. network output, for the critic this metric is the TD error and for the actor it's the return; λ is the trace decay rate which controls how quickly do prior gradients decay in the eligibility trace.

The idea of extending IDHP to a multi-step version leads one to also consider the case of extending IDHP with eligibility traces as well, as the history of their inception is closely intertwined. This connection is explored in several works, one of such works is by Singh and Sutton [128] who explored the similarities of eligibility traces algorithms and MC algorithms, which are the infinite-step extreme of multi-step algorithms. Another such work is by van Seijen [129], who derived the distinction between the eligibility trace algorithm TD(λ) and the λ return algorithm which is the prototypical multi-step algorithm. In fact, van Seijen proved that the two algorithms are asymptotically identical for infinitely small learning rates.

As opposed to the multi-step augmentation, eligibility traces will only be applied to the actor update equations. This is a decision made as a result of empirical experiments which concluded that IDHP learning is more stable when only the actor uses eligibility traces.

As it turns out, eligibility traces can be formulated in several manners [130], these formulations each record eligibility traces slightly differently. For the present thesis, two options will be experimented with. They are namely the; accumulating trace, and the replacing trace, for which they are written below for the actor updates. These two trace's generic form can be obtained by swapping the partial derivative term with $\nabla f(x)$, gradient of performance metric w.r.t. function parameters.

1. Accumulating traces:
$$\mathbf{E}_{t+1} = \lambda\gamma\mathbf{E}_t + \nabla W_{a,t} \tag{3.32}$$
2. Replacing traces:
$$\mathbf{E}_{t+1} = \begin{cases} \nabla W_{a,t} & \text{if} \quad ||\nabla W_{a,t}|| > ||\lambda\gamma\mathbf{E}_{t-1}|| \\ \lambda\gamma\mathbf{E}_{t-1} & \text{otherwise} \end{cases} \tag{3.33}$$

It can be seen that the first option, accumulating traces, is simply the original form of eligibility traces shown in Equation 3.31.

These two traces have different effects on how an agent learns, which can be roughly illustrated with Figure 3.5. With accumulating traces, when one state is visited several times, the gradient update which results from the observed state-reward pair is compounded on each other, which can cause faster network weight changes. These compounded updates will be persistently made to the network for several time steps following this visit, albeit at decayed amounts. On the other hand, with replacing traces, when one state is visited several times even in quick succession, the magnitude of network weight updates will not exceed that of the original network weight gradients. However, the effect of this state-reward pair update will persist after the state visit, as the eligibility trace will continue to update the network with the observed gradient, albeit again with decaying amounts.

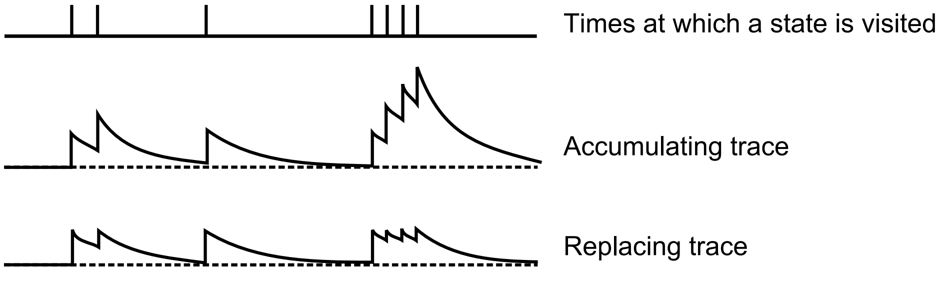

Figure 3.5: Accumulating and replacing trace illustrated, recreated from [128].

To arrive at the final network weight update procedure, the eligibility traces can be used to update actor weights according to Equation 3.31 with δ_t being the return gradient shown in Equation 3.34.

$$\delta_{a,t} = \frac{\partial R_t}{\partial a_t} = \left[\frac{\partial r_{t-1}}{\partial x_t} + \gamma\lambda(s_t)\right] G_t \tag{3.34}$$

Eligibility Trace and Momentum Gradient Descent

An interesting note can be made about the differences between eligibility traces and momentum-based gradient descent algorithms.

The high-level ideas of the two algorithms are similar. In neural networks, momentum-based algorithms for network weight optimization roughly take the following form:

$$\begin{aligned} W_{t+1} &= W_t + \eta \mathbf{M}_t \\ \mathbf{M}_{t+1} &= \lambda \mathbf{M}_t + \delta_t \nabla W_t, \quad \mathbf{M}_0 = 0 \end{aligned} \tag{3.35}$$

The most important difference in the momentum-based update equations is the metric gradient term δ_t, which is moved from the weight update to the momentum/trace update. Note that the momentum variable $\mathbf{M}$ is equivalent to $\mathbf{M}$ in its function, they both serve to store past updates for use in future weight updates.

This difference can be used intuitively to deduce that momentum-based optimization for actor or critic optimization will result in poorer performance than eligibility trace-based optimization. Using the case of actor training for illustration, the term $\delta_{a,t}$, in that case, is an estimate of the true return derivative, as can be seen by Equation 3.34 where the critic's value gradient estimate λ is used to create $\delta_{a,t}$. For earlier time steps, such an estimate is likely to be less accurate than later time steps, as the critic slowly begins to be trained. Since momentum-based approaches accumulate the total weight update in the $\mathbf{M}$ term using $\delta_{a,t}$ from each time step, all subsequent actor updates will be influenced by these poorer prior $\delta_{a,t}$ estimates. Thus, intuitively, it can be said that momentum-based approaches introduce unwanted bias into the learning process. As opposed to eligibility trace approaches, where only the latest $\delta_{a,t}$ estimate is used.

A similar argument can be seen made in literature for the case of TD value function learning. For instance, Nichols [123], who applied both eligibility trace and momentum to the SARSA algorithm, empirically demonstrated that eligibility traces yielded an algorithm more likely to succeed and had greater sample efficiency. Similarly, Gupta [122] also showed that momentum on the TD algorithm hinders learning whereas eligibility traces on TD, i.e. TD(λ), results in better learning performance than the baseline TD algorithm.

3.4. IDHP Algorithm

The IDHP algorithm combines the various components introduced in Section 3.2: the RLS model, the actor, and the critic, to create the reinforcement learning agent. To initialize the algorithm, initial values for several algorithm variables as well as the algorithm's hyperparameters are set, Table 3.3 lists all the variables and hyperparameters to be initialized.

For the undecided hyperparameters, the experiments conducted involve running several different sets of learning and decay rates, thus values for these parameters will be stated in Section 3.5 instead. On the other hand, the hyperparameters γ, τ, ρ and variable initialization will be identical across all experiments, and their values are given in Table 3.3. Regarding the choice of values for γ, τ, and ρ, these values were taken directly from previous research, specifically from the works of Heyer [4] and Teirlinck [112]. The initialization values for variables in Table 3.3 are either decided based on a combination of values from research plus trial and error, where the main goal in deciding most of the values was to keep the algorithm simple, so using identity or null matrices and numbers as much as possible.

Note that the eligibility trace variable is initialized even if the algorithm is set not to use eligibility traces, this is because the eligibility trace update procedure is simply the general form of the network update procedure. Specifically, one obtains the original network weight update equations by setting the eligibility decay rate λ to 0.

Table 3.3: IDHP initialization variables and hyperparameters.

Hyperparameters		Variable initialization			
Actor learning rates:	$\eta_{a,h}$,$\eta_{a,l}$	Eligibility trace:	$\mathbf{E}_0$	$=$	$\mathbf{0}$
Critic learning rates:	$\eta_{c,h}$,$\eta_{c,l}$	RLS model parameter:	Θ_0	$=$	$\mathbf{0}$
Eligibility trace decay rates:	λ_h,λ_l	RLS model covariance:	Σ_0	$=$	$10^6 \cdot \mathbb{I}$
MDP reward scaling factor:	κ	actor-network weights:	$W_{a,0}$	$\sim$	$\mathcal{N}(0,\, 0.1^2)$
MDP reward discount factor:	$\gamma = 0.6$	critic-network weights:	$W_{c,0}$	$\sim$	$\mathcal{N}(0, 0.1^2)$
Target critic mixing factor:	$\tau = 0.01$	Model states:	x_0	$=$	$\mathbf{0}$
RLS forgetting factor:	$\rho = 1$	MDP states:	s_0	$=$	$\mathbf{0}$
		Model & MDP action:	a_0	$=$	$\mathbf{0}$

After initialization, the main algorithm loop begins. First, one MDP step is taken, by sampling an action from the actor given the initial MDP state and performing that action in the environment. Second, the appropriate η is selected depending on the current error and warmup period, and the Σ is adapted depending on the warmup period and model error. Third, the critic, actor, and model are updated using the appropriate equations: the critic is updated using either a single or two-step TD error with the target critic weights moving slightly towards the critic weights, the actor is updated using the eligibility trace variables with λ being 0 if traces are not used and λ non-zero otherwise, finally the RLS model is updated using the latest model state and actor action to produce an estimate for the system model to use in the next time step. The algorithm then repeats this cycle, until the episode duration has reached the limit T. The algorithm is summarized in Algorithm 5.

Algorithm 5 IDHP algorithm.

1: **Initialize**:
Set initial variable values and hyperparameters listed in Table 3.3.
2: **Online loop**:
For $t = 0$ **to** T/dt **do**

// *Sample and perform action*

$a_t \leftarrow \pi(s_t; W_{a,t})$

$s_{t+1}, r_{t+1} \leftarrow \text{Environment}(a_t)$

// *Adapt* η *and* Σ *accordingly*

$$\eta_a, \eta_c \leftarrow \begin{cases} \eta_{\cdot,h} & \text{if} \quad t < 3 \text{ or } ||e_{[t-2,t]}|| > 1 \\ \eta_{\cdot,l} & \text{otherwise} \end{cases}$$

$$\Sigma_{t+1} \leftarrow \begin{cases} \text{Reset to } \Sigma_0 & \text{if} \quad ||\epsilon_t|| > 9 \times 10^{-5} \\ \text{Update using Equation 3.14} & \text{otherwise} \end{cases}$$

$$\Theta_{t+1} \leftarrow \begin{cases} \text{Reset to } \Theta_0 & \text{if} \quad ||\epsilon_t|| > 9 \times 10^{-5} \\ \text{Update using Equation 3.13} & \text{otherwise} \end{cases}$$

// *Update critic and target critic*

If using multi-step IDHP **then**

$$\delta_t = \lambda_{t-2} - \left(\frac{\partial r_{t-2}}{\partial x_{t-2}} + \gamma \frac{\partial r_{t-1}}{\partial x_{t-1}} \frac{\partial x_{t-1}}{\partial x_{t-2}}\bigg|_{t-1} + \gamma^2 \lambda'_t \frac{\partial x_t}{\partial x_{t-1}}\bigg|_t \frac{\partial x_{t-1}}{\partial x_{t-2}}\bigg|_{t-1}\right)$$

Else

$$\delta_t = \lambda_{t-1} - \frac{\partial r_{t-1}}{\partial x_{t-1}} - \gamma \lambda'_t \frac{\partial x_t}{\partial x_{t-1}}\bigg|_t$$

End If

$\frac{\partial E_t}{\partial W_c} = \delta_t \frac{\partial \lambda(\cdot)}{\partial W_c}$

$W_{c,t+1} = W_{c,t} + \eta_c \frac{\partial E_t}{\partial W_c}$

$W_{c',t+1} = \tau W_{c,t} + (1-\tau) W_{c',t}$

// *Update actor*

$\mathbf{E}_{t+1} \leftarrow$ accumulating trace (3.32) or replacing trace (3.33) $\triangleright$ $\lambda = 0$ *if not using eligibility traces*

$\frac{\partial R_t}{\partial W_a} = \left[\frac{\partial r_{t-1}}{\partial x_t} + \gamma \lambda(s_t)\right] G_t \mathbf{E}_t$

$W_{a,t+1} = W_{a,t} + \eta_a \frac{\partial R_t}{\partial W_a}$

// *Update model*

$F_{t+1}, G_{t+1} \leftarrow$Algorithm 4

3.5. Experiments and Evaluated IDHP Variants

The experiments conducted will evaluate and compare the proposed augmentations against the baseline IDHP algorithm. While two augmentations were proposed, three augmented IDHP algorithms are created:

1. IDHP(λ): baseline IDHP with the actor augmented by *accumulating* eligibility trace.
2. MIDHP: baseline IDHP with the critic augmented by multi-step update.
3. MIDHP(λ): baseline IDHP with the critic augmented by multi-step update and the actor augmented by *replacing* eligibility trace.

First, one study into how the augmentations affect the network gradients in the IDHP algorithm is conducted. This study will present a high-level discussion on the observed differences between the four algorithms when it comes to actor and critic updates over time. This study will run each algorithm on a sinusoidal AoA tracking problem for 5 s. The hyperparameters for this study were chosen out of convenience and kept simple, as the main focus here is on the augmentations. Meaning the most important factor when it comes to the hyperparameters used is for all algorithms to use the same values. A second consideration when choosing the hyperparameters was in concern of elucidating the differences between all algorithms, in order for the results to be more readily understandable. To this end, the eligibility decay rate λ was chosen to be at a relatively high value of 0.9, such that the results of this study will more clearly show the effect of using eligibility traces. The hyperparameters used for this study are reported in Table 3.4.

Table 3.4: Hyperparameters used during the weight gradients study.

Hyperparameters		
κ	$=$	1000
$\eta_{a,h}, \eta_{a,l}$	$=$	$2.0, 0.02$
$\eta_{c,h}, \eta_{c,l}$	$=$	$0.2, 0$
$\lambda_{a,h}, \lambda_{a,l}$	$=$	$0.9, 0.9$

Then, two Mone Carlo experiments will be conducted to study the effect of the augmentations on IDHP in terms of how they control the aircraft.

The first of such experiments involves studying the effect of only incorporating IDHP with each of the augmentations, where no changes to the hyperparameters or random number seeds used will be made. Since the initial network weights are sampled from a probability distribution, fixing the set of random number seeds used is important, as this ensures that the only differences across the four algorithms are the augmentations present, or lack thereof. All four agents will be given a step reference signal to track with no faults being introduced, 100 flights per algorithm will be conducted with the agent at the beginning of each flight being initialized to the initial variables listed under Table 3.3. Here, the main metrics for comparison are settling time t_s, defined as the time for tracking error to settle below 1.5 deg, and final error e_f, which is the absolute tracking error at the end of an episode/flight. The first metric, t_s, gives explicit information on how long the tracking error takes to settle, this is considered to be an indirect way of looking at how long the agents take to converge to their final policy; if an agent takes more time to converge to their final policy, it should take more time for the tracking error to settle, and vice versa. The second metric, e_f, is used to indicate the quality of the converged policy; a policy more optimal than another should logically have a smaller tracking error at the end of the episode. This experiment will use the same hyperparameters as the weight gradient study, except for the trace decay rates λ, where less aggressive values are used for better learning stability.

The second experiment involves studying the impact of the proposed augmentations on IDHP, by incorporating IDHP with each augmentation and tuning the hyperparameters of each algorithm. This means that different hyperparameters are used for each algorithm. In this experiment, the agents will be given a sinusoidal reference signal to track, while being introduced to faults 20 s into the flight. Just like the first experiment, each agent will repeat this control problem 100 times.

For hyperparameter tuning, the algorithm performances are optimized for the cg shift fault scenario to minimize tracking error, this resulted in different hyperparameters for each studied algorithm. A random search algorithm was used in these hyperparameter tuning procedures, where 15 hyperparameters are tested in parallel to speed up optimization using the multi-processing library of Python. Once again, the set of random number seeds used in all four algorithms is fixed. Here, the main metric used is the transient absolute tracking error e from the fault start to 10 s after. This metric is used to give an indication of how quickly the agents can adapt to the change in the MDP, and thus how adaptive the flight controller can be to a fault, a more adaptive controller should logically have a smaller error in the transient period after a fault.

Specifications of the two experiments along with the hyperparameters used are summarized in Table 3.5.

3.5.1. Reliability of Results: Coefficient of Variation

To demonstrate the reliability of the gathered metrics in the Monte Carlo experiments, the sample group's coefficient of variation C_v should stabilize. Broadly speaking, the more samples that can be drawn for a study, the more reliable the statistics are. This is because the underlying distribution that

Table 3.5: Specifications of the two experiments, experiment 1 uses the same hyperparameters for all algorithms, while experiment 2 uses different hyperparameters for each algorithm.

Experiment 1		Experiment 2	
Reference signal [deg]:	$\alpha_{ref,t} = 10$	Reference signal [deg]:	$\alpha_{ref,t} = 5\sin(2\pi\frac{t}{10})$
Metrics:	t_s, e_f	Metric:	$e = \sum_{t=20s}^{30s} \lvert\lvert\alpha_t - \alpha_{ref,t}\rvert\rvert$
Faults:	*None*	Faults @ 20 s:	*Shifted CG, damped elevator, inverted elevator*
Hyperparameters:		Hyperparameters:	
IDHP, IDHP(λ), MIDHP, MIDHP(λ)		IDHP	IDHP(λ)
$\kappa = 1000$		$\kappa = 1320$	$\kappa = 1211$
$\eta_{a,h}, \eta_{a,l} = 2.0, 0.02$		$\eta_{a,h}, \eta_{a,l} = 4.273, 0.059$	$\eta_{a,h}, \eta_{a,l} = 3.568, 0.054$
$\eta_{c,h}, \eta_{c,l} = 0.2, 0$		$\eta_{c,h}, \eta_{c,l} = 0.471, 0$	$\eta_{c,h}, \eta_{c,l} = 0.472, 0$
$\lambda_{a,h}, \lambda_{a,l} = 0.5, 0.1$		$\lambda_{a,h}, \lambda_{a,l} = 0, 0$	$\lambda_{a,h}, \lambda_{a,l} = 0.57, 0.257$
		MIDHP	MIDHP(λ)
		$\kappa = 1254$	$\kappa = 1289$
		$\eta_{a,h}, \eta_{a,l} = 3.2, 0.058$	$\eta_{a,h}, \eta_{a,l} = 3.398, 0.09$
		$\eta_{c,h}, \eta_{c,l} = 0.462, 0$	$\eta_{c,h}, \eta_{c,l} = 0.378, 0$
		$\lambda_{a,h}, \lambda_{a,l} = 0, 0$	$\lambda_{a,h}, \lambda_{a,l} = 0.236, 0.137$

represents the data can be more accurately approximated, assuming that the distributions are stationary. To show that the number of samples gathered is sufficient to approximate their underlying distribution, one can calculate the ratio of standard deviation to mean: this is the C_v statistic:

$$C_{v_i} = \frac{\sigma_i}{\mu_i} \tag{3.36}$$

Where the i subscript denotes the number of samples used to determine the variable. I.e., $C_{v_{10}}$ is the standard deviation of 10 samples divided by the mean of the same 10 samples. One simple way to calculate this variable is to do so as the Monte Carlo study is conducted, for every new sample n, an associated C_{v_n} can be calculated using the n samples collected thus far. By continuously calculating this variable throughout a Monte Carlo study, one should expect to see the C_v value stabilize at some stable level, at which point it can be said that the Monte Carlo study has *converged* and that the resulting statistics are reliable to some degree. A similar measure of reliability is used by Ballio and Guadagnini [131] who use the stabilization of mean and variance over the number of samples as a measure of convergence.

3.5.2. Statistical Significance of Results: t-test and a-test

To provide further rigour on the results gathered, the statistical significance of the observations can be found quantitatively. This is done in two ways, the first is using Student's t-test [132], and the second is using Vargha and Delaney's a-test[133].

Student's t-test is one form of statistical test used to conclude whether two groups of samples can be said to belong to the same population or underlying distribution. With the t-test, a null hypothesis is made stating that the mean and variance of the population underlying the two groups are the same. Thus, disproving this null hypothesis would mean the two groups in fact belong to different populations. To prove or disprove this null hypothesis, the t-test produces a p-value, which on a high level can be interpreted as the probability that the null hypothesis is true and ranges between 0 and 1. This p-value should be below a threshold in order to conclude that the null hypothesis is false, the common choice for such a threshold is 0.05 or 5%, which is the threshold chosen in the present research as well.

Vargha and Delaney's a-test is another form of statistical test, this test is used to provide information on the magnitude of difference between two groups of samples. In more mathematical terms, this statistical test determines what the stochastic ordering of the two groups is: whether one random variable is larger, smaller, or equal, to another random variable. In the a-test, an A-value is calculated between two groups of samples a and b representing the stochastic order of the two groups, this value ranges between 0 and 1. This A-value is the stochastic superiority of group a over group b, it $A > 0.5$, then group a generally has sample values which are higher than group b, i.e. group a is stochastically superior compared to group b. The reverse is also true, if $A < 0.5$, then group a is stochastically inferior compared to group b.

Applying the a-test to hypothetical settling time t_s samples as an example, suppose an a-test between t_s of MIDHP and IDHP returns an A-value of 0.3, this means that the settling times of MIDHP are generally smaller than the settling times of IDHP. Then, if an a-test between t_s of IDHP(λ) and IDHP returns an A-value of 0.55, two conclusions can now be drawn: first is that the settling times of IDHP(λ) are generally larger than IDHP, and second is that the settling times of IDHP(λ) are also larger than that of MIDHP. Final note, a property of the a-test is that the A-value is symmetric, i.e. if the A-value between group a and b is 0.3, then the A-value between group b and a is 0.7. This property follows from the definition of A from Vargha and Delanye's work [133].

By using these two statistical tests in conjunction, the metrics of different algorithms can be verified to be statistically significant as well as how they rank relative to each other, done using Student's t-test and Vargha Delaney's a-test respectively, foregoing subjective conclusions.

3.6. Results & Discussions

This section presents simulated flight control performances of the IDHP algorithm and its derivatives. This section presents the simulation results on the nominal performance and fault tolerance of the four present algorithms: IDHP, IDHP(λ), MIDHP, and MIDHP(λ). The main goal of this section is to provide a quantitative and qualitative evaluation regarding how the proposed augmentations affect the performance of the baseline IDHP algorithm through the results.

3.6.1. Weight Gradients Study

The four algorithms are given a test MDP problem to tackle to gather time traces of the algorithm's actor and critic updates. The chosen problem is a control task where the aircraft's AoA is controlled to follow a sinusoidal AoA reference signal. The gradient time traces are shown in Figure 3.6, from the top row of figures to the bottom row, the order of gradient plots are: IDHP, IDHP(λ), MIDHP, and MIDHP(λ). The left column of plots corresponds to the actor updates, while the right column corresponds to the critic updates.

Comparing the second row to the first row, the actor update time traces can be seen to be shifted leftwards in the second row, same observation is made for the critic updates. Additionally, the magnitude of actor updates is in general higher, even though the shape of the update time traces between the first and second row are very similar for both actor and critic updates. This makes sense on a theoretical level, the use of eligibility traces in IDHP(λ) on the actor means that the updates which the actor receives will include the updates of the previous time steps. Looking at the figures in row 1, the weight updates which the actor receives do not change in sign often, or exhibit any oscillatory action, for the first second the updates are either monotonically increasing or decreasing. Therefore, when these updates are accumulated using eligibility traces, it can be predicted that the actor updates will simply be a quicker and higher magnitude version of the updates from the baseline algorithm.

Comparing the third row of figures to the first, this time the actor updates are more similar than in the first comparison between the first and second row. However, the critic updates between the first and the third row look dissimilar where in the third row a lot more new updates, albeit relatively small magnitudes, are happening after the initial spike of critic updates. This shows that using a multi-step TD error for updating the critic introduced new update steps to the critic which would not have been present otherwise. In the upcoming Monte Carlo experiments, it will be seen what the effect of this is on the algorithm’s control performance.

Finally, comparing the fourth row of figures to the first row. One observation here is that the differences between the critic update of the fourth row to the first row are very similar to that of the third row and the first row: smaller updates are made to the critic after the initial spike of large updates. To add further, it would appear that the use of replacing eligibility traces on the actor updates was relatively mild compared to the effect which accumulating eligibility traces had. In fact, the only difference that can be discerned between the actor updates of the fourth row and that of the first row is the oscillatory updates around 1.3 s, seen after the initial update spike of updates. Otherwise, the differences in actor updates between the two rows are minute.

Despite some differences existing on close inspection, the four rows of figures seem similar at a glance, which might lead one to conclude that the augmentations did not meaningfully affect the algorithm. But to really understand how the augmentations affected the characteristics of the algorithm which are important, analysis of the Monte Carlo experiments results are needed.

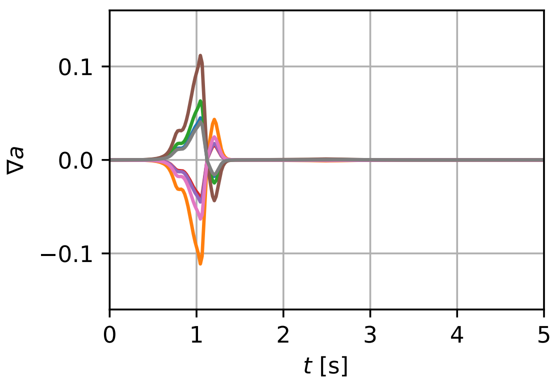

(a) IDHP actor updates.

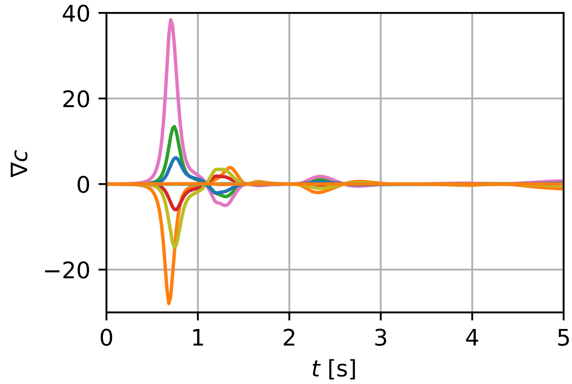

(b) IDHP critc updates.

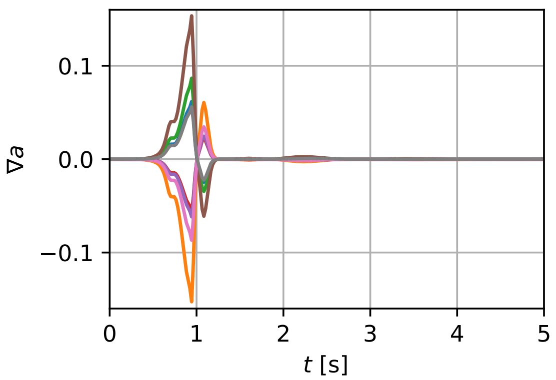

(c) IDHP(λ) actor updates.

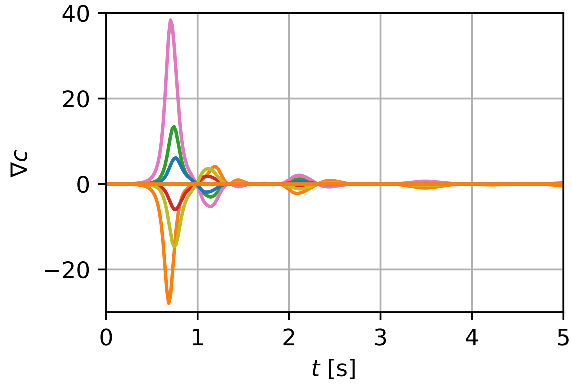

(d) IDHP(λ) critic updates.

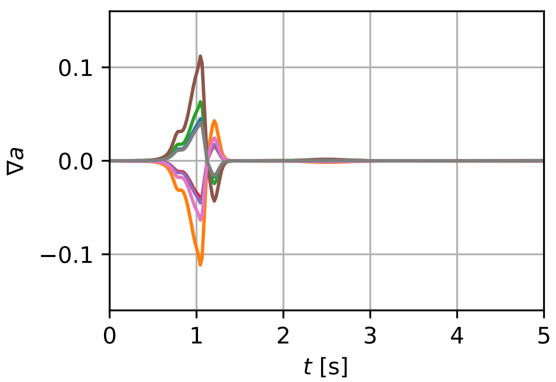

(e) MIDHP actor updates.

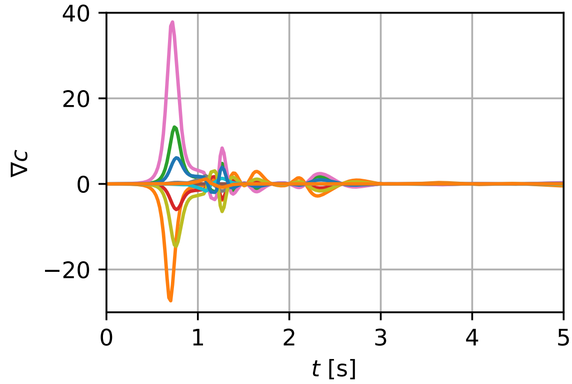

(f) MIDHP critic updates.

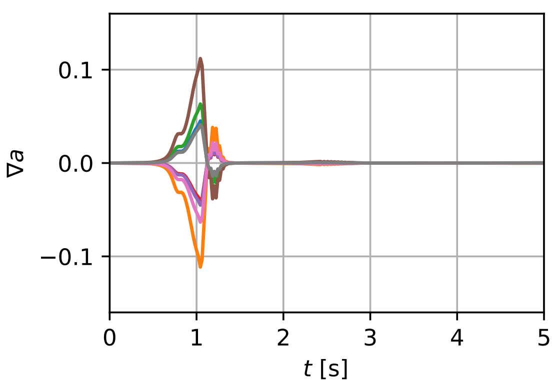

(g) MIDHP(λ) actor updates.

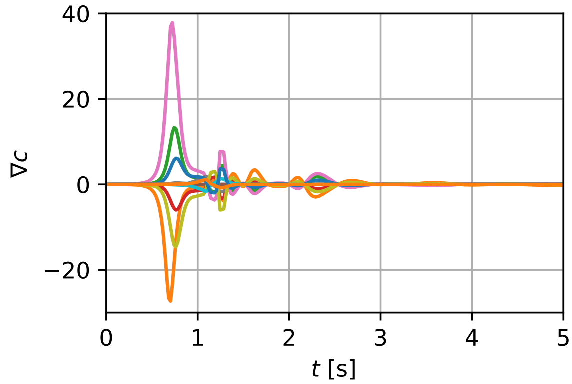

(h) MIDHP(λ) critic updates.

Figure 3.6: Actor and critic update over 5 s of the four algorithms solving the same control task.

3.6.2. Experiment 1

The control task for this experiment is a step AoA reference tracking problem, roughly speaking, the optimal control action is for the controller to smoothly increase the deflection of the elevator until the aircraft's AoA meets the reference value. Shown in Figure 3.7 is the Monte Carlo response of the IDHP agent for experiment 1, with the mean responses and their spread plotted over time.

From Figure 3.7a, the response akin to that of a purely proportional feedback controller can be seen, where the system state rises sharply and oscillates before settling around the reference value. This observation of a proportional controller-like response is expected, because the policy input, the MDP state space, is simply the tracking error. This means that the output of the policy function can only be some factor multiplied by the tracking error, thus the policy function behaves like a proportional gain.

The tracking error of this controller can be seen in Figure 3.7b, showing that the tracking error settles below 1.5 deg around 2 to 3 s and has a non-zero error at the end of each episode.

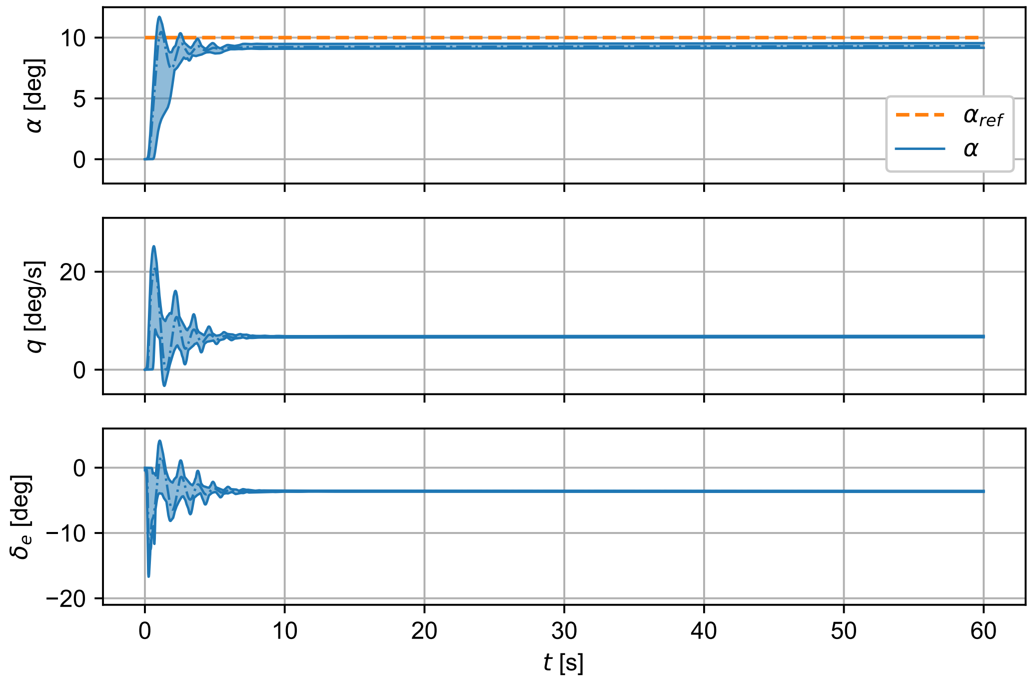

(a) State and action time traces.

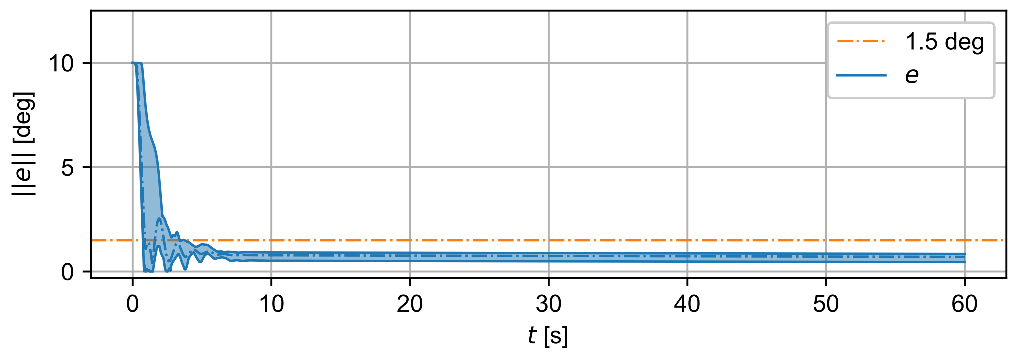

(b) AoA tracking error time trace with the 1.5 deg settling time threshold shown in dash-dotted orange, minimum and maximum shown by shaded area, mean shown by dash dot line.

Figure 3.7: IDHP step tracking result.

To compare the performances of all four algorithms, their corresponding t_s and e_f metrics from the 100 Monte Carlo runs are presented as boxplot diagrams in Figure 3.8. The key numerical statistics from the boxplots are presented in Table 3.6.

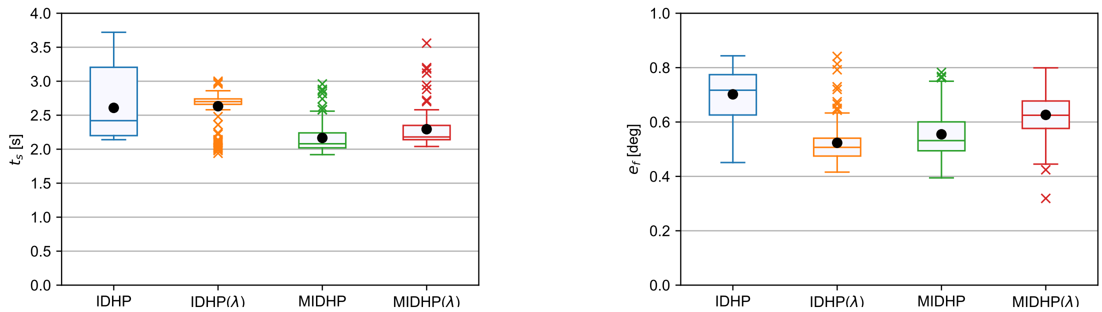

(a) Settling time t_s.

(b) Final error e_f.

Figure 3.8: Boxplots of experiment 1 metrics from the 100 runs conducted of each algorithm, black dots are the mean values.

Table 3.6: Settling time t_f and final error e_f statistics.

	t_f [s]				e_f [deg]			
	IDHP	IDHP(λ)	MIDHP	MIDHP(λ)	IDHP	IDHP(λ)	MIDHP	MIDHP(λ)
Maximum:	3.72	3	2.96	3.56	0.84	0.84	0.78	0.8
Minimum:	2.14	1.94	1.92	2.04	0.44	0.42	0.38	0.32
Upper quartile:	3.2	2.73	2.24	2.34	0.78	0.54	0.6	0.68
Lower quartile:	2.2	2.66	2.02	2.14	0.62	0.48	0.49	0.57
Median:	2.42	2.7	2.08	2.18	0.72	0.51	0.53	0.62
Mean:	2.6	2.63	2.17	2.29	0.7	0.52	0.55	0.53
No. outliers (above, below):	$\{0, 0\}$	$\{3, 14\}$	$\{7, 0\}$	$\{8, 0\}$	$\{0, 0\}$	$\{9, 0\}$	$\{3, 0\}$	$\{0, 2\}$

Starting with the analysis of the t_s comparisons shown in Figure 3.8a, the range of settling times for all algorithms ranged between 1.9 to 3.75 s, where IDHP and MIDHP produced the highest and lowest settling time respectively. The baseline IDHP algorithm overall had the widest spread in settling time with an Inter Quartile Range (IQR) of 1 s, this is in contrast to the derivative algorithms which all had a much smaller IQR, which at the smallest was 0.7 for IDHP(λ) and at the largest was 0.22 for MIDHP. While the spread of the median 50% of the settling times was much tighter for the derivative algorithms, their median times were generally lower. For IDHP, the median settling time was 2.42 s, while MIDHP had a median time as low as 2.08 s, which is 14% quicker. IDHP(λ), however, had a higher median settling time, at 2.7 s or 11.6% higher. Despite this higher median settling time, IDHP(λ) yielded a lower minimum and maximum settling time compared to IDHP, the same can be said when comparing MIDHP or MIDHP(λ) to IDHP where IDHP had the higher settling time in all the quantiles.

Thus overall, it can be said that two of the three derivative algorithms improved the settling time of the flight controller, with the exception of IDHP(λ) which arguably increased the settling time slightly. Furthermore, the augmentations in general result in less sensitivity to network initialization, evident by the much smaller settling time IQR, which is a desirable quality in controller robustness. That being said, any practical controller should not be initialized by random sampling from any distribution, but instead use some pre-determined values, which could be decided on randomly or through more systematic means.

Moving on to the analysis of e_f, the range of e_f stood between 0.84 and 0.32 deg, where IDHP and MIDHP(λ) produced controllers that gave the highest and lowest e_f respectively. In this metric, the IQR of all four algorithms are more similar than with the t_s metric but still significant, with the highest being 0.16 deg from IDHP and the lowest being 0.06 deg from IDHP(λ), which is a 62.5% difference. Another distinction between IDHP and its derivatives can be gleaned from these statistics. The median and mean e_f of the derivative algorithms are all smaller than IDHP, the smallest improvement is found in MIDHP(λ) which has a 13.9% improvement, while the largest improvement is found in IDHP(λ) which had an e_f that was 29.2% smaller at 0.51 deg.

Considering the whole set of data, a clear picture can be seen by observing Figure 3.8b that IDHP generally has a worse e_f. This is to say that the augmentations allowed the agent to learn a policy which reached a lower asymptotic error than the baseline algorithm under a step reference tracking task, albeit still with non-zero error.

With these statistics, it can be stated that the augmentations can improve the flight control performance of the IDHP algorithm since all factors aside from the augmentations have been held constant across all four Monte Carlo studies. A more nuanced point to be made is to what degree they improved performance. Of all the algorithms, MIDHP yielded the largest improvements in both t_s and e_f, for which the upper quartiles were both in the neighbourhood or lower than the lower quartile of the same statistics in the IDHP algorithm. This is to say that the multi-step augmentation provided the biggest likelihood for improvement in the controller's step tracking performance, as well as being more unilaterally better in both metrics. As opposed to IDHP(λ), which while having much lower e_f, was not likely to have lower t_s than the IDHP controller.

Coefficient of Variation

The C_v plots for t_s and e_f of the four algorithms are presented in Figure 3.9 and Figure 3.10, the ends of each plot have boxes bounding the graphs above and below to within 5% of the final C_v values. It can be seen that the C_v graphs mostly converge within this bounding box in the final few samples, meaning that the t_s and e_f metrics from the samples taken have mostly converged.

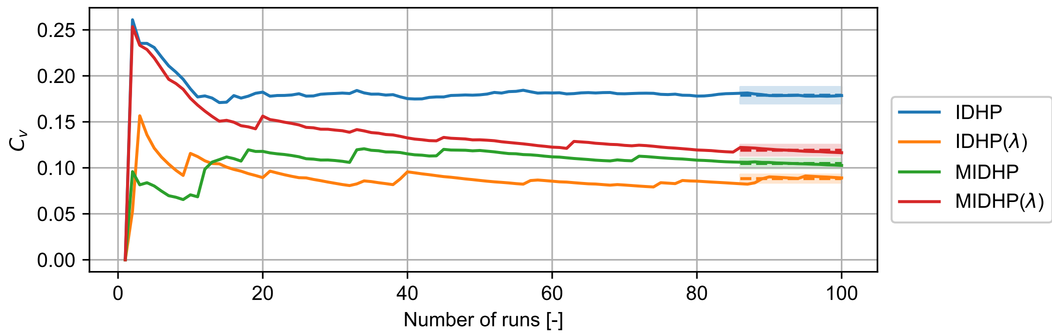

Figure 3.9: C_v plot for t_s, bounding boxes show mean of final 15 runs plus minus 5%.

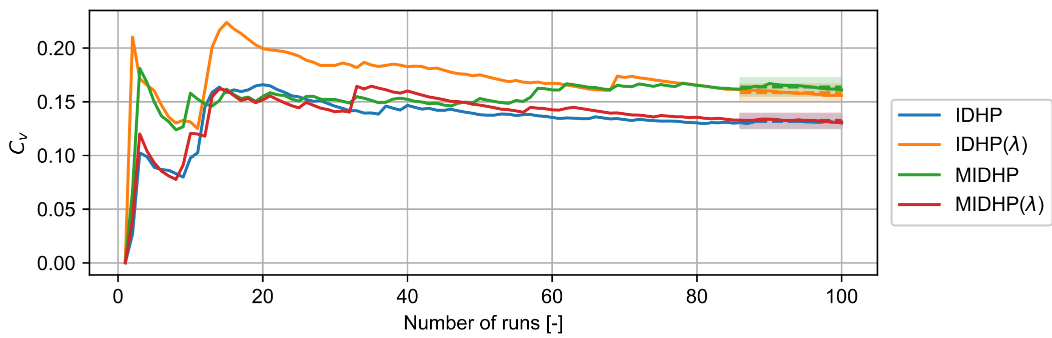

Figure 3.10: C_v plot for e_f, bounding boxes show mean of final 15 runs plus minus 5%.

Statistical Tests

A pair-wise statistical testing is done between the sampled metrics from each of the three derivative algorithms and the baseline IDHP algorithm. The statistical test results are summarized in Table 3.7. From these tests, it can be concluded that the difference between the derivative and baseline IDHP are all statistically significant except for the t_s samples of IDHP(λ), whose p-value is greater than 0.05. From these statistical tests, it is concluded that MIDHP showed the biggest improvement in nominal flight since it had the smallest A-value for t_s and the second smallest A-value for e_f. Which respectively indicates having the lowest t_s and second lowest e_f overall.

Table 3.7: Statistical testing results of experiment 1, p-values indicating statistically significant and insignificant differences shown in green and red respectively.

Statistical tests				
		IDHP(λ) vs IDHP	MIDHP vs IDHP	MIDHP(λ) vs IDHP
t_s	p-value	0.6447	3.9650×10^{-15}	2.3549×10^{-8}
	A-value	0.573	0.1436	0.2653
e_f	p-value	1.0678×10^{-32}	1.7971×10^{-23}	5.3592×10^{-9}
	A-value	0.0862	0.1364	0.2683

3.6.3. Experiment 2

The control task for this experiment is a sinusoidal AoA reference tracking task with faults being introduced 20 s into the flight. The three faults of shifted CG, damped elevator, and inverted elevator as listed in Table 3.5 and explained in Section 3.1.3 are used. Since the introduction of augmentations changed what hyperparameters gave the optimal performance, it was decided that a comparison of the algorithms under tailored hyperparameters would give a broader and more fair evaluation of the algorithms.

This experiment's objective is to study the effect of the augmentations on the fault tolerance of the IDHP controller, by measuring the impact of introducing fault on the total tracking performance metric e of the aircraft between when the fault is introduced and 10 s after. This metric is effectively equivalent to measuring the settling time in a step tracking task, as a low e would mean that the controller steered the aircraft AoA quickly back to the reference value.

Figure 3.11 shows the tracking performance of the IDHP controller for the sinusoidal tracking task with the elevator damaged 20 s into the flight. As can be seen from Figure 3.11b, the introduction of the fault led to a deterioration in the controller's tracking performance, however, this did not last as the tracking error began to steadily decrease after the error's peak. In fact, the 100 different agents seemingly converged to a more similar policy than before the fault, as the spread of tracking errors in Figure 3.11b became tighter after the 20 s mark.

The IDHP agent continually identifies a system model using RLS, and it is interesting to observe the prediction error of this model. This can be done by inspecting the $||\epsilon||$ over time, where ϵ is the model innovation or prediction error. Such a plot is shown in Figure 3.12. Observing this graph, $||\epsilon||$ immediately before the fault has been steadily decreasing, showing that the model's prediction accuracy was gradually improving. Immediately after the fault, $||\epsilon||$ jumps up sharply past the RLS covariance reset threshold of 9×10^{-5}. This triggers the model to reset, and the RLS algorithm re-identifies the system dynamics. Thereafter, the model innovation can be observed to continuously fall, indicating the identified model dynamics are once again converging towards the true system dynamics.

To dive into the comparative performances of the four algorithms, the transient tracking error e from the Monte Carlo studies are once again graphed in boxplots, these graphs are presented and analyzed in the following texts.

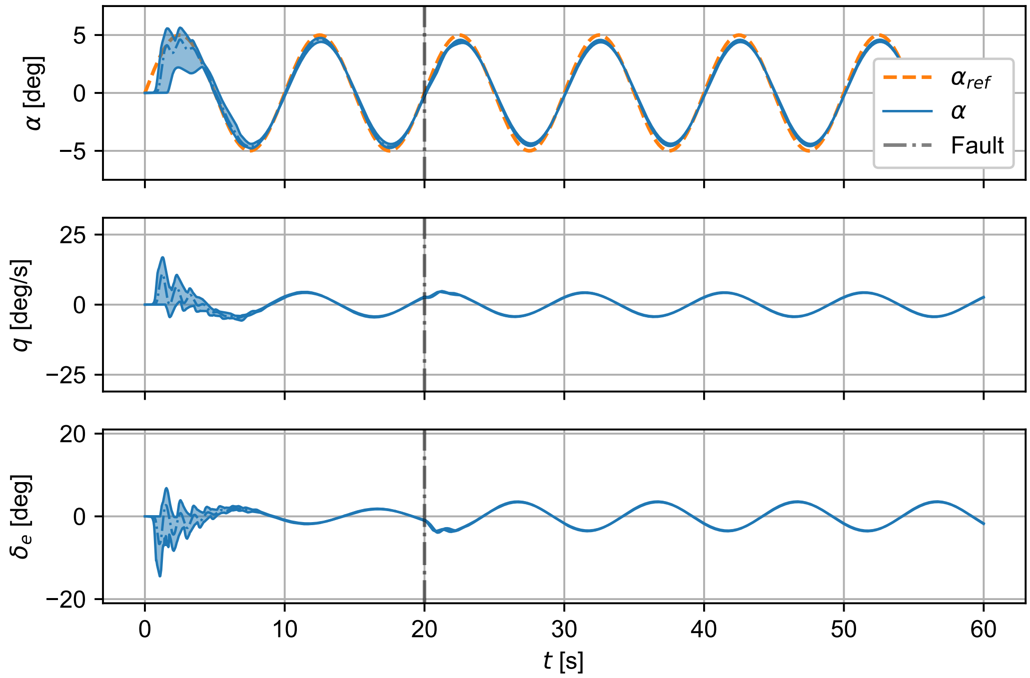

(a) State and action time traces.

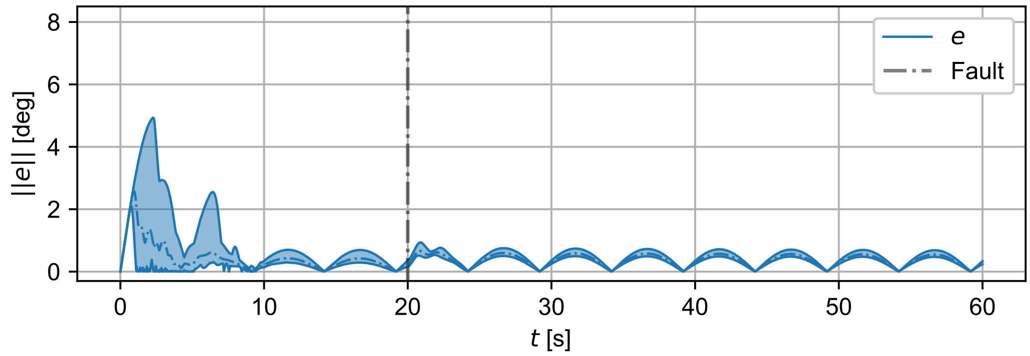

(b) AoA tracking error time trace.

Figure 3.11: IDHP sinusoidal tracking results with the elevator damage initiated at 20 s, minimum and maximum shown by the shaded area, mean shown by dash dot line.

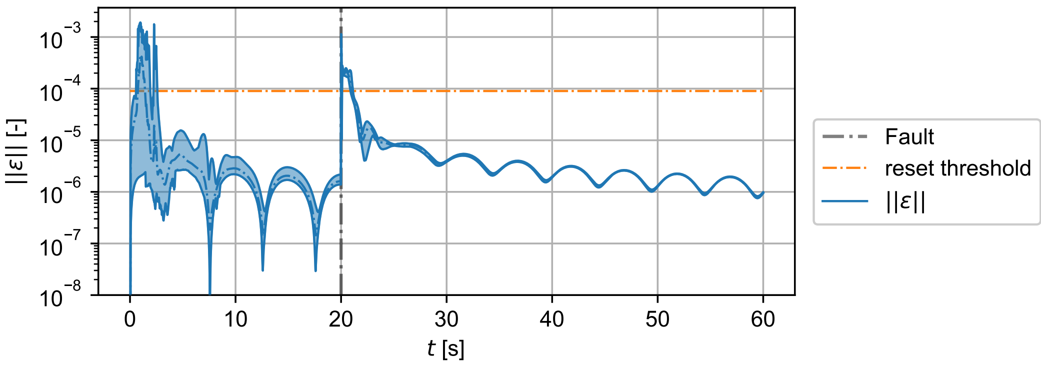

Figure 3.12: Monte Carlo result of RLS innovation norm $||\epsilon||$ over time, minimum and maximum shown by shaded area, mean shown by dash dot line.

Shifted Centre of Gravity

Figure 3.13 shows the e boxplots of the four algorithms after a shift in the CG, the numerical statistics are presented in Table 3.8. The values of e found with this fault ranged from a maximum of 4.49 deg from the IDHP(λ) algorithm to a minimum of 3.15 deg also from the same algorithm. The transient error of the IDHP(λ) controller is relatively large, as shown in Figure 3.13. This is in contrast with the MIDHP(λ) algorithm, which had a maximum and minimum of 4.2 and 3.41 deg, which is a 41% smaller spread. This difference can also be seen in the e time traces, which are shown zoomed in around the 20 s mark in Figure 3.14a. As a reference, the baseline result of IDHP is shown in Figure 3.14b.

While IDHP(λ) had the largest spread of e, it also had a lower median and lower quartile e than IDHP, meaning that IDHP(λ) had more runs whose error converged faster after the CG shift fault. The multi-step augmentations gave both a lower and higher overall e than the baseline IDHP e spread, where the spread of e from MIDHP(λ) was around the lower quartile of e samples from IDHP, therefore most MIDHP(λ) controllers recovered quicker from the CG shift fault. On the other hand, the group of e samples from MIDHP was slightly higher than the median e of IDHP.

The maximum difference between the median e of IDHP and any of its derivative algorithms is 5.77% between IDHP and MIDHP(λ), which had a median e of 3.81 and 3.89 deg respectively. This is a comparatively small improvement compared to the ones observed in experiment 1 under Section 3.6.2.

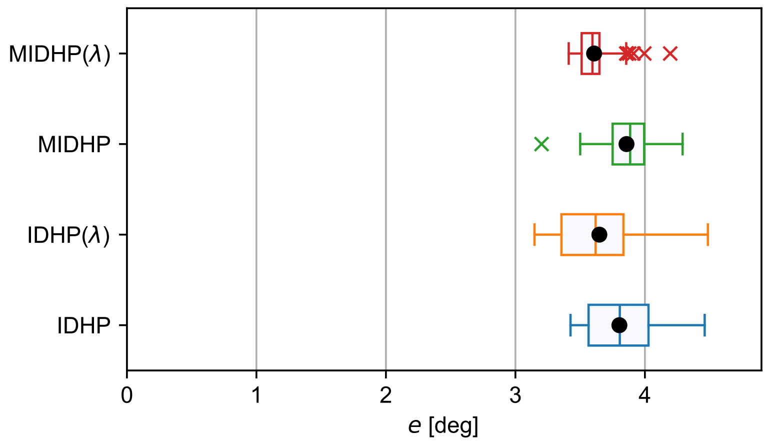

Figure 3.13: e boxplots of experiment 2 with the CG shift fault, black dots are the mean values.

Table 3.8: Transient error e statistics after the CG shift fault.

	e [deg]			
	IDHP	IDHP(λ)	MIDHP	MIDHP(λ)
Maximum:	4.46	4.49	4.29	4.2
Minimum:	3.43	3.15	3.2	3.41
Upper quartile:	4.02	3.83	3.99	3.65
Lower quartile:	3.56	3.36	3.75	3.51
Median:	3.81	3.62	3.89	3.59
Mean:	3.8	3.65	3.86	3.61
No. outliers (above, below):	$\{0, 0\}$	$\{0, 0\}$	$\{0, 1\}$	$\{6, 0\}$

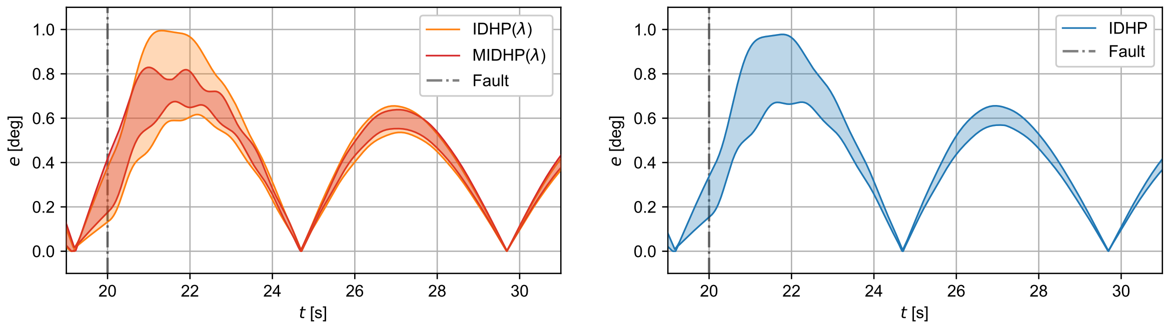

(a) IDHP(λ) and MIDHP(λ) e.

(b) IDHP e.

Figure 3.14: Minimum and maximum e error over time for three of the tested controllers.

The C_v plots for the group of e samples for the CG shift fault experiment is shown in Figure 3.15, where it can be seen the C_v stabilizes towards the end of the Monte Carlo runs.

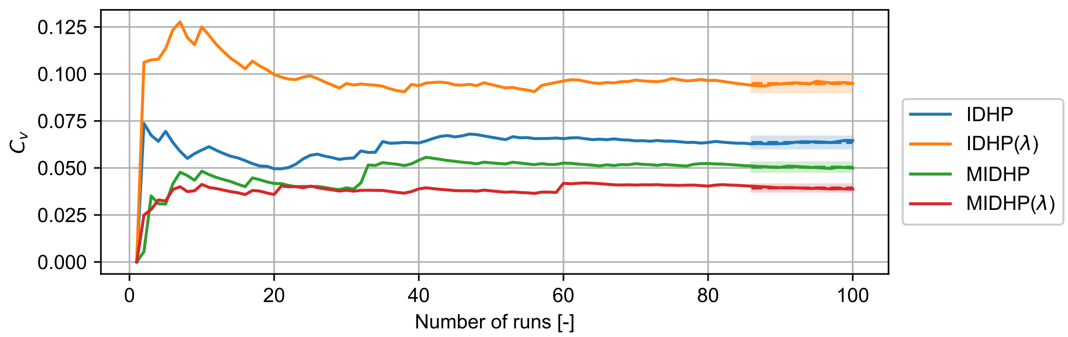

Figure 3.15: C_v plot for e under the CG shift fault in experiment 2, bounding boxes show mean of final 15 runs plus minus 5%.

The statistical testing results for the samples from this experiment are shown in Table 3.9. The statistical tests show that the difference between the derivative algorithms and the baseline are statistically significant, except for MIDHP versus IDHP where the p-value is 0.0813. It is also shown that MIDHP(λ) yielded the largest improvement in transient error since it's A-value is the smallest.

Table 3.9: Statistical testing results of experiment 2 with the shifted CG fault, p-values indicating statistically significant and insignificant differences shown in green and red respectively.

	Statistical tests		
	IDHP(λ) vs IDHP	MIDHP vs IDHP	MIDHP(λ) vs IDHP
p-value	3.687×10^{-4}	0.0813	7.9148×10^{-11}
A-value	0.334	0.5762	0.2734

Damaged Elevator

The next fault scenario lowers the control effectiveness of the elevator by 50% to represent a damaged elevator. The group of e samples are shown in boxplots in Figure 3.16, and the statistics are numerically recorded in Table 3.10. At a quick glance, the boxplots for this fault case and the shifted CG scenario are very similar, see Figure 3.13: The IDHP(λ) algorithm has the largest spread, followed by MIDHP, then IDHP, and ending with MIDHP(λ) which has the smallest spread. Additionally, the median e value of MIDHP(λ) as well as its median 50% of the e values are smaller than that of the IDHP algorithm. This time, the median e of MIDHP(λ) is 3.14 deg which is 5.14% smaller than the median of IDHP which is at 3.31 deg. Reading the statistics, MIDHP(λ) has a much more consistent spread of transient errors at a smaller spread than the baseline IDHP, meaning that it adapts better to the presented fault, this difference is also shown by the e time traces shown in Figure 3.17. Note that for the MIDHP(λ) time trace, the maximum e value was an outlier that is far from the upper quartile range, thus most of the controllers have a smaller e than is apparent in Figure 3.17.

In this fault scenario, the combination of multi-step TD update on the critic and eligibility traces for actor update contributed to a more robust and consistent controller: the recovery from a damaged elevator was quicker and the agent converged to a more optimal policy than the baseline IDHP.

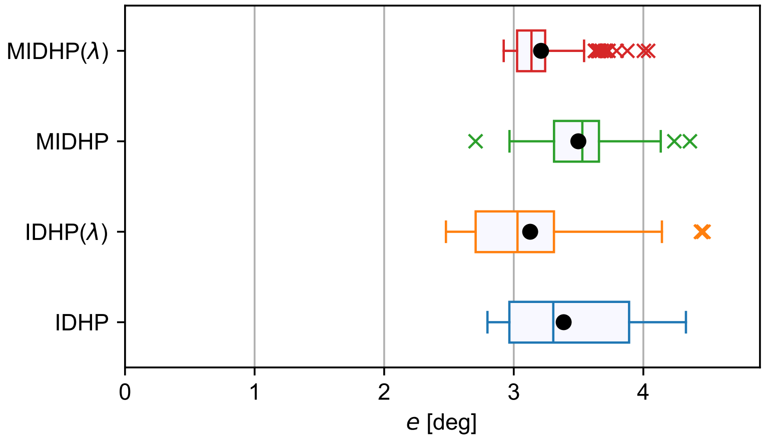

Figure 3.16: e boxplots of experiment 2 with the damaged elevator fault of each algorithm, black dots are the mean values.

Table 3.10: Transient error e statistics after the damaged elevator fault.

	e [deg]			
	IDHP	IDHP(λ)	MIDHP	MIDHP(λ)
Maximum:	4.33	4.46	4.36	4.04
Minimum:	3.80	2.48	2.70	2.92
Upper quartile:	3.89	3.31	3.66	3.24
Lower quartile:	2.97	2.71	3.31	3.03
Median:	3.31	3.01	3.53	3.14
Mean:	3.39	3.13	3.50	3.21
No. outliers (above, below):	$\{0,0\}$	$\{4,0\}$	$\{2,1\}$	$\{16,0\}$

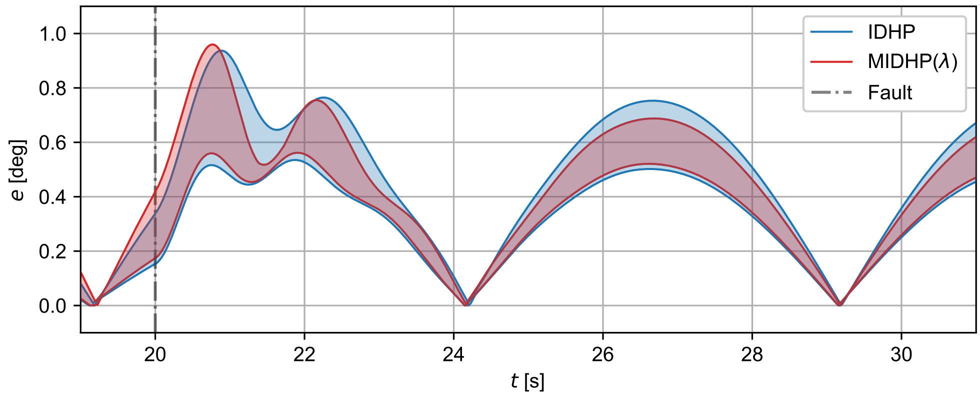

Figure 3.17: Experiment 2 with damaged elevator, minimum and maximum e over time for IDHP and MIDHP(λ).

The C_v plots of the e sample population for the damaged elevator fault experiment are shown in Figure 3.15, where it can be seen that once again the C_v stabilizes towards the end of the Monte Carlo runs.

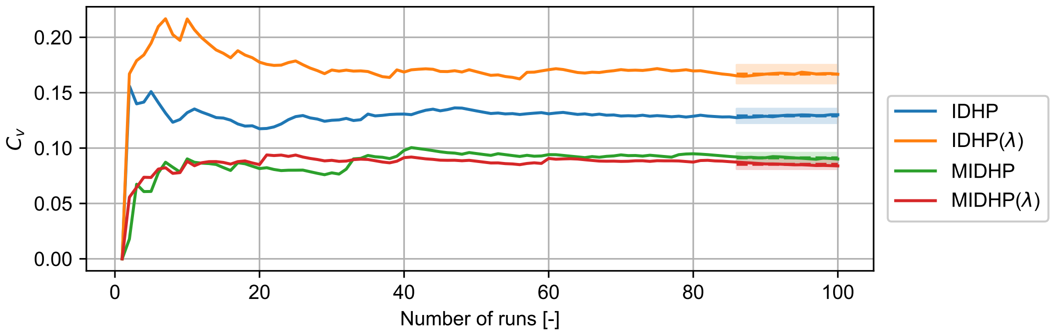

Figure 3.18: C_v plot for e under the damaged elevator fault in experiment 2, bounding boxes show mean of final 15 runs plus minus 5%.

The statistical testing results for the samples from this experiment are shown in Table 3.11. The statistical tests show that the difference of all three derivative algorithms from the baseline is statistically significant and that IDHP(λ) yielded the biggest improvement, with the lowest A-value.

Table 3.11: Statistical testing results of experiment 2 with the damaged elevator fault, p-values indicating statistically significant and insignificant differences shown in green and red respectively.

Statistical tests			
	IDHP(λ) vs IDHP	MIDHP vs IDHP	MIDHP(λ) vs IDHP
p-value	2.1594×10^{-4}	0.0388	9.2228×10^{-4}
A-value	0.3145	0.6037	0.4069

Reversed Elevator

The last fault scenario is the reversed elevator fault. The boxplot of transient errors e from stable controllers is shown in Figure 3.19, and the associated statistics are recorded in Table 3.12, a stable controller here means one which does not produce excessively oscillatory or unresponsive actions. Note that the final row of Table 3.12 records the number of agents which had an unstable or marginally stable controller after the reversed elevator fault is triggered. Furthermore, only the e of stable controllers are recorded and plotted in the boxplots such that these diagrams illustrate the performance of the algorithms only when they converge to a stable controller; leaving the matter of likelihood for the algorithm to produce stable controllers to be seen through the number of diverged controllers.

Reading from Table 3.12, it can be seen that for IDHP(λ), 98% of controllers were unstable or marginally stable. For other algorithms, while the portion of stable controllers is higher, the portion of unstable or marginally stable controllers is still significantly high. The most successful algorithm in this fault scenario was IDHP which had 74 stable controllers, followed closely by MIDHP(λ) which had 71 stable controllers.

From Figure 3.19, it can be seen that the stable IDHP controllers generally had the lowest error from the four algorithm's controllers. The median error of stable IDHP controllers is 12.02 deg, and the next closest median e is MIDHP(λ) whose median e is 13.32 deg or 9.76% higher.

Overall, the baseline IDHP algorithm can handle the reversed elevator fault scenario better than any of its derivative algorithms, both in terms of proportion and quality of stable controllers.

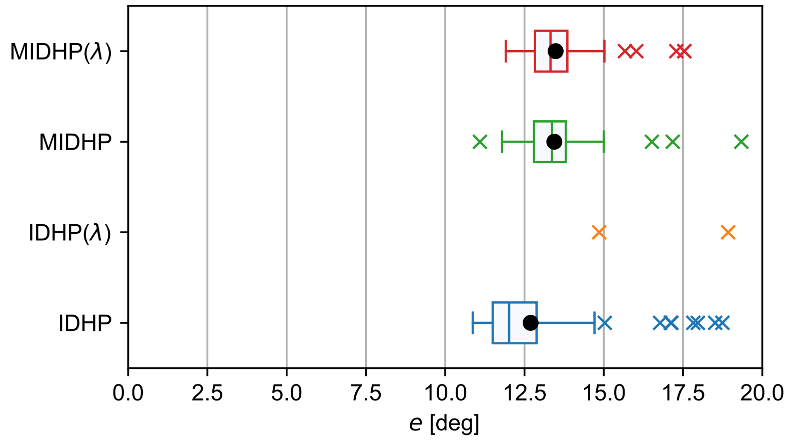

Figure 3.19: e boxplots of experiment 2 with the reversed elevator fault of each algorithm, black dots are the mean values.

Table 3.12: Transient error e statistics after the reversed elevator fault.

	e [deg]			
	IDHP	IDHP(λ)	MIDHP	MIDHP(λ)
Maximum:	18.74	18.9	19.33	17.53
Minimum:	10.86	14.82	11.08	11.90
Upper quartile:	12.86	3.31	13.82	13.84
Lower quartile:	11.50	2.71	12.78	12.82
Median:	12.02	3.01	13.34	13.32
Mean:	12.70	3.13	13.42	13.49
No. outliers (above, below):	$\{8, 0\}$	$\{0, 0\}$	$\{2, 1\}$	$\{5, 0\}$
No. diverged :	26	98	52	29

The inverted elevator fault was the most difficult scenario for all algorithms to adapt to, where many of the Monte Carlo runs had agents which would converge to an unstable or marginally stable controller, exhibiting highly oscillatory control action or stuck at full elevator deflection after the fault was introduced.

To investigate this matter, it would be useful to understand what the policy function looks like for a controller which is stable versus one which is not. Such a study is simple to conduct if only one instantaneous policy is studied, or if the policy function does not adapt and change over time. However, the policy function in the IDHP algorithm does evolve over time, with the policy function producing a different mapping at every time step of the simulation. Therefore, to be able to represent this temporal variation clearly, a scalar field plotted as a colour map is used. Specifically, at every time step, the policy function over the domain $e = [-5, 5]$ deg is recorded, by determining what the elevator deflection is over this domain of errors. This record is done at every single timestep, and the result can be plotted as a scalar field where the x and y axes are t and e, and the z axis is δ_e. The z axis is then mapped to a range of colours to represent the magnitude of elevator deflection.

These actor colourmaps and the corresponding state time trace are shown in Figure 3.21 for an unstable and a stable controller. To add further information, three snapshots of the policy function are presented in Figure 3.21 as well, these snapshots show what the policy function looks like at the select time steps: i.e. the mapping of what elevator deflection the agent will command for a given tracking error.

Inspecting these two controllers, a clear difference between them. For a stable controller, the actor-network would map the tracking error to a smooth control action, as evident by the smooth colour transitions in and the smooth policy function shown in Figure 3.21b at $t = 19.5$ s. This smooth actor-network can also be seen in the unstable network as well, but only before the reversed elevator fault is triggered. After the elevator is reversed, the actor-network converges to a very abrupt policy for the unstable controller, where any input away from zero tracking error results in the agent commanding a full negative or positive elevator deflection, see Figure 3.21a. This policy function resembles a step function more than a $\tanh$ function. Whereas for the stable controller, the agent managed to arrive at a policy function which is as smooth as before the fault, with only the gradient of the function being flipped. For a policy function to look smooth, such as the stable controllers, the weights of the actor-network cannot be too large in magnitude, since the higher the weights are the more extreme ranges of the $\tanh$ function will the inputs be mapped to. This deduction is confirmed by inspecting the actor-network weights of the stable and unstable controller, shown in Figure 3.20.

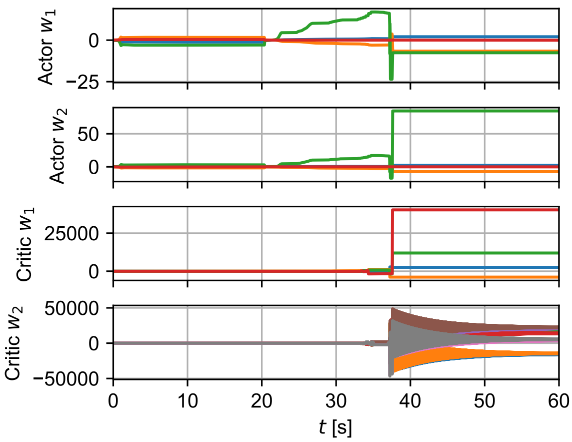

(a) IDHP(λ) unstable controller.

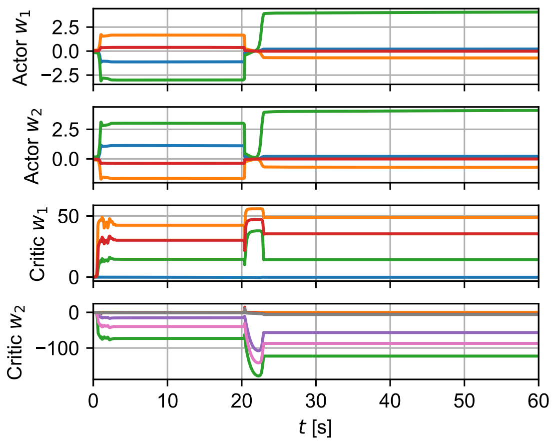

(b) MIDHP(λ) stable controller.

Figure 3.20: Actor and critic weights evolution comparison between an unstable and a stable controller in experiment 2 with the reversed elevator fault.

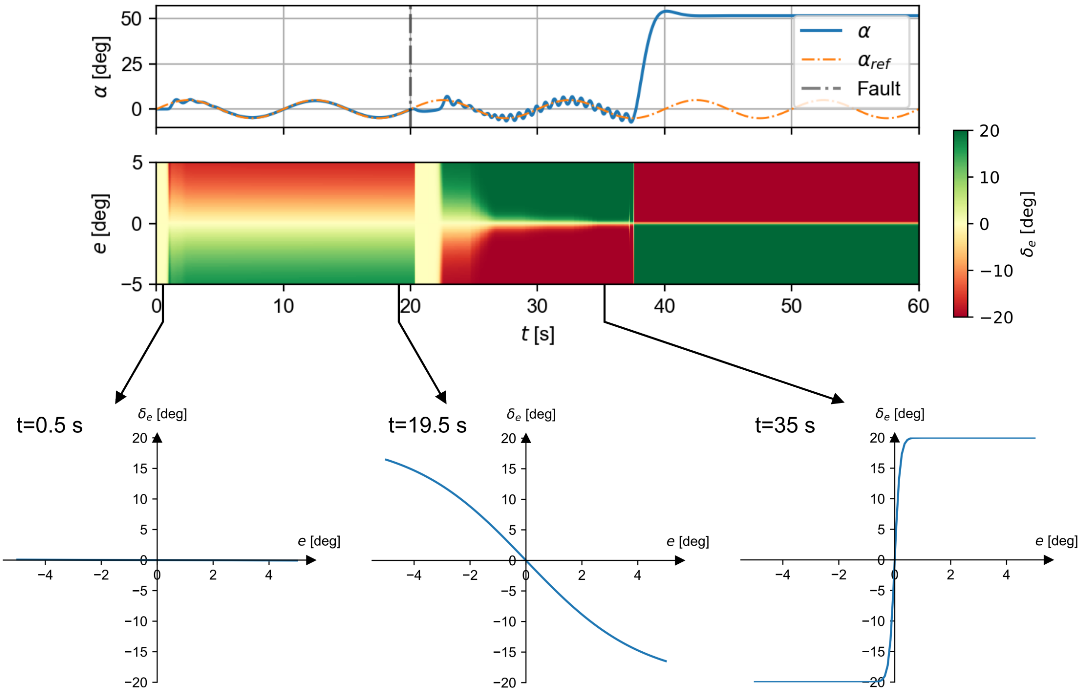

(a) IDHP(λ) unstable controller.

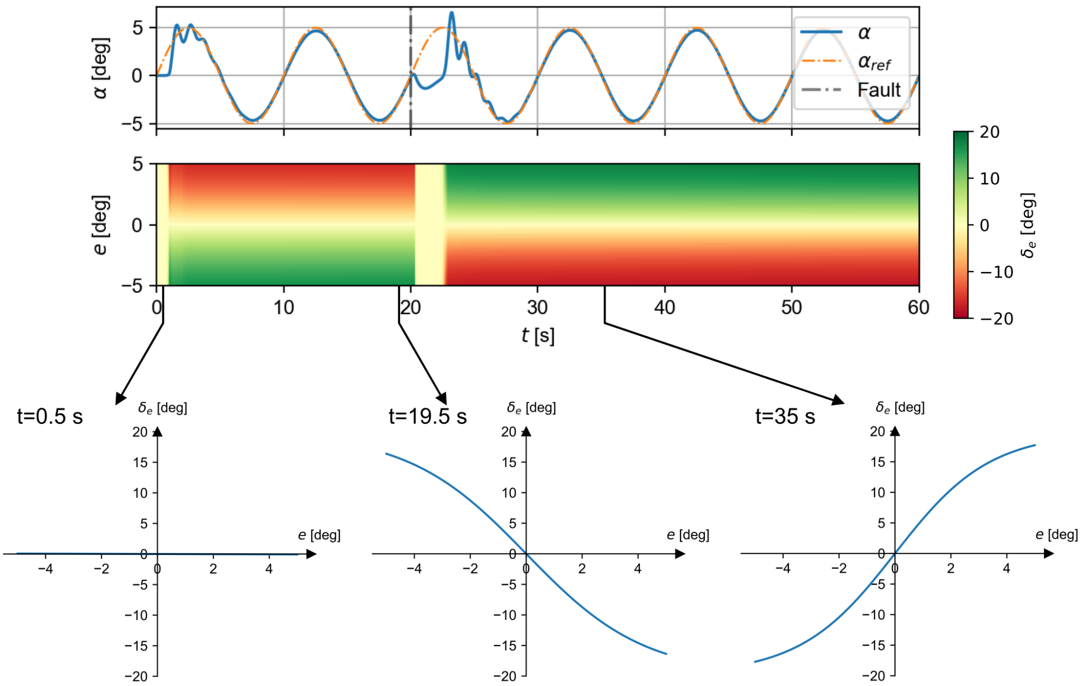

(b) MIDHP(λ) stable controller.

Figure 3.21: Comparison of stable and unstable controllers on the reversed elevator fault, in 3.21a and 3.21b, first the aircraft and reference α overtime is plotted, then the policy function plotted over time is plotted as a colour plot, finally three snapshots of the policy function are shown at $t = 0.5,\ 19.5,\ 35$ s.

The C_v plots for the group of e samples in the reversed elevator fault experiment are shown in Figure 3.15. Unlike the C_v plots of the previous two faults, the graphs are cut short by the number of runs with unstable or marginally stable controllers, i.e. the presented C_v plots only show the C_v of the runs with stable controllers. Observing this graph, the C_v values for all algorithms are not as stable or converged as the plots of Figure 3.15 and Figure 3.18. The most unstable of the C_v plot is for the IDHP(λ) controllers, where only two stable controllers were found, and for which the group of e statistics are not very indicative for the ensemble transient errors for all IDHP(λ) controllers. Nonetheless, the present result can still be used to draw some conclusions about the eligibility trace augmentation for the reversed elevator fault, which is that this augmentation detracts from the tolerance of the controller to this fault.

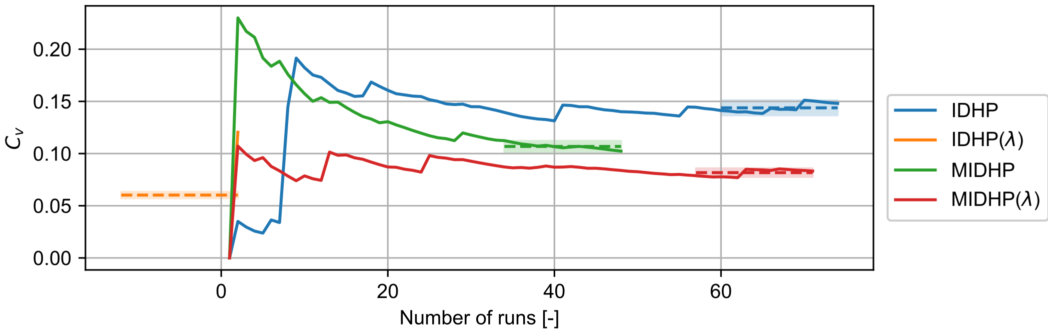

Figure 3.22: C_v plot for e under the reversed elevator fault in experiment 2, bounding boxes show mean of final 15 runs plus minus 5%.

The statistical testing results for the samples from this experiment are shown in Table 3.13.

Table 3.13: Statistical testing results of experiment 2 with the reversed elevator fault, p-values indicating statistically significant and insignificant differences shown in green and red respectively.

	Statistical tests		
	IDHP(λ) vs IDHP	MIDHP vs IDHP	MIDHP(λ) vs IDHP
p-value	0.1213	0.3649	0.2036
A-value	1.0	1.0	1.0

3.7. Conclusion

This chapter demonstrated the effect of incorporating the IDHP algorithm with the three augmentations proposed: accumulating traces, multi-step update, and replacing traces plus multi-step update.

Prior to discussing the results, the method for incorporating the proposed augmentations with IDHP was presented. The MDP concerning flight control of the PH-LAB was also presented, along with explanations and specifications of what flight dynamics models were to be used, considerations for how to design the MDP variables and thus what kind of flight controller is to be designed. These sections help with partially answering **Q2** from the research questions.

The effects of the augmentations on the behaviour of IDHP were presented and discussed in the study of weight gradients. This showed that some differences are present in the actor and critic updates of the agent depending on what augmentations were used. These differences came in the form of larger magnitude updates, quicker updates, and more persistent updates compared to the updates found in the baseline IDHP algorithm.

In the first Monte Carlo experiment, the settling time and final error results from the four algorithms in a step tracking control task were presented. The two metrics used gave some level of indication of the simulation time needed for the agents to converge to their final policy, and what the quality of this final policy was. From the gathered results, it was observed that the proposed augmentations generally converged to a policy with more optimal tracking performance than the baseline algorithm. However, the time needed for IDHP augmented with eligibility traces to converge was slightly longer than IDHP.

That said, the two other augmentations were found to have a smaller settling time, and thus indicating they could converge to their final policy quicker.

In the second Monte Carlo experiment, the transient error results of the four algorithms in a sinusoidal tracking task with faults were presented. From the CG shift and damaged elevator fault scenarios, the augmentations generally showed slightly lower transient error than the baseline algorithm, except when IDHP is only augmented with multi-step TD updates which had a slightly higher transient error. In the reversed elevator fault, it was found that all augmentations led to a poorer rate of the algorithm arriving at a stable controller, with only the double augmentation of eligibility traces and multi-step TD updates giving somewhat similar rates of stable controllers. In all augmentations, the transient error of stable controllers was poorer than that of the baseline IDHP algorithm.

With these various studies, partial answers are given for *Q3.1, 3.2, 3.2, 3.4* of the research questions.

That being said, the answers thus provided are produced on flight control of the short-period model of the PH-LAB, and more detailed flight models should be used to provide insights into how the augmented algorithms will handle the dynamics more closely resembling a real aircraft. Therefore, further research is needed.

Finally, the A-value for the gathered metrics from the conducted experiments is used to rank the four algorithms for each metric and experiment, and the resulting ranks are shown in Table 3.14. These ranks are decided based on which algorithm had the lowest A-value for the concerned metric, where the lowest A-value would have a rank of 1, and the highest A-value would have a rank of 4. The A-value of IDHP for all metrics is set to be 0.5, which stands for no difference in the sample values with IDHP. Note that the ranking for the reversed elevator experiment is done using how many runs out of the 100 conducted Monte Carlo runs yielded a stable controller.

Table 3.14: Ranking of the four algorithms according to each metric, rank 1 is best, rank 4 is worst, algorithm names are coloured to distinguish amongst variants easier.

	Experiment 1		Experiment 2		
	t_s	e_f	shifted CG e	damaged elevator e	reversed elevator
Rank 1	MIDHP	IDHP(λ)	MIDHP(λ)	IDHP(λ)	IDHP
Rank 2	MIDHP(λ)	MIDHP	IDHP(λ)	MIDHP(λ)	MIDHP(λ)
Rank 3	IDHP	MIDHP(λ)	IDHP	IDHP	MIDHP
Rank 4	IDHP(λ)	IDHP	MIDHP	MIDHP	IDHP(λ)

From the Table 3.14, it can be seen that the baseline algorithm overall had ranks 3 or 4 for all the metrics, with IDHP only coming 1st in the reversed elevator fault, thus demonstrating that the proposed augmentations yielded more fault-tolerant and performant controllers. Regarding which augmented algorithm is the best, since MIDHP(λ) had ranked 1st in one metric, 2nd in three metrics, and 3rd in one metric, this algorithm is overall the best. However, IDHP(λ) can also arguably be said to be as good if not better, since it ranked 1st in two metrics, 2nd in one metric, but 4th in two metrics.

These rankings can be discussed with a little more nuance, MIDHP(λ) ranked as the best algorithm in the fault tolerance experiments, ranking 1st in the shifted CG fault case, and 2nd in both the damaged and reversed elevator fault cases. But in nominal flight, which looks at the settling time and final error of the algorithms, it can be seen that MIDHP performed best, as it ranked 1st in terms of settling time, and 2nd in terms of final error.

Thus, MIDHP(λ) yields the most fault-tolerant controller, and MIDHP yields the most performant controller under nominal flight conditions.

Part III

Additional Results

4 Monte Carlo Hyperparameter Tuning

In total six IDHP variants are possible with the proposed augmentations; IDHP could either use multi-step updates or not, use replacing traces, or use accumulating traces. During the preliminary phases of the thesis, efforts were dedicated to evaluating how all six variants perform, this chapter presents the results of these efforts.

During hyperparameter tuning of the IDHP controllers for the results of Chapter 3, a large number of around 300 hyperparameters were randomly sampled and all six possible IDHP variants as shown in Figure 4.1 were run 30 times on each of these samples under the reversed elevator fault. To arrive at a hyperparameter selection for one IDHP variant then becomes a matter of selecting whichever hyperparameter resulted in the best performance for that variant.

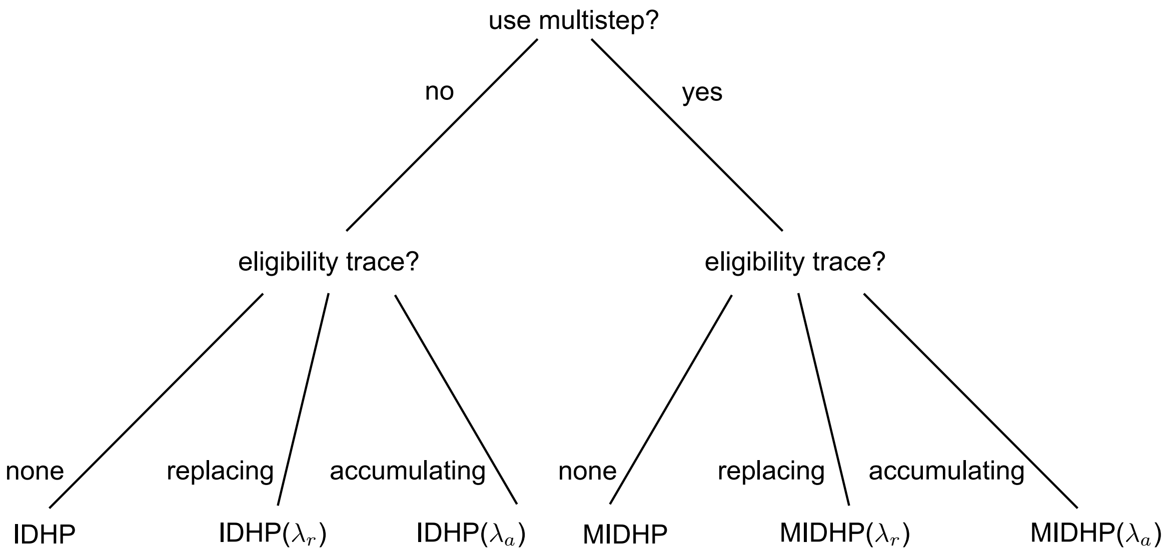

Figure 4.1: Possible variants of the IDHP algorithm, M prefix stands for multi-step, λ_r stands for replacing trace, λ_a stands for accumulating trace.

A byproduct of selecting and running a large number of hyperparameters for all IDHP variants is the resulting data, the performance of all algorithms on each of the hyperparameters can then be studied to surmise qualitatively what the effect of the augmentations was. To do so, three performance metrics are recorded. These three metrics are average Root Squared Error (RSE) of the α tracking error over one flight, t_c the average time needed to recover from the inverted elevator fault, and N_d the number of runs which took longer than 10 s to recover from the fault.

These results are graphed as scatter plots in Figure 4.2, each of the subplots is one IDHP variant identified by the acronym at the top of each subplot, each scatter point corresponds to one sample of hyperparameter, and each point's coordinate corresponds to the performance of each hyperparameter. The origin of the subplots is the *utopia point*, the point signifying perfect performance with no tracking error, no delayed recoveries, and the quickest possible recovery time from the fault.

It can be seen that in the top row of scatter plots, the points cluster along vertical lines with somewhat of an even spacing. These line clusters are a result of experiments where the same number of controllers converged to an extremely unusable policy. Specifically, policies which ended up causing the agent to rapidly command full elevator deflection as soon as the elevator reversal fault was triggered. For instance, the leftmost line corresponds to samples which did not have any controllers converging to such a policy, the line cluster one-over are samples with one such controller, the line one-more-over are samples with 2 such controllers, and so on.

In contrast, the bottom row of plots do not have these vertical clusters, which is due to these rapid policy changes not occurring in these variants. However, the policies of these variants would converge to such extreme policies at random points after the elevator reversal fault.

Another interesting observation is that the accumulating trace and multi-step update augmentations generally resulted in more hyperparameter samples in the neighbourhood of the utopia point, which implies that these augmentations generally resulted in agents that performed better throughout the flight. Nonetheless, there is another side to this story, where the multi-step variants had many more samples with a high number of delayed convergences.

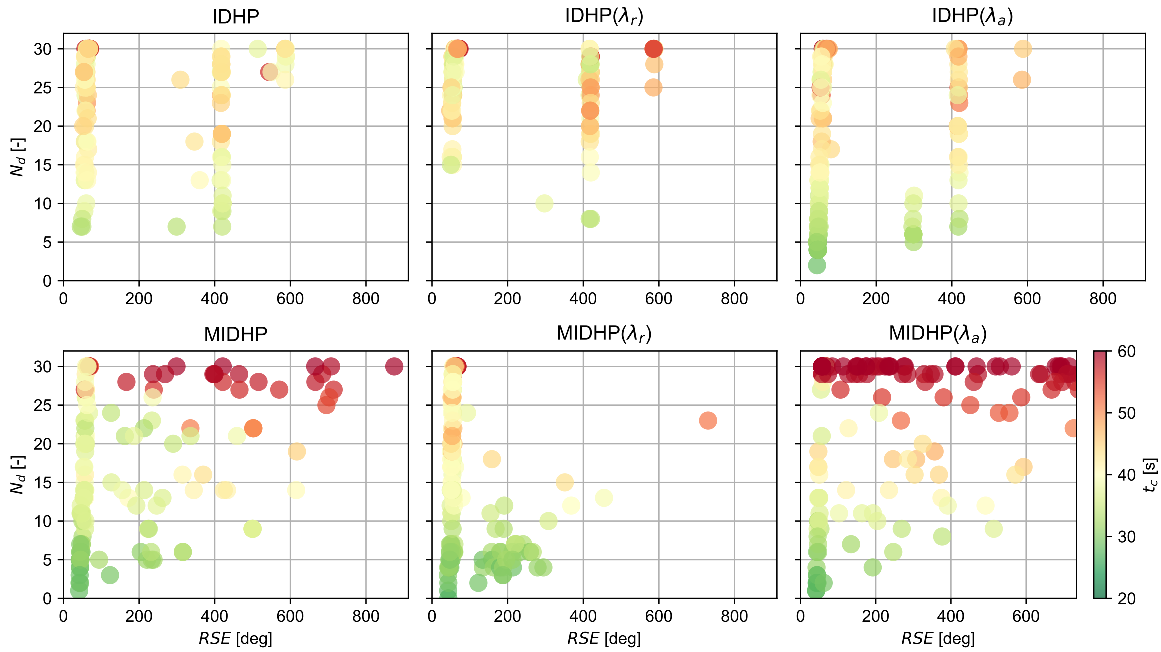

Figure 4.2: Hyperparameter scatter plots.

In light of these results, a decision was made to omit the analysis of two variants for the preliminary results, specifically IDHP(λ_r), and MIDHP(λ_a). This decision was made to compromise between presenting an excessive amount of graphs and data in the report, while still covering as many of the augmentations as possible, hence it was decided to maintain one variant with only eligibility traces IDHP(λ_a), one with only multi-step updates MIDHP, one with both augmentations MIDHP(λ_r), and one eligibility trace variant for each of the presented eligibility trace options IDHP(λ_a) and MIDHP(λ_r).

5 Rate Saturation on Controller Performance

From the results of the scientific paper, observing the oscillatory control actions in spite of adding a Conditioning for Action Policy Smoothness (CAPS) penalty, a question arose of whether introducing deflection rate saturation on the elevator surfaces would help alleviate this issue. Since such a saturation would restrict the sharp changes in elevator deflection rate. Therefore, the actuator dynamics of the aircraft model were extended to include a saturation on the deflection rates, placing a saturation limit according to the following block diagram:

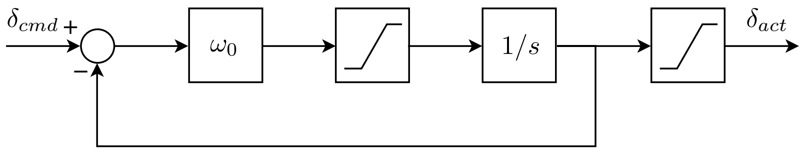

Figure 5.1: Block diagram of actuator model with deflection rate and angle saturation.

With the input δ_{cmd} being the commanded deflection, δ_{act} the actual deflection, and ω_0 the time constant of the first order transfer function.

With this extended actuator model, the four algorithms from Part 2, namely: IDHP, IDHP(λ) with accumulating trace, MIDHP, and MIDHP(λ) with accumulating trace; are re-tuned, finding the new hyperparameters which gave them the best performances. Subsequently, the same experiment from the scientific paper of five tests with 100 samples per test is conducted. For clarity, the table describing the five tests is reproduced:

Table 5.1: The five tests used in evaluating the proposed augmentations on IDHP.

		Test 1	Test 2	Test 3	Test 4	Test 5
Phase	:	Warmup (0 to 55 s)	Manoeuvering (55 to 90 s)	Manoeuvering (55 to 90 s)	Manoeuvering (55 to 90 s)	Manoeuvering (55 to 90 s)
Faults	:	N/A	None	Shifted CG	Damaged Elevator	Damaged and saturated elevator
Metrics	:	RSE, Sm				

Shown in the figure below are 100 runs of IDHP(λ) on test 4 with both a rate saturated and no rate saturation actuator models, where a damaged elevator is introduced at 60 s.

From Figure 5.2, it can be seen that the introduction of rate saturation has led to more runs converging to unstable policies during the warmup phase, with a small number of policies converging to a policy that always maximally deflects the elevator as seen in Figure 5.2b. Despite these drawbacks, the controllers that converge to a stable policy are noticeably less oscillatory during the high pitch segment from 60 to 80 s.

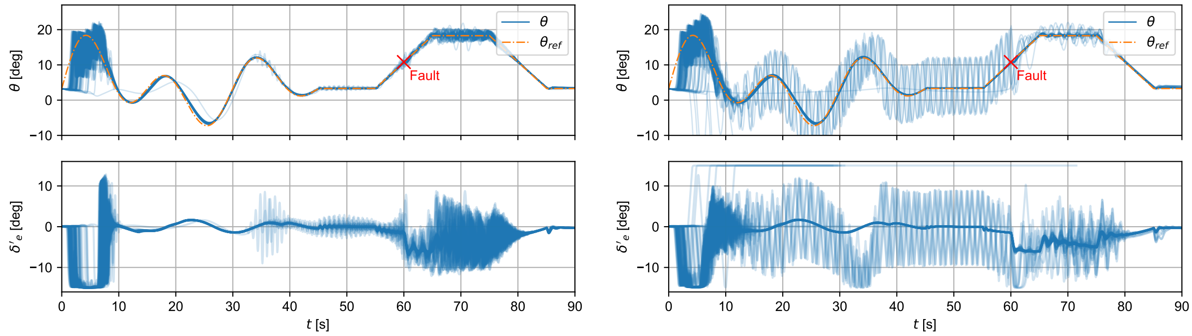

(a) Without rate saturation. **(b)** With rate saturation

Figure 5.2: Monte Carlo runs of IDHP(λ) with and without rate saturation, elevator damaged at 60 s.

The RSE and Sm metrics of the five tests are presented in boxplots under Figure 5.3 and Figure 5.4, and statistical testing results of the data are tabulated in Table 5.2 and Table 5.3 to provide a similar analysis of augmentation performance from the scientific paper, with the only difference being the introduction of deflection rate saturation in the actuator model.

The first observation from the results is that the action smoothing effect of multi-step updates no longer holds with the rate saturated actuator, and that all three augmented IDHP algorithms result in noisier control actions. However, the same trends in RSE can still be observed during the manoeuvering phase, and improvements in RSE from the augmented algorithms are also seen during the warmup phase.

With these results, it seems possible that the introduction of acceleration saturation on the actuator might lead to further smoothing of control action. This comes as one of the logical next steps in experimenting with RL for control, as introducing acceleration saturation in the actuator models will make the actuator dynamics slightly more realistic.

Test 1: warmup

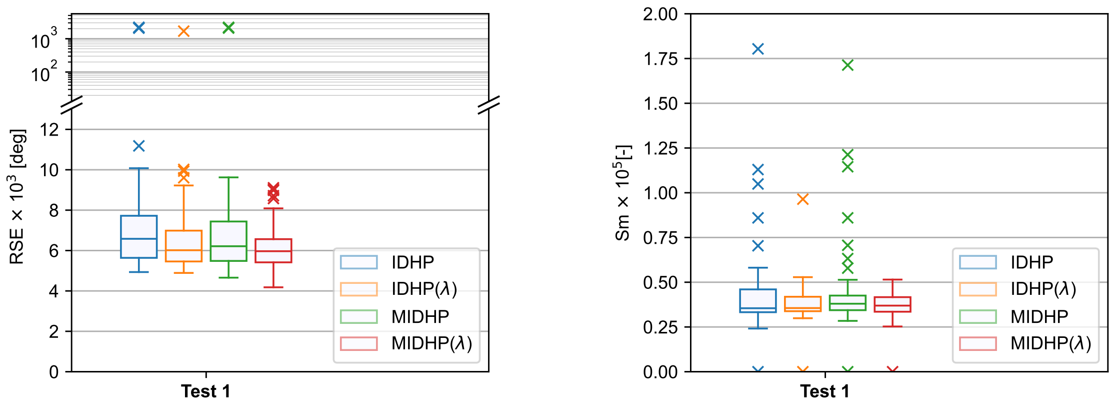

(a) RSE. **(b)** Sm.

Figure 5.3: Test 1 RSE & Sm result boxplots.

Table 5.2: VD's A-values on the RSE & Sm results on the first test, red A-value indicates statistically insignificant result according to Student's t-test (p-value > 0.05), A-value < 0.5 indicate the augmented algorithm's metrics are smaller than IDHP's and vice versa.

		Test 1	
		RSE	Sm
IDHP(λ) vs *IDHP*	:	0.391	0.510
MIDHP vs *IDHP*	:	0.380	0.542
MIDHP(λ) vs *IDHP*	:	0.320	0.522

Test 2-5: manoeuvering

Note that in Table 5.3, the RSE A-value in test 2 for the comparison between MIDHP and IDHP is 0.342 despite the spread of RSE samples from MIDHP being much wider and frequently at higher values than IDHP. This seemingly strange result is due to the fact that VD's A-value is computed based on the ranking of two samples, but not on the absolute distance between two samples.

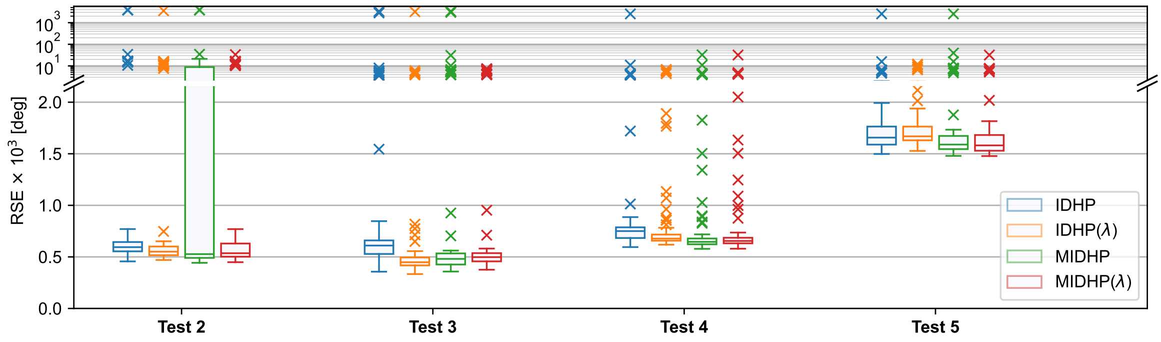

(a) RSE.

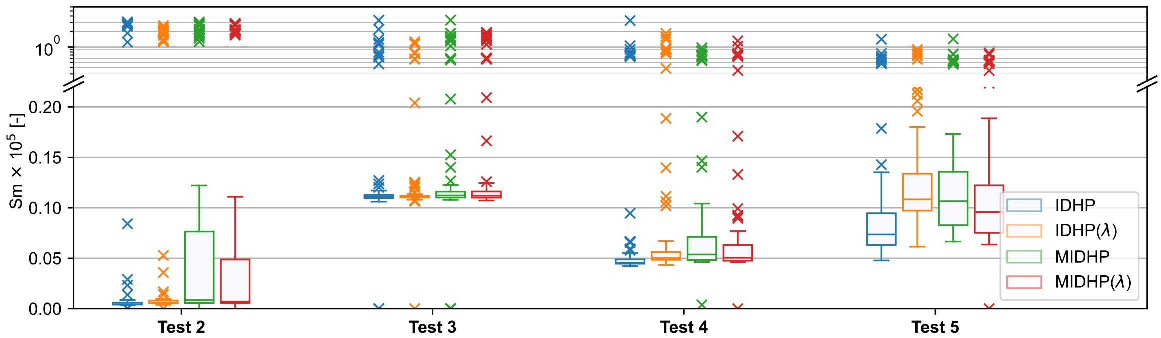

(b) Sm.

Figure 5.4: Test 2, 3, 4, and 5 RSE & Sm result boxplots.

Table 5.3: VD's A-values on the RSE & Sm results on the second to fifth tests, red A-value indicates statistically insignificant result according to Student's t-test (p-value $= 0.05$), A-value < 0.5 indicate the augmented algorithm's metrics are smaller than IDHP's and vice versa.

(a) RSE.

		Test 2	Test 3	Test 4	Test 5
IDHP(λ) vs *IDHP*	:	0.301	0.100	0.282	0.591
MIDHP vs *IDHP*	:	0.342	0.163	0.178	0.277
MIDHP(λ) vs *IDHP*	:	0.229	0.182	0.186	0.278

(b) Sm.

		Test 2	Test 3	Test 4	Test 5
IDHP(λ) vs *IDHP*	:	0.826	0.501	0.927	0.892
MIDHP vs *IDHP*	:	0.750	0.618	0.927	0.825
MIDHP(λ) vs *IDHP*	:	0.837	0.641	0.834	0.769

6

Neural Network Jacobian

Implementation of the eligibility traces requires having the derivative of the function approximator being used. In the early uses of eligibility traces, reinforcement learning algorithms used function approximators which are linear or had relatively few parameters as compared to deep or shallow neural networks [128]. The nonlinearity which are inherent to neural networks, due to the use of nonlinear activation functions, and the use of one or more hidden layers, causes the computation of such derivatives to be cumbersome.

Luckily, standard with many machine learning libraries are auto-differentiation functionalities. Using such libraries, it is possible to obtain the eligibility trace of a neural network by taking the derivative of the network's output with respect to all of its weights. Nonetheless, for the purposes of understanding how the eligibility trace of a neural network, or the network Jacobian, is obtained, it is useful to have a glimpse at what operations lead to the final result.

For the purpose of illustration, a small neural network similar to those used in the scientific paper will be defined.

Take a neural network with two input nodes, one hidden layer with five nodes, and two output nodes. Define the hidden and output layer to have an $\tanh$ activation function. This results in the following functional form of the neural network:

$$y = tanh(W_2 x_1) \tag{6.1}$$

$$x_1 = tanh(W_1 x) \tag{6.2}$$

$$x \in \mathcal{R}^2, \quad x_1 \in \mathcal{R}^5, \quad y \in \mathcal{R}^2, \quad W_1 \in \mathcal{R}^{2\times 5}, \quad W_2 \in \mathcal{R}^{5\times 2}$$

Where y is the neural network output, x is the input, W_1 and W_2 are the network layer weights, and x_1 is an intermediate variable.

Such a network will have a jacobian as follows:

$$\nabla y = \begin{bmatrix} \frac{\partial y}{\partial W_2} & \frac{\partial y}{\partial W_1} \end{bmatrix} \in \mathcal{R}^{2\times 20} \tag{6.3}$$

The jacobian may also be expressed as a three-dimensional array or a tensor, rather than a matrix. Along the first dimension of this matrix are the two outputs of the network, along the second dimension of this matrix are all the 20 individual weights which parameterize the neural network. This matrix is then computed in two steps, first by finding $\frac{\partial y}{\partial W_2}$, and second by finding $\frac{\partial y}{\partial W_1}$.

Determining $\frac{\partial y}{\partial W_2}$

Observing Equation 6.1, there is a direct relationship between y and W_2, thus this partial derivative is relatively straightforward. The weight W_2 is represented as a matrix with 2 rows and 5 columns, and the term $\frac{\partial y}{\partial W_2}$ is accordingly a matrix with 2 rows and 10 columns, which can be considered to be composed of 2 rows of 2 sub-blocks with each sub-block a row-vector of 5 columns:

$$\frac{\partial y}{\partial W_2} = \begin{bmatrix} (1-y_1^2)x_1 & \mathbf{0}_{1\times 5} \\ \mathbf{0}_{1\times 5} & (1-y_2^2)x_1 \end{bmatrix} \tag{6.4}$$

With y_1 being the first output or first element of y, and y_2 the second output.

Determining $\frac{\partial y}{\partial W_1}$

The relationship between y and W_1 is more indirect, going through two activation functions and one weight matrix. This means the partial derivative will require evaluating a longer chain of derivatives.

The weight W_1 is represented as a matrix with 5 rows and 2 columns, and once again the partial $\frac{\partial y}{\partial W_1}$ is also represented as a matrix with 2 rows and 10 columns. This time, the partial is considered as a matrix with 2 rows of 5 sub-blocks, with each sub-block being a row-vector with 2 columns:

$$\frac{\partial y}{\partial W_1} = \begin{bmatrix} \frac{\partial y_1}{\partial W_{1:1,\cdot}} & \frac{\partial y_1}{\partial W_{1:2,\cdot}} & \frac{\partial y_1}{\partial W_{1:3,\cdot}} & \frac{\partial y_1}{\partial W_{1:4,\cdot}} & \frac{\partial y_1}{\partial W_{1:5,\cdot}} \\ \frac{\partial y_2}{\partial W_{1:1,\cdot}} & \frac{\partial y_2}{\partial W_{1:2,\cdot}} & \frac{\partial y_2}{\partial W_{1:3,\cdot}} & \frac{\partial y_2}{\partial W_{1:4,\cdot}} & \frac{\partial y_2}{\partial W_{1:5,\cdot}} \end{bmatrix} \tag{6.5}$$

Where $W_{1:1,\cdot}$ is the first row of the weight matrix W_1, and $\frac{\partial y_1}{\partial W_{1:1,\cdot}}$ the derivative between the first network output y_1 to the first row of the weight matrix W_1, which can be determined as follows:

$$\frac{\partial y_i}{\partial W_{1:j,\cdot}} = [(1 - y_i^2)(W_{2:i,j})(1 - x_{1:j}^2)]x \tag{6.6}$$

The Jacobian for Deeper Networks

As a neural network increases in depth, the more linear the relationship between input and output becomes. This inevitably leads to the derivative of the weights closer to the input to depend more and more on weights closer to the output. Practically, this leads to the Jacobian becoming more difficult to compute, but this is an issue that can be readily overcome through auto-differentiation. But when it comes to the implications on algorithm performance, deeper networks can cause the gradients accumulated during past time steps to inaccurately indicate which parameters are more eligible for updates, this is evident in Equation 6.6, where the partial derivative or eligibility of the j-th row of W_1 is influenced by the *value* of $W_{2:i,j}$. Such parameter dependence causes an issue referred to as *gradient divergence* by Kobayashi, who proposed adaptively decaying the eligibility traces according to the extent of such divergences [130].

7 Verification and Validation

To provide credibility to the results presented in the present thesis, in addition to the statistical testing of results, a verification and validation procedure is conducted to assure the software produced is *correct*. Such a procedure concludes whether the final software is correct by asking two questions. First, is the question of *is the software built right*, which refers to whether the RL algorithm and the MDP models have been implemented correctly. Second, is the question of *is the right software being built*, which in the context of the present work refers primarily to whether the dynamic model used in the MDPss correspond with the dynamics observed in the real aircraft, this is validation.

7.1. Verification

7.1.1. RL Algorithm

The present work is based on the implementation and experimentation of the IDHP algorithm. The implemented algorithms are first derived and understood on a mathematical level, by studying the work of Zhou et al. [52], and once a pseudo-code consistent with the algorithm of IDHP has been reproduced, it is implemented as Python code. The Python implementation is then further compared to previous implementations of IDHP for algorithmic consistency.

The primary verification needed to ensure that the IDHP implemented is correct, is to compare whether the present implementation can learn a usable control policy. Furthermore, that the implemented algorithm can do so in approximately the same time frame and to roughly the same quality as previous works. Such a verification is performed in several ways. First, the algorithm is shown to be able to produce usable policies by the results presented in Chapter 3, where the aircraft state is steered correctly to follow the reference state. Second, the tracking performance from Chapter 3 is compared to the results of Lee [111] and of Heyer [4]. In the present and both referenced works, the IDHP controller are able to track the reference state from initialization in roughly 5 s, with errors less than 1 deg. The only exception here is the tracking performance of Heyer, which is much lower than the present work and that of Lee. This difference is likely due to the difference in the inputs taken by the actor and critic, which in the works of Heyer includes the tracking error as well as AoA and pitch rate, this input is more extensive than that used in the experiments of Chapter 3.

This then provides credence that the IDHP implemented learns as expected. Verifying if the proposed augmentations are correct is done in a similar manner, by first deriving and understanding the mathematical formulation of the eligibility traces and multi-step updates, and subsequently ensuring that the implemented code is done according to the written formulae.

Finally, as the IDHP algorithms used in Part 2 are duplicates of the algorithms used in Part 1, this extends the confidence in the correct implementation of IDHP to the algorithms used in Part 1.

7.1.2. Aircraft Dynamics

Verification of aircraft dynamics is done in two parts. The first is to verify that the dynamics implemented for the short-period model in Part 1 is as intended. As this dynamics model is taken directly from TUDelft's lecture notes, the primary method of verification is to ensure that the state space models, control and stability coefficients implemented in Python are exactly that of the lecture notes [116]. This is helped by defining the coefficients in Python with the same names as used in the lecture notes, allowing for the values of coefficients and the creation of the state space matrices to be compared directly.

The aircraft dynamics model used in Part 2 requires a different method of verification. Here, the model used is a `.pyd` C-code executable in Python, compiled from the CitAST Simulink model developed by the Control and Simulations group of TUDelft [134]. Thus, the aircraft of dynamics in Part 2 need to be verified by model matching with the dynamics of the Simulink model, this is done by commanding the same control signals to both the `.pyd` and Simulink models.

Three model matching tests are done, all inspecting the attitude rates of the aircraft, as this is the fastest and therefore most critical dynamic to ensure model consistency. The first test feeds the trim input to both models, and its results are shown in Figure 7.1. The second is a sinusoidal input to the three control surfaces, shown in Figure 7.2. The third is a sinusoidal input to the three control surfaces in addition to a Centre of Gravity shift at 20 s, which is a mechanic coded directly into the Simulink model and thus needs to be verified to behave identically in the `.pyd` model, these results are shown in Figure 7.3. As can be seen, while the errors in attitude rates are minimal, with the differences between the two models being hardly distinguishable by the naked eye, there is nonetheless a non-zero error between the two. This difference is assumed to be due to some rounding or conversion errors in model constants when compiling the Simulink model to `.pyd`.

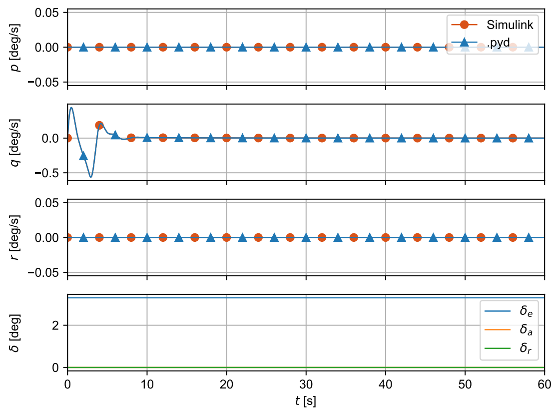

(a) Attitude rates of both models and commanded trim input.

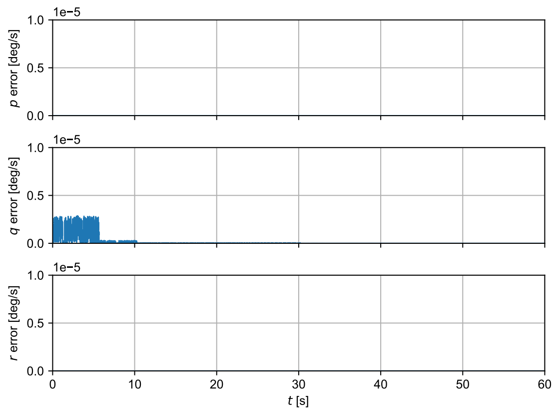

(b) Attitude rate errors.

Figure 7.1: Trim input model matching, the response of .pyd and Simulink models shown in circle and triangle dotted lines respectively.

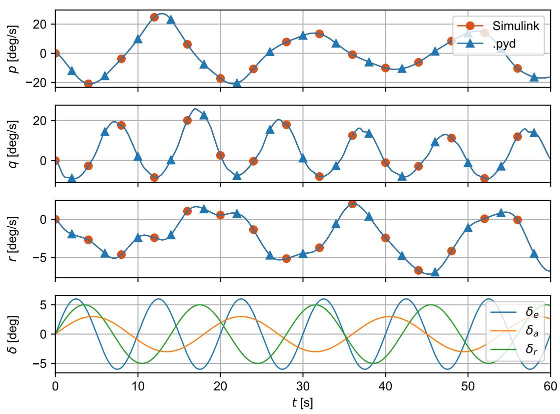

(a) Attitude rates of both models and commanded sinusoidal input.

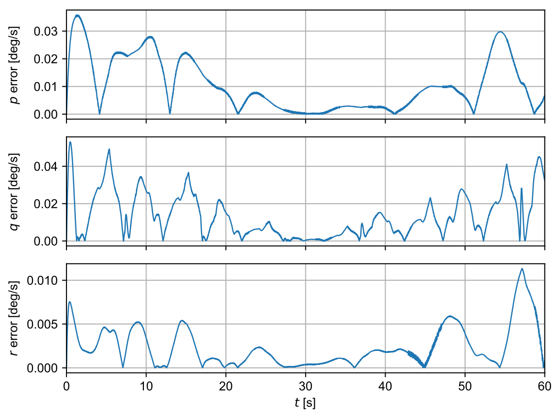

(b) Attitude rate errors.

Figure 7.2: Sinusoidal input model matching, the response of .pyd and Simulink models shown in circle and triangle dotted lines respectively.

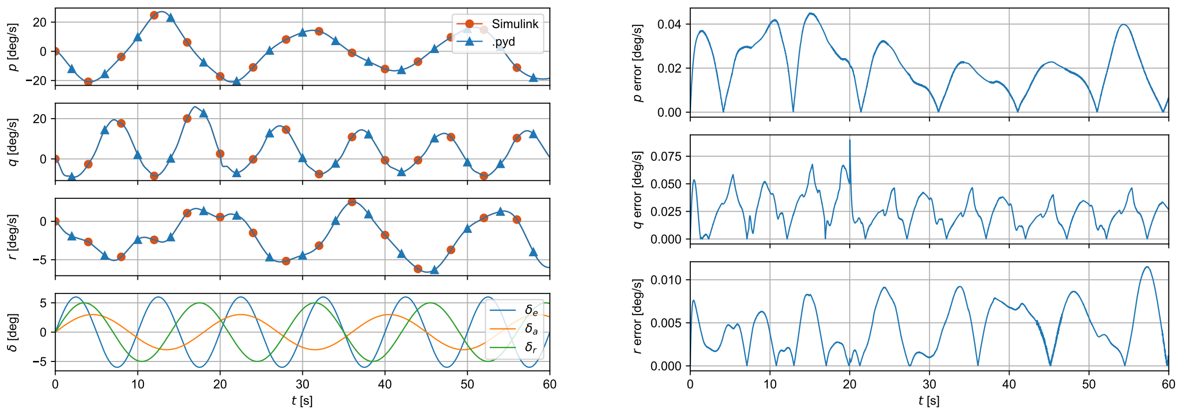

(a) Attitude rates of both models and commanded sinusoidal input.

(b) Attitude rate errors.

Figure 7.3: Shifted CG and sinusoidal input model matching, the response of .pyd and Simulink models shown in circle and triangle dotted lines respectively.

7.2. Validation

Validity of the dynamic results is a key factor in the ability of the presented results to be replicated in a real aircraft. The main factor here is the degree of fidelity with which the Simulink CitAST model matches that of a real aircraft. The CitAST model is developed as a computational model of the PH-LAB, a Cessna Citation 2 single-aisle twin-engine business jet. The latest model uses model coefficients identified from flight test data of the PH-LAB [135], the fidelity of these coefficients is shown through the fit statistics of the various force and moment coefficients specifically the coefficient of determination and relative root mean square error:

	C_X	C_Y	C_Z	C_l	C_m	C_n
R^2	0.60	0.55	0.64	0.25	0.00	0.50
$RRMSE$ (%)	8.79	7.34	7.97	8.65	12.65	8.50

Table 7.1: Fit statistics of the force and moment coefficients used in the CitAST Simulink model.

In addition to the fitting quality of model coefficients, several assumptions made regarding the aircraft dynamics limit to some extent the validity of the CitAST model. Several of these assumptions and simplifications made, and how they may affect the RL algorithm's learning, are listed in the following:

1. Constant 100 Hz sampling rate of all system states, which is not necessarily the case in real sensors where states are sampled at different intervals depending on the sensor used and state sampled. Since the three modules of IDHP (actor, critic, incremental model) are only updated whenever new state samples are tasked, the actual time needed to warm up the agent and perhaps its quality will depend on the sampling rate.
2. While the CitAST model allows for sensor dynamics and noise, the present study disabled such effects. These stochastic effects will affect what updates the three agent modules receive and, therefore, the quality of the final controller.
3. Actuator dynamics are modelled as simple first-order transfer functions, with identical time constants for aileron, elevator, and rudder surfaces. Actual actuator dynamics may resemble higher-order transfer functions more.
4. No turbulence effect on aircraft dynamics, which makes the control task easier to accomplish for the agent.

Part IV

Closure

8 Conclusion

Reinforcement learning can potentially be an effective means for creating fault-tolerant controllers, it does not have the model dependence of robust, model predictive, or dynamic inversion controllers, and it can adapt its parameters to changes mid-operation.

To foray beyond the current state of research, the present thesis was undertaken, with the following stated objective:

Research Objective

To improve the fault-tolerance of reinforcement learning based flight controllers by advancing the state of the art, through researching novel augmentations to reinforcement learning algorithms.

To more concretely guide the research process, this research objective was broken down into several research questions aimed to be answered by the end of the thesis. These answers are stated in the present chapter.

8.1. Answering Research Questions

Research Question 1

Q1 What promising reinforcement learning algorithm for fault-tolerance and tracking performance should be further studied in the present research?

Q1.1 What reinforcement learning algorithms are considered to be state-of-the-art?
Q1.2 How is fault-tolerance defined and tested in past research?
Q1.3 Which algorithms have been shown to provide the best fault-tolerance?
Q1.4 What reference tracking performance have these algorithms shown in past research?
Q1.5 What promising augmentations to reinforcement learning algorithms can be made and experimented with?

The first of the research questions is used to guide the initial learning process for learning the basis of reinforcement learning, how it may be used for flight control, and state-of-the-art research in reinforcement learning agents applied to flight control.

The answers to this first question can be found in Chapter 2, summarized in the following.

Reinforcement learning sprung out of the confluence of two streams of research around the late 20th century: dynamic programming for optimal control, and mathematical modelling of the biological learning process of animals. This heritage can still be observed in state-of-the-art algorithms, which can be considered to be in two sub-fields, ADP with groups of algorithms such as ACD, and deep reinforcement learning with algorithms such as SAC and TD3. These algorithms have been developed and extended through myriads of ways, such as the extension of DHP into a highly adaptive online version known as IDHP, or the extension of the update equations of SAC to learn a full probability distribution for the action-value function. Such extensions and the algorithms which form their basis can be considered to be state-of-the-art, and thus this answers *Q1.1*. For further information, the reader is referred to

Section 2.2 and Section 2.3.

In previous research towards reinforcement learning for flight control, with a focus on fault-tolerance, straightforward means for testing how fault-tolerant such flight controllers are presented. Primarily, this involved designing flight scenarios where either faults are introduced mid-flight, or where the controller is trained offline on the nominal aircraft and subsequently introduced to an aircraft with faults as represented by a different dynamics model. The resulting tracking performance of these controllers is then used as the primary indicator for determining how fault-tolerant a controller is. Further information can be found under Section 2.4.2. This answers *Q1.2*.

The two fields of ADP and DRL both provide valid solutions to the problem of fault-tolerant flight control. In ADP, the way fault-tolerance is achieved is through adapting the controller parameters online, i.e. through the adaptive controller paradigm. This is possible since such algorithms typically use function approximators with fewer parameters, such as small neural networks, and their learning algorithms are formulated from the theories of optimal control with proven optimality in linear cases; a strong basis for creating controllers. In DRL, the approach of using these algorithms to fault-tolerant control leverages the abilities of deep neural networks to approximate complex input-output relationships. Using a large number of offline flights, the agent is provided with ample data on which to learn a general relationship between aircraft states and aircraft action to achieve reference tracking. This relationship is general enough to hold sufficiently true even with the introduction of faults to the aircraft, as well as changes to operating conditions such as altitude, yielding fault-tolerant control. This then results in a Pareto non-dominance of the available algorithms when it comes to the question of "... best fault-tolerance.", this tie is broken by deciding that controller adaptiveness is more important than the generality of controller parameters. Thus answering *Q1.3* with the choice of IDHP, a highly adaptive ACD algorithm, further information can be found under Section 2.2.3, Section 2.3, and Section 2.4.

In the same research used to help answer *Q1.2*, reference tracking performances of ADP algorithms, specifically IDHP based controllers, are presented, found in Section 2.4.2. This helps answer *Q1.4*.

Lastly, the literature has also presented several ideas which have been successfully augmented into state-of-the-art reinforcement learning algorithms. For the present thesis, two such ideas are identified: eligibility traces, and multi-step updates or multi-step TD error as presented in Section 2.2.3. These ideas are then proposed to be augmented to the IDHP algorithm. Thus, *Q1.5* is answered.

Research Question 2

Q2 How can the identified algorithm be applied to control the PH-LAB research aircraft?

- *Q2.1* How can the identified augmentations be made to the reinforcement learning algorithm studied?
- *Q2.2* How should the flight control system be structured?
- *Q2.3* What are the variables defining the MDP in the case of controlling the PH-LAB?

The second question guides the implementation of a reinforcement learning algorithm as a flight controller. This is answered primarily in Chapter 3, which focuses on developing the agent and the flight controller by sacrificing dynamics fidelity, as a minimal aircraft model is used; specifically a model of the short-period dynamics, a longitudinal aircraft eigenmode.

First, the matter of how eligibility traces and multi-step updates can be augmented to the IDHP algorithm is answered. Eligibility traces are relatively simple to augment, as they only require finding the derivative of the actor or critic neural network, i.e. the network Jacobian. Multi-step updates are slightly more complex, as additional terms need to be added in the error equations used to update the IDHP critic. Both these augmentations are derived in Section 3.3. Thus, *Q2.1* is answered.

Regarding flight control structure, keeping in mind the objective of the present thesis is regarding fault tolerance of the reinforcement learning algorithm, not of how to optimally structure the control system or integrate the RL agent to the structure, a choice was made to use a minimal control structure. Specifically, by either only feeding the controller with the tracking error, or the tracking error plus some aircraft states. Further information can be found under Section 3.1 and the scientific paper. This helps answers *Q2.2* and *Q2.3*.

Research Question 3

Q3 How does the developed flight controller perform during nominal flight and in the presence of faults?

Q3.1 What flight scenarios should be designed to test the proposed controller's nominal performance and fault tolerance?
Q3.2 How should a controller's nominal performance and fault tolerance be measured?
Q3.3 What is the implemented controller's nominal performance and fault tolerance?
Q3.4 How do the proposed augmentations affect the nominal performance and fault tolerance of the baseline reinforcement learning algorithm?

The final question sets the experiments for studying the proposed augmentations. This was partly answered in the preliminary results of Chapter 3, but is mainly answered through the scientific paper.

In section III.D of the paper, a pitch reference tracking task was proposed, where the flight scenario begins with a warmup phase and is succeeded by a simple pitch-up pitch-down manoeuvre. This answers *Q3.1*.

The agents are tested on the designed flight scenario using both the nominal aircraft dynamics and with faults suddenly introduced. These flights are repeated 100 times to provide a sample of what tracking performances the agents provide in both cases, which is then used to measure the nominal performance and fault tolerance of the controllers. Thus answering *Q3.2*.

In section IV of the paper, the performance of the baseline algorithm, IDHP, and the proposed augmented algorithms, referred to as IDHP(λ), MIDHP, and MIDHP(λ), can be found. All algorithms can successfully control the aircraft whether faults are introduced or not, with several runs out of the 100 tried producing highly oscillatory control actions. Interestingly, the introduction of faults seems to improve the tracking performance of the 100 runs, as their control smoothness improved in flights where faults are introduced. This answers *Q3.3*.

Finally, the results from the conducted experiments are used to evaluate how the proposed augmentations compare to the baseline IDHP. Section IV of the paper shows that in the majority of the tests, the augmented algorithms have better tracking performance and smoother control actions, with the strange exception of MIDHP having many more unstable runs when controlling the nominal aircraft. Ultimately, MIDHP(λ) was shown to have the smoothest control action and tracking performance. However, if deflection rate saturation is introduced to the elevator, the advantage in action smoothness from MIDHP(λ) is diminished. With these findings, *Q3.4* is answered.

8.2. Closing Remarks

In the wider picture, state-of-the-art reinforcement learning has already demonstrated successful applications in the fields of robotics and control systems, this has been achieved with algorithms built from biological emulation and from optimal control.

As a non-model based method for controller synthesis, reinforcement learning based control systems stand as an exciting alternative paradigm to model based controller synthesis methods. To realize the opportunities which this alternative control synthesis paradigm promises, such as fault tolerance, autonomous cockpit, and enabling of novel aircraft designs, it is imperative that research takes place in the field of reinforcement learning based flight controllers. Realizing this, the present thesis stands as one such effort to investigate some of the unexplored directions of this research field.

Specifically, the present thesis aims to study how eligibility traces and multi-step updates can be applied to one of the latest ACD algorithms, IDHP, and how these augmentations affect the control performance of the resulting controller.

Through conducting flight control experiments on the CitAST, these augmentations are shown to be able to improve the overall tracking performance of IDHP, as well as their tolerance of faults. Nonetheless, it was shown that there is a significant chance of the resulting controller having highly oscillatory control actions mainly at higher pitch angles. This may be overcome by redesigning how the agents are warmed up, such as by exposing the agents to higher pitch angles.

9 Recommendations

Several questions and directions were not studied in the present thesis, due to both time and scope restrictions. This chapter lists and describes these points.

1. **Study and identification of oscillatory actors.**

   Being aware of the problems of passenger comfort and flight safety, the issue of marginally stable RL agents, or oscillatory control actions, should be investigated further. This could be done by performing deeper data analysis between controllers with noisy actions versus smooth actions, e.g. testing if their weights are close. Alternatively, one could investigate how to label certain actor networks as being marginally stable, thus providing a means of avoiding such networks in the learning process. This would be akin to finding the RL control equivalence of a marginally stable pole from linear control theory.
2. **More complex control structures, and the role of RL agents in them.**

   The present thesis only used single-loop controller structures. In established control system design practices, it is commonplace to use cascaded feedback loops in order to allow the user to command reference signals for slower varying states. Such as an altitude command. This was done in other studies into reinforcement learning for flight control, but a comprehensive evaluation and comparison of the various control structures and how an RL agent can be embedded in them would provide useful guidance for further RL flight control research. The question of how augmentations such as eligibility traces and multi-step updates would perform in such control structures would then be one of the logical sub-questions.

   The applicability of RL agents in the popular C-star or Q-star control flight control laws is also an interesting avenue to explore.
3. **The matter of the form of the incremental model.**

   Specifically concerning the utility or validity of estimating an incremental model of the MDP states, allowing for variables such as tracking error to be in the MDP state space, as opposed to an incremental model of the aircraft dynamics states.

   From a modelling perspective, such a model goes along the lines of trying to find the relationship between subsequent tracking errors. This idea is a bit dubious if one thinks a little deeper since it supposes that by knowing the tracking error at one time step one can predict what the tracking error of the next time step is. For instance, whether the error will be higher or lower at the next time step, which is an estimation that could be biased by observations: seeing the error go down over the previous time step might cause the model to predict an ever-decreasing error, but such an observation should not necessarily mean a decreased error at the next time step.

   However, finding a model for the tracking error is useful and arguably logical from the IDHP or adaptive dynamic programming perspective. Since the use of the RLS estimated model in the case of IDHP is to find the relationship between:

   - The MDP state variable and the control action i.e. the agent policy $\frac{\partial s}{\partial u}$.
   - The MDP state variable between subsequent time steps $\frac{\partial s_{t+1}}{\partial s_t}$, or equivalently $\frac{\partial s_t}{\partial s_{t-1}}$.

Furthermore, estimating such a model can be practically implemented, one simply has to feed the increment of the MDP state to the RLS estimator. But more importantly, doing so could reduce the complexity of the learning task for the IDHP critic, as one can restrict the IDHP critic to solely estimate the value function gradient over the MDP state space, instead of estimating such a gradient over the model state space or some augmented space thereof. This is beneficial when considering MDP state spaces which are either strict subsets of the model state space or are smaller in dimension.

4. **Alternative function classes for function approximation.**

   In state-of-the-art research, much focus is placed on neural networks, especially deep neural networks, as the function approximator of choice. This has been empirically shown to have merits, as deep neural networks have immense function approximation power, being capable of learning extremely complex function mappings between high dimensional input and output spaces.

   However, it would be interesting to investigate the use of alternate function approximators such as radial basis functions, which provide more authority over local domains. This could arguably make sense for control of dynamical systems such as an aircraft, where dynamics in various regions of the flight envelope exist at different time scales, or even evolve entirely differently, e.g. the lift coefficient function near low angles of attack versus near stall.

5. **Increase real-life fidelity of aircraft model used.**

   The present thesis considered a high fidelity aircraft model in terms of flight dynamics, yet it is nonetheless a deterministic model. Stochastic effects and practicalities of flight control such as turbulence, gusts, off-normal or slightly perturbed aircraft characteristics, sensor noise-biases-and-delays, and actuator disturbances, are some of the real-world phenomena that commercial flight control systems have to successfully handle. Incorporating such factors is recommended for bridging the simulation to reality gap.

   The most elaborate form of this would be to fly on the real-life PH-LAB aircraft, which already sees ongoing research with RL-based flight controllers [136].

Bibliography

[1] I. Savage, “Comparing the fatality risks in united states transportation across modes and over time,” *Research in Transportation Economics*, vol. 43, no. 1, pp. 9–22, 2013, The Economics of Transportation Safety, ISSN: 0739-8859. DOI: https://doi.org/10.1016/j.retrec.2012.12.011.

[2] I. A. T. Association, *Loss of control in-flight accident analysis report*, Distributed by IATA, 2019.

[3] K. Dally and E.-J. Van Kampen, “Soft actor-critic deep reinforcement learning for fault tolerant flight control,” in *AIAA SCITECH 2022 Forum*, 2022, p. 2078.

[4] S. Heyer, D. Kroezen, and E.-J. Van Kampen, “Online adaptive incremental reinforcement learning flight control for a cs-25 class aircraft,” Jan. 2020. DOI: 10.2514/6.2020-1844.

[5] G. J. Balas, “Flight control law design: An industry perspective,” *European Journal of Control*, vol. 9, no. 2-3, pp. 207–226, 2003.

[6] D. Lee, D. Fahey, A. Skowron, M. Allen, U. Burkhardt, Q. Chen, S. Doherty, S. Freeman, P. Forster, J. Fuglestvedt, A. Gettelman, R. De León, L. Lim, M. Lund, R. Millar, B. Owen, J. Penner, G. Pitari, M. Prather, R. Sausen, and L. Wilcox, “The contribution of global aviation to anthropogenic climate forcing for 2000 to 2018,” *Atmospheric Environment*, vol. 244, p. 117 834, 2021, ISSN: 1352-2310. DOI: https://doi.org/10.1016/j.atmosenv.2020.117834.

[7] M. Klöwer, M. R. Allen, D. S. Lee, S. R. Proud, L. Gallagher, and A. Skowron, “Quantifying aviation’s contribution to global warming,” *Environmental Research Letters*, vol. 16, no. 10, p. 104 027, Nov. 2021. DOI: 10.1088/1748-9326/ac286e.

[8] J. Benad and R. Vos, “Design of a flying v subsonic transport,” in *33rd Congress of the International Council of the Aeronautical Sciences*, 2022.

[9] D. Silver, T. Hubert, J. Schrittwieser, I. Antonoglou, M. Lai, A. Guez, M. Lanctot, L. Sifre, D. Kumaran, T. Graepel, T. P. Lillicrap, K. Simonyan, and D. Hassabis, “Mastering chess and shogi by self-play with a general reinforcement learning algorithm,” *CoRR*, vol. abs/1712.01815, 2017. arXiv: 1712.01815.

[10] OpenAI, M. Andrychowicz, B. Baker, M. Chociej, R. Jozefowicz, B. McGrew, J. Pachocki, A. Petron, M. Plappert, G. Powell, A. Ray, J. Schneider, S. Sidor, J. Tobin, P. Welinder, L. Weng, and W. Zaremba, “Learning dexterous in-hand manipulation,” 2019. arXiv: 1808.00177.

[11] M. Szuster and Z. Hendzel, “Discrete globalised dual heuristic dynamic programming in control of the two-wheeled mobile robot,” *Mathematical Problems in Engineering*, vol. 2014, p. 628 798, 2014. DOI: 10.1155/2014/628798.

[12] H. Modares, F. L. Lewis, and Z.-P. Jiang, “H_∞ Tracking control of completely unknown continuous-time systems via off-policy reinforcement learning,” *IEEE Transactions on Neural Networks and Learning Systems*, vol. 26, no. 10, pp. 2550–2562, 2015. DOI: 10.1109/TNNLS.2015.2441749.

[13] S. Roshanravan and S. Shamaghdari, “Adaptive fault-tolerant tracking control for affine nonlinear systems with unknown dynamics via reinforcement learning,” *IEEE Transactions on Automation Science and Engineering*, vol. 21, no. 1, pp. 569–580, 2024. DOI: 10.1109/TASE.2022.3223702.

[14] L. Mark and S. Richard. “The markov property.” (2005), [Online]. Available: https://shorturl.at/brtJ6 (visited on 02/11/2024).

[15] E. L. Thorndike, *Animal intelligence*. New York, The Macmillan Company, 1911.

[16] R. Bellman, *Dynamic Programming*. Princeton University Press, 1957.

[17] R. Sutton and A. Barto, *Reinforcement Learning: An Introduction*. The MIT Press, 2018.

[18] A. Plaat, *Deep reinforcement learning, a textbook*. Springer Singapore, 2022.

[19] M. Towers, J. K. Terry, A. Kwiatkowski, J. U. Balis, G. d. Cola, T. Deleu, M. Goulão, A. Kallinteris, A. KG, M. Krimmel, R. Perez-Vicente, A. Pierré, S. Schulhoff, J. J. Tai, A. T. J. Shen, and O. G. Younis, *Gymnasium*, Mar. 2023. DOI: 10.5281/zenodo.8127026.

[20] E. Torenbeek, *Synthesis of subsonic airplane design: an introduction to the preliminary design of subsonic general aviation and transport aircraft, with emphasis on layout, aerodynamic design, propulsion and performance*. Springer Science & Business Media, 2013.

[21] R. C. Nelson *et al.*, *Flight stability and automatic control*. WCB/McGraw Hill New York, 1998, vol. 2.

[22] M. Palermo and R. Vos, "Experimental aerodynamic analysis of a 4.6%-scale flying-v subsonic transport," in *AIAA Scitech 2020 Forum*, 2020, p. 2228.

[23] C. Liu, "Turboelectric distributed propulsion system modelling," 2013.

[24] L. Buşoniu, R. Babuvska, B. De Schutter, and D. Ernst, *Reinforcement learning and dynamic programming using function approximators*. CRC Press, 2010.

[25] W. T. Miller, R. S. Sutton, and P. J. Werbos, "A menu of designs for reinforcement learning over time," in *Neural Networks for Control*. 1995, pp. 67–95.

[26] Q. Wei, D. Liu, and H. Lin, "Value iteration adaptive dynamic programming for optimal control of discrete-time nonlinear systems," *IEEE Transactions on Cybernetics*, vol. 46, no. 3, pp. 840–853, 2016. DOI: 10.1109/TCYB.2015.2492242.

[27] F. L. Lewis and D. Vrabie, "Reinforcement learning and adaptive dynamic programming for feedback control," *IEEE Circuits and Systems Magazine*, vol. 9, no. 3, pp. 32–50, 2009. DOI: 10.1109/MCAS.2009.933854.

[28] F. L. Lewis, D. Vrabie, and K. G. Vamvoudakis, "Reinforcement learning and feedback control: Using natural decision methods to design optimal adaptive controllers," *IEEE Control Systems Magazine*, vol. 32, no. 6, pp. 76–105, 2012. DOI: 10.1109/MCS.2012.2214134.

[29] X. Wang and X. Tian, "Value approximation with least squares support vector machine in reinforcement learning system," *Journal of Computational and Theoretical Nanoscience*, vol. 4, pp. 1290–1294, Nov. 2007. DOI: 10.1166/jctn.2007.013.

[30] D. Bertsekas, *Dynamic programming and optimal control: Volume I*. Athena scientific, 2012, vol. 4.

[31] Q. Wei, D. Liu, and X. Yang, "Infinite horizon self-learning optimal control of nonaffine discrete-time nonlinear systems," *IEEE Transactions on Neural Networks and Learning Systems*, vol. 26, no. 4, pp. 866–879, 2015. DOI: 10.1109/TNNLS.2015.2401334.

[32] M. Lin, B. Zhao, D. Liu, X. Liu, and F. Luo, "Generalized policy iteration-based reinforcement learning algorithm for optimal control of unknown discrete-time systems," in *33rd Chinese Control and Decision Conference (CCDC)*, 2021, pp. 3650–3655. DOI: 10.1109/CCDC52312.2021.9601467.

[33] Y. Zhou, E.-J. v. Kampen, and Q. Chu, "Nonlinear adaptive flight control using incremental approximate dynamic programming and output feedback," *Journal of Guidance, Control, and Dynamics*, vol. 40, no. 2, pp. 493–496, 2017. DOI: 10.2514/1.G001762.

[34] Y. Zhou, E. v. Kampen, and Q. Chu, "Incremental approximate dynamic programming for nonlinear adaptive tracking control with partial observability," *Journal of Guidance, Control, and Dynamics*, vol. 41, pp. 2554–2567, 12 2018. DOI: 10.2514/1.g003472.

[35] B. Luo, D. Liu, T. Huang, X. Yang, and H. Ma, "Multi-step heuristic dynamic programming for optimal control of nonlinear discrete-time systems," *Information Sciences*, vol. 411, pp. 66–83, 2017, ISSN: 0020-0255. DOI: https://doi.org/10.1016/j.ins.2017.05.005.

[36] D. Wang, J. Wang, M. Zhao, P. Xin, and J. Qiao, "Adaptive multi-step evaluation design with stability guarantee for discrete-time optimal learning control," *IEEE/CAA Journal of Automatica Sinica*, vol. 10, no. 9, pp. 1797–1809, 2023. DOI: 10.1109/JAS.2023.123684.

[37] T. Li, D. Zhao, and J. Yi, "Heuristic dynamic programming strategy with eligibility traces," in *2008 American Control Conference*, 2008, pp. 4535–4540. DOI: 10.1109/ACC.2008.4587210.

[38] J. Ye, Y. Bian, B. Xu, Z. Qin, and M. Hu, "Online optimal control of discrete-time systems based on globalized dual heuristic programming with eligibility traces," in *2021 3rd International Conference on Industrial Artificial Intelligence (IAI)*, 2021, pp. 1–6. DOI: `10.1109/IAI53119.2021.9619346`.

[39] D. Prokhorov and D. Wunsch, "Adaptive critic designs," *IEEE Transactions on Neural Networks*, vol. 8, no. 5, pp. 997–1007, 1997. DOI: `10.1109/72.623201`.

[40] D. Liu, S. Xue, B. Zhao, B. Luo, and Q. Wei, "Adaptive dynamic programming for control: A survey and recent advances," *IEEE Transactions on Systems, Man, and Cybernetics: Systems*, vol. 51, no. 1, pp. 142–160, 2021. DOI: `10.1109/TSMC.2020.3042876`.

[41] T. Hanselmann, L. Noakes, and A. Zaknich, "Continuous-time adaptive critics," *IEEE Transactions on Neural Networks*, vol. 18, no. 3, pp. 631–647, 2007. DOI: `10.1109/TNN.2006.889499`.

[42] L. Yu, W. Liu, Y. Liu, and F. E. Alsaadi, "Learning-based t-shdp() for optimal control of a class of nonlinear discrete-time systems," *International Journal of Robust and Nonlinear Control*, vol. 32, no. 5, pp. 2624–2643, 2022. DOI: `https://doi.org/10.1002/rnc.5847`.

[43] D. Liu, X. Xiong, and Y. Zhang, "Action-dependent adaptive critic designs," in *IJCNN'01. International Joint Conference on Neural Networks Proceedings*, vol. 2, 2001, 990–995 vol.2. DOI: `10.1109/IJCNN.2001.939495`.

[44] J. Ye, Y. Bian, B. Luo, M. Hu, B. Xu, and R. Ding, "Costate-supplement adp for model-free optimal control of discrete-time nonlinear systems," *IEEE Transactions on Neural Networks and Learning Systems*, vol. 35, no. 1, pp. 45–59, 2024. DOI: `10.1109/TNNLS.2022.3172126`.

[45] D. Liu and Q. Wei, "Policy iteration adaptive dynamic programming algorithm for discrete-time nonlinear systems," *IEEE Transactions on Neural Networks and Learning Systems*, vol. 25, no. 3, pp. 621–634, 2014. DOI: `10.1109/TNNLS.2013.2281663`.

[46] Y. Zhou, E.-J. Van Kampen, and Q. Chu, "Incremental model based heuristic dynamic programming for nonlinear adaptive flight control," Oct. 2016.

[47] Y. Zhou, E.-J. Van Kampen, and Q. Chu, "Launch vehicle adaptive flight control with incremental model based heuristic dynamic programming," Sep. 2017.

[48] G. Venayagamoorthy, R. Harley, and D. Wunsch, "Comparison of heuristic dynamic programming and dual heuristic programming adaptive critics for neurocontrol of a turbogenerator," *IEEE transactions on neural networks*, vol. 13, pp. 764–73, Feb. 2002. DOI: `10.1109/TNN.2002.1000146`.

[49] D. Liu, Y. Xu, Q. Wei, and X. Liu, "Residential energy scheduling for variable weather solar energy based on adaptive dynamic programming," *IEEE/CAA Journal of Automatica Sinica*, vol. 5, no. 1, pp. 36–46, 2018. DOI: `10.1109/JAS.2017.7510739`.

[50] J. Qiao, M. Zhao, D. Wang, and M. Li, "Action-dependent heuristic dynamic programming with experience replay for wastewater treatment processes," *IEEE Transactions on Industrial Informatics*, vol. PP, pp. 1–9, Jan. 2024. DOI: `10.1109/TII.2023.3344130`.

[51] C. Mu, Z. Ni, C. Sun, and H. He, "Data-driven tracking control with adaptive dynamic programming for a class of continuous-time nonlinear systems," *IEEE Transactions on Cybernetics*, vol. 47, no. 6, pp. 1460–1470, 2017. DOI: `10.1109/TCYB.2016.2548941`.

[52] Y. Zhou, E.-J. Van Kampen, and Q. Chu, "Incremental model based online dual heuristic programming for nonlinear adaptive control," *Control Engineering Practice*, vol. 73, pp. 13–25, Apr. 2018. DOI: `10.1016/j.conengprac.2017.12.011`.

[53] B. Sun and E.-J. van Kampen, "Incremental model-based global dual heuristic programming with explicit analytical calculations applied to flight control," *Engineering Applications of Artificial Intelligence*, vol. 89, p. 103 425, 2020, ISSN: 0952-1976. DOI: `https://doi.org/10.1016/j.engappai.2019.103425`.

[54] M. Fairbank, E. Alonso, and D. Prokhorov, "Simple and fast calculation of the second-order gradients for globalized dual heuristic dynamic programming in neural networks," *IEEE Transactions on Neural Networks and Learning Systems*, vol. 23, no. 10, pp. 1671–1676, 2012. DOI: `10.1109/TNNLS.2012.2205268`.

[55] G. Yen and P. DeLima, “Improving the performance of globalized dual heuristic programming for fault tolerant control through an online learning supervisor,” *IEEE Transactions on Automation Science and Engineering*, vol. 2, no. 2, pp. 121–131, 2005. DOI: `10.1109/TASE.2005.844122`.

[56] D. Liu, D. Wang, D. Zhao, Q. Wei, and N. Jin, “Neural-network-based optimal control for a class of unknown discrete-time nonlinear systems using globalized dual heuristic programming,” *IEEE Transactions on Automation Science and Engineering*, vol. 9, no. 3, pp. 628–634, 2012. DOI: `10.1109/TASE.2012.2198057`.

[57] J. Yi, S. Chen, X. Zhong, W. Zhou, and H. He, “Event-triggered globalized dual heuristic programming and its application to networked control systems,” *IEEE Transactions on Industrial Informatics*, vol. 15, no. 3, pp. 1383–1392, 2019. DOI: `10.1109/TII.2018.2850001`.

[58] Y. Zhou, “Efficient online globalized dual heuristic programming with an associated dual network,” *IEEE Transactions on Neural Networks and Learning Systems*, vol. 34, no. 12, pp. 10 079–10 090, 2023. DOI: `10.1109/TNNLS.2022.3164727`.

[59] L. Baird, “Residual algorithms: Reinforcement learning with function approximation,” in *Machine Learning Proceedings*, San Francisco: Morgan Kaufmann, 1995, pp. 30–37, ISBN: 978-1-55860-377-6. DOI: `https://doi.org/10.1016/B978-1-55860-377-6.50013-X`.

[60] A. G. Ivakhnenko, “Polynomial theory of complex systems,” *IEEE Transactions on Systems, Man, and Cybernetics*, vol. SMC-1, no. 4, pp. 364–378, 1971. DOI: `10.1109/TSMC.1971.4308320`.

[61] S. Liang and R. Srikant, “Why deep neural networks for function approximation?” In *International Conference on Learning Representations*, 2016. DOI: `10.48550/arXiv.1610.04161`.

[62] Y. LeCun, B. Boser, J. S. Denker, D. Henderson, R. E. Howard, W. Hubbard, and L. D. Jackel, “Backpropagation applied to handwritten zip code recognition,” *Neural Computation*, vol. 1, no. 4, pp. 541–551, 1989. DOI: `10.1162/neco.1989.1.4.541`.

[63] A. Graves, “Generating sequences with recurrent neural networks,” *arXiv preprint*, 2014. DOI: `10.48550/arXiv.1308.0850`.

[64] R. Jozefowicz, O. Vinyals, M. Schuster, N. Shazeer, and Y. Wu, “Exploring the limits of language modeling,” *arXiv preprint*, 2016. DOI: `10.48550/arXiv.1602.02410`.

[65] C. Farabet, C. Couprie, L. Najman, and Y. Lecun, “Learning hierarchical features for scene labeling,” *IEEE Transactions on Pattern Analysis and Machine Intelligence*, vol. 35, no. 8, pp. 1915–1929, Aug. 2013. DOI: `10.1109/TPAMI.2012.231`.

[66] A. Krizhevsky, I. Sutskever, and G. Hinton, “Imagenet classification with deep convolutional neural networks,” *Neural Information Processing Systems*, vol. 25, Jan. 2012. DOI: `10.1145/3065386`.

[67] G. E. Dahl, D. Yu, L. Deng, and A. Acero, “Context-dependent pre-trained deep neural networks for large-vocabulary speech recognition,” *IEEE Transactions on Audio, Speech, and Language Processing*, vol. 20, no. 1, pp. 30–42, DOI: `10.1109/TASL.2011.2134090`.

[68] G. E. Dahl, D. Yu, L. Deng, and A. Acero, “Context-dependent pre-trained deep neural networks for large-vocabulary speech recognition,” *IEEE Transactions on Audio, Speech, and Language Processing*, vol. 20, no. 1, pp. 30–42, 2012. DOI: `10.1109/TASL.2011.2134090`.

[69] S. Ruder, “An overview of gradient descent optimization algorithms,” *arXiv preprint*, 2016. DOI: `10.48550/arXiv.1609.04747`.

[70] D. Silver, G. Lever, N. Heess, T. Degris, D. Wierstra, and M. Riedmiller, “Deterministic policy gradient algorithms,” in *International conference on machine learning*, Pmlr, 2014, pp. 387–395.

[71] V. Mnih, K. Kavukcuoglu, D. Silver, A. Graves, I. Antonoglou, D. Wierstra, and M. A. Riedmiller, “Playing atari with deep reinforcement learning,” *arXiv preprint*, 2013. DOI: `10.48550/arXiv.1312.5602`.

[72] M. Hessel, J. Modayil, H. van Hasselt, T. Schaul, G. Ostrovski, W. Dabney, D. Horgan, B. Piot, M. G. Azar, and D. Silver, “Rainbow: Combining improvements in deep reinforcement learning,” *arXiv preprint*, 2017. DOI: `10.48550/arXiv.1710.02298`.

[73] H. van Hasselt, A. Guez, and D. Silver, “Pedestrian detection with unsupervised multi-stage feature learning,” in *Proceedings of the AAAI conference on Artificial Intelligence*, vol. 30, 2016. DOI: `10.1609/aaai.v30i1.10295`.

[74] H. Hasselt, “Double q-learning,” in *Advances in Neural Information Processing Systems*, vol. 23, Curran Associates, Inc., 2010.

[75] T. Schaul, J. Quan, I. Antonoglou, and D. Silver, “Prioritized experience replay,” *arXiv preprint*, 2015. DOI: 10.48550/arXiv.1511.05952.

[76] Z. Wang, N. de Freitas, M. Lanctot, T. Schaul, M. Hessel, and H. van Hasselt, “Dueling network architectures for deep reinforcement learning,” *arXiv preprint*, 2016. DOI: 10.48550/arXiv.1511.06581.

[77] V. Mnih, A. P. Badia, M. Mirza, A. Graves, T. P. Lillicrap, T. Harley, D. Silver, and K. Kavukcuoglu, “Asynchronous methods for deep reinforcement learning,” *arXiv preprint*, 2016. DOI: 10.48550/arXiv.1602.01783.

[78] R. S. Sutton, “Learning to predict by the methods of temporal differences,” *Machine Learning*, vol. 3, no. 1, pp. 9–44, Aug. 1988, ISSN: 1573-0565. DOI: 10.1007/BF00115009.

[79] M. G. Bellemare, W. Dabney, and R. Munos, “A distributional perspective on reinforcement learning,” *arXiv preprint*, 2017. DOI: 10.48550/arXiv.1707.06887.

[80] W. Dabney, M. Rowland, M. G. Bellemare, and R. Munos, “Distributional reinforcement learning with quantile regression,” *arXiv preprint*, 2017. DOI: 10.48550/arXiv.1710.10044.

[81] M. Fortunato, M. G. Azar, B. Piot, J. Menick, I. Osband, A. Graves, V. Mnih, R. Munos, D. Hassabis, O. Pietquin, C. Blundell, and S. Legg, “Noisy networks for exploration,” *arXiv preprint*, 2017. DOI: 10.48550/arXiv.1706.10295.

[82] R. J. Williams, “Simple statistical gradient-following algorithms for connectionist reinforcement learning,” *Machine learning*, vol. 8, pp. 229–256, 1992.

[83] J. Schulman, S. Levine, P. Moritz, M. I. Jordan, and P. Abbeel, “Trust region policy optimization,” *arXiv preprint*, 2015. DOI: 10.48550/arXiv.1502.05477.

[84] S. Kullback and R. A. Leibler, “On information and sufficiency,” *The annals of mathematical statistics*, vol. 22, no. 1, pp. 79–86, 1951.

[85] M. P. Deisenroth, G. Neumann, J. Peters, *et al.*, “A survey on policy search for robotics,” *Foundations and Trends® in Robotics*, vol. 2, no. 1–2, pp. 1–142, 2013.

[86] H. Bai, R. Cheng, and Y. Jin, “Evolutionary reinforcement learning: A survey,” *Intelligent Computing*, vol. 2, p. 0025, 2023.

[87] J. Schulman, F. Wolski, P. Dhariwal, A. Radford, and O. Klimov, “Proximal policy optimization algorithms,” *arXiv preprint arXiv:1707.06347*, 2017.

[88] T. P. Lillicrap, J. J. Hunt, A. Pritzel, N. Heess, T. Erez, Y. Tassa, D. Silver, and D. Wierstra, “Continuous control with deep reinforcement learning,” *arXiv preprint arXiv:1509.02971*, 2015.

[89] S. Fujimoto, H. Hoof, and D. Meger, “Addressing function approximation error in actor-critic methods,” in *International conference on machine learning*, PMLR, 2018, pp. 1587–1596.

[90] T. Haarnoja, A. Zhou, P. Abbeel, and S. Levine, “Soft actor-critic: Off-policy maximum entropy deep reinforcement learning with a stochastic actor,” in *International conference on machine learning*, PMLR, 2018, pp. 1861–1870.

[91] B. D. Ziebart, *Modeling purposeful adaptive behavior with the principle of maximum causal entropy*. Carnegie Mellon University, 2010.

[92] M. G. Bellemare, W. Dabney, and R. Munos, “A distributional perspective on reinforcement learning,” in *International conference on machine learning*, PMLR, 2017, pp. 449–458.

[93] S. Skogestad and I. Postlethwaite, *Multivariable Feedback Control: Analysis and Design*. Hoboken, NJ, USA: John Wiley & Sons, Inc., 2005, ISBN: 0470011688.

[94] M. Voutilainen, L. Viitasaari, and P. Ilmonen, “Note on ar(1)-characterisation of stationary processes and model fitting,” *Modern Stochastics: Theory and Applications*, vol. 6, no. 2, pp. 195–207, 2019, ISSN: 2351-6046. DOI: 10.15559/19-VMSTA132.

[95] R. V. Jategaonkar and F. Thielecke, “Evaluation of parameter estimation methods for unstable aircraft,” *Journal of Aircraft*, vol. 31, no. 3, pp. 510–519, 1994. DOI: 10.2514/3.46523.

[96] J. C. Gibson, "Handling qualities for unstable combat aircraft," in *ICAS, Congress, 15 th, London, England*, 1986, pp. 433–445.

[97] C. Kamali, A. Pashilkar, and J. Raol, "Real-time parameter estimation for reconfigurablecontrol of unstable aircraft," *Defence Science Journal*, vol. 57, no. 4, p. 381, 2007.

[98] A. K. Kundu, *Aircraft design*. Cambridge University Press, 2010, vol. 27.

[99] E. Torenbeek, *Synthesis of subsonic airplane design: an introduction to the preliminary design of subsonic general aviation and transport aircraft, with emphasis on layout, aerodynamic design, propulsion and performance*. Springer Science & Business Media, 2013.

[100] P. Abbeel, A. Coates, M. Quigley, and A. Ng, "An application of reinforcement learning to aerobatic helicopter flight," *Advances in neural information processing systems*, vol. 19, 2006.

[101] F. Fei, Z. Tu, J. Zhang, and X. Deng, "Learning extreme hummingbird maneuvers on flapping wing robots," in *2019 International Conference on Robotics and Automation (ICRA)*, IEEE, 2019, pp. 109–115.

[102] Y. Duan, X. Chen, R. Houthooft, J. Schulman, and P. Abbeel, "Benchmarking deep reinforcement learning for continuous control," *arXiv preprint arXiv:1707.06347*, 2016.

[103] A. De Marco, P. M. D'Onza, and S. Manfredi, "A deep reinforcement learning control approach for high-performance aircraft," *Nonlinear Dynamics*, vol. 111, no. 18, pp. 17 037–17 077, 2023.

[104] C. Tang and Y.-C. Lai, "Deep reinforcement learning automatic landing control of fixed-wing aircraft using deep deterministic policy gradient," in *2020 International Conference on Unmanned Aircraft Systems (ICUAS)*, 2020, pp. 1–9. DOI: `10.1109/ICUAS48674.2020.9213987`.

[105] A. Adetifa, P. Okonkwo, B. B. Muhammed, and D. Udekwe, "Deep reinforcement learning for aircraft longitudinal control augmentation system," *Nigerian Journal of Technology*, vol. 42, no. 1, pp. 144–151, 2023.

[106] P. Seres, C. Liu, and E.-J. van Kampen, "Risk-sensitive distributional reinforcement learning for flight control," *IFAC-PapersOnLine*, vol. 56, no. 2, pp. 2013–2018, 2023.

[107] M. Zahmatkesh, S. A. Emami, A. Banazadeh, and P. Castaldi, "Robust attitude control of an agile aircraft using improved q-learning," in *Actuators*, MDPI, vol. 11, 2022, p. 374.

[108] R. Enns and J. Si, "Helicopter trimming and tracking control using direct neural dynamic programming," *IEEE Transactions on Neural networks*, vol. 14, no. 4, pp. 929–939, 2003.

[109] S. Ferrari and R. F. Stengel, "Online adaptive critic flight control," *Journal of Guidance, Control, and Dynamics*, vol. 27, no. 5, pp. 777–786, 2004.

[110] H. Li, L. Sun, W. Tan, X. Liu, and W. Dang, "Incremental dual heuristic dynamic programming based hybrid approach for multi-channel control of unstable tailless aircraft," *IEEE Access*, vol. 10, pp. 31 677–31 691, 2022.

[111] J. H. Lee and E.-J. Van Kampen, "Online reinforcement learning for fixed-wing aircraft longitudinal control," in *AIAA Scitech 2021 Forum*, 2021, p. 0392.

[112] C. Teirlinck and E.-J. Van Kampen, "Hybrid soft actor-critic and incremental dual heuristic programming reinforcement learning for fault-tolerant flight control," in *AIAA SCITECH 2024 Forum*, 2024, p. 2406.

[113] R. Konatala, E.-J. Van Kampen, and G. Looye, "Reinforcement learning based online adaptive flight control for the cessna citation ii (ph-lab) aircraft," in *AIAA Scitech 2021 Forum*, 2021, p. 0883.

[114] J. Rao, J. Wang, J. Xu, and S. Zhao, "Optimal control of nonlinear system based on deterministic policy gradient with eligibility traces," *Nonlinear Dynamics*, vol. 111, no. 21, pp. 20 041–20 053, 2023. DOI: `10.1007/s11071-023-08909-6`.

[115] S. Baldi, Z. Zhang, and D. Liu, "Eligibility traces and forgetting factor in recursive least-squares-based temporal difference," *International Journal of Adaptive Control and Signal Processing*, vol. 36, no. 2, pp. 334–353, 2022. DOI: `https://doi.org/10.1002/acs.3282`.

[116] J. Mulder, W. van Staveren, J. van der Vaart, E. de Weerdt, C. de Visser, A. in 't Veld, and E. Mooij, *Flight Dynamics Lecture Notes*. Delft, Netherlands: Delft University of Technology, 2013.

[117] J. Sola and J. Sevilla, "Importance of input data normalization for the application of neural networks to complex industrial problems," *IEEE Transactions on Nuclear Science*, vol. 44, no. 3, pp. 1464–1468, 1997. DOI: 10.1109/23.589532.

[118] K. Doel, U. Ascher, and E. Haber, "The lost honor of ℓ 2 -based regularization," in Aug. 2013, pp. 181–203, ISBN: 978-3-11-028222-1. DOI: 10.1515/9783110282269.181.

[119] D. Slock and T. Kailath, "Numerically stable fast transversal filters for recursive least squares adaptive filtering," *IEEE Transactions on Signal Processing*, vol. 39, no. 1, pp. 92–114, 1991. DOI: 10.1109/78.80769.

[120] Y. Zhou, "Online reinforcement learning control for aerospace systems," Available at https://doi.org/10.4233/uuid:5b875915-2518-4ec8-a1a0-07ad057edab4, PhD thesis, Delft University of Technology, Delft, The Netherlands, Apr. 2018.

[121] S. S. Haykin, *Adaptive filter theory*. Pearson Education India, 2002.

[122] D. Gupta, "Applicability of momentum in the methods of temporal learning," 2020.

[123] B. D. Nichols, "A comparison of eligibility trace and momentum on sarsa in continuous state-and action-space," in *2017 9th Computer Science and Electronic Engineering (CEEC)*, IEEE, 2017, pp. 55–59.

[124] D. Lee and N. He, "Target-based temporal-difference learning," in *Proceedings of the 36th International Conference on Machine Learning*, K. Chaudhuri and R. Salakhutdinov, Eds., ser. Proceedings of Machine Learning Research, vol. 97, PMLR, Jun. 2019, pp. 3713–3722.

[125] R. Rojas and R. Rojas, "The backpropagation algorithm," *Neural networks: a systematic introduction*, pp. 149–182, 1996.

[126] C. J. C. H. Watkins, "Learning from delayed rewards," 1989.

[127] P. Cichosz, "Truncating temporal differences: On the efficient implementation of td (lambda) for reinforcement learning," *Journal of Artificial Intelligence Research*, vol. 2, pp. 287–318, 1994.

[128] S. P. Singh and R. S. Sutton, "Reinforcement learning with replacing eligibility traces," *Machine learning*, vol. 22, no. 1, pp. 123–158, 1996.

[129] H. van Seijen, "Effective multi-step temporal-difference learning for non-linear function approximation," *arXiv preprint arXiv:1608.05151*, 2016.

[130] T. Kobayashi, "Adaptive and multiple time-scale eligibility traces for online deep reinforcement learning," *Robotics and Autonomous Systems*, vol. 151, p. 104 019, 2022, ISSN: 0921-8890. DOI: https://doi.org/10.1016/j.robot.2021.104019.

[131] F. Ballio and A. Guadagnini, "Convergence assessment of numerical monte carlo simulations in groundwater hydrology," *Water resources research*, vol. 40, no. 4, 2004.

[132] Student, "The probable error of a mean," *Biometrika*, pp. 1–25, 1908.

[133] A. Vargha and H. D. Delaney, "A critique and improvement of the cl common language effect size statistics of mcgraw and wong," *Journal of Educational and Behavioral Statistics*, vol. 25, no. 2, pp. 101–132, 2000.

[134] C. Van Der Linden, "Dasmat-delft university aircraft simulation model and analysis tool: A matlab/simulink environment for flight dynamics and control analysis," *Series 03: Control and Simulation 03*, 1998.

[135] M. Van den Hoek, C. de Visser, and D. Pool, "Identification of a cessna citation ii model based on flight test data," in *Advances in Aerospace Guidance, Navigation and Control: Selected Papers of the Fourth CEAS Specialist Conference on Guidance, Navigation and Control Held in Warsaw, Poland, April 2017*, Springer, 2018, pp. 259–277.

[136] R. B. Konatala, E.-J. Van Kampen, G. Looye, D. Milz, and C. Weiser, "Flight testing reinforcement learning based online adaptive flight control laws on cs-25 class aircraft," in *AIAA SCITECH 2024 Forum*, 2024, p. 2402.